AD-A033 885 NORTHROP CORP DES PLAINES ILL DEFENSE SYSTEMS DEPT F/G 17/4 •
LOW COST EXPENDABLE TWT AMPLIFIER FOR ECM.(U)
AUG 76 O DOEHLER, R MOATS
UNCLASSIFIED 094-007576 N00173-75-C-0464
NL

1 OF 2
ADA033885

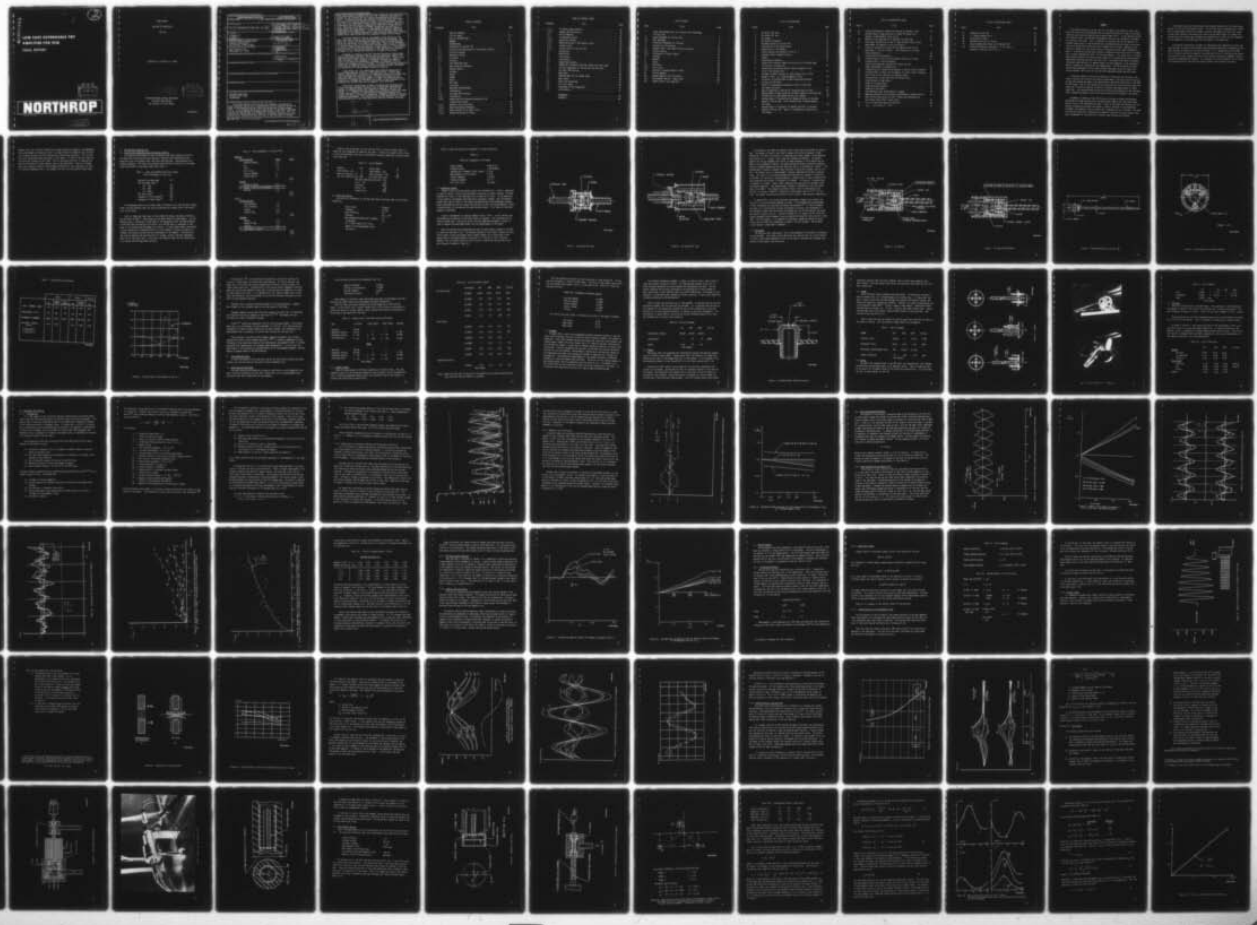

LOW COST EXPENDABLE TWT AMPLIFIER FOR ECM

FINAL REPORT

NORTHROP

Northrop Corporation Electronics Division Defense Systems Department

FINAL REPORT

LOW COST TWT AMPLIFIER

FOR ECM

Prepared by O. Doehler & R. Moats

Northrop Defense Systems Department
Electron Tube Section
Des Plaines, Illinois 60018

094-007576

SECURITY CLASSIFICATION OF THIS PAGE (When Data Entered)

REPORT DOCUMENTATION PAGE

READ INSTRUCTIONS BEFORE COMPLETING FORM

1. REPORT NUMBER

2. GOVT ACCESSION NO.

3. RECIPIENT'S CATALOG NUMBER

4. TITLE (and Subtitle)

(6) Low Cost Expendable TWT Amplifier for ECM.

(9) Final Report. 23 Apr '75 - 1 May '76,
Period: 4/23/75 - 5/1/76

6. PERFORMING ORG. REPORT NUMBER

(14) 094-007576

7. AUTHOR(s)

(10) O. Doehler
R. Moats

8. CONTRACT OR GRANT NUMBER(s)

(15) N00173-75-C-0464

9. PERFORMING ORGANIZATION NAME AND ADDRESS
Northrop Defense Systems Dept.
Electron Tube Section
Des Plaines, Illinois 60018

10. PROGRAM ELEMENT, PROJECT, TASK AREA & WORK UNIT NUMBERS

(12) 114 p.

11. CONTROLLING OFFICE NAME AND ADDRESS
Naval Research Lab.
Washington, D.C. 20375

(11) 12. REPORT DATE
August 1976

13. NUMBER OF PAGES
112

14. MONITORING AGENCY NAME & ADDRESS (if different from Controlling Office)

15. SECURITY CLASS. (of this report)
Unclassified

15a. DECLASSIFICATION/DOWNGRADING SCHEDULE

16. DISTRIBUTION STATEMENT (of this Report)

DISTRIBUTION STATEMENT A
Approved for public release;
Distribution Unlimited

17. DISTRIBUTION STATEMENT (of the abstract entered in Block 20, if different from Report)

18. SUPPLEMENTARY NOTES

19. KEY WORDS (Continue on reverse side if necessary and identify by block number)

Microwave Amplifiers
Traveling Wave Tubes
Expendables

20. ABSTRACT (Continue on reverse side if necessary and identify by block number)

Preliminary design of the low cost TWT included a cost analysis, which indicated the division of approximately 50% for material and 50% for labor at the manufacturing cost level was appropriate to medium power TWT's. It was observed during this analysis that a significant percentage of the labor was devoted to alignment and testing of the tube. Thus, in addition to reducing the cost of material in assembly labor going in tube construction, consideration must be given to the realization of design

DD FORM 1 JAN 73 1473 EDITION OF 1 NOV 65 IS OBSOLETE

SECURITY CLASSIFICATION OF THIS PAGE (When Data Entered)

409 984

which would minimize alignment and test time. Mechanical and electrical designs for the electron gun and focusing structure were considered in detail. Alternative designs were studied to determine which would yield the lowest cost, without compromising shelf life and performance. This study led to a stacked metal-ceramic electron gun construction capable of withstanding the high bake-out temperatures required to obtain the shelf life. The study of the metal-to-ceramic vacuum seal was confined to a beaded header utilizing Hybralox, a new inexpensive material capable of withstanding high temperatures. The PPM focusing structure constructed independent of the vacuum envelope was shown to be the lowest cost focusing method, which could be realized with reasonable weight and efficiency.

A detailed trade-off study on the methods of fabrication for the major cost items in the gun and focusing structure was considered. The parts cost for the gun and focusing system was shown to be approximately $30.00 for quantities in the 2000 to 5000 range. Some initial estimates of construction of the circuit and body indicated that it would be feasible to realize a $250.00 tube manufactured in those quantities. The estimates were exclusive of tooling and packaging of the completed tube, although estimates of parts fabrication tooling are included in the report.

Alignment or shimming of the PPM focusing structure to obtain satisfactory performance and beam focusing over the operational range of the tube contributes several hours to the manufacturing labor. Study of non-ideal PPM focusing was conducted to determine the means and degree of control required on the dimensions, alignment, and magnetic field to reduce this alignment time to a minimum. The study utilized both analytical techniques and numerical studies utilizing a digital computer programmed for the analysis of electron beam forming and focusing.

A beam tester was also constructed, which enabled observation of electron beam behavior inside of a PPM focusing field. Initial test results obtained were limited due to reduced beam current and voltage, but were consistent with analytical study. Further verification of the analytical results by the beam tester will enable the specification of electron gun alignment and concentricity as well as the tolerances on the dimensions of the PPM stack and the magnetic field amplitude.

Preliminary investigation of means of constructing the interaction circuit and tube and body, RF seals, and collector were conducted preparatory to determining the work required to complete a low cost TWT design. A "T" shaped helix wire locked into a dielectric barrel was shown to have the possibility of eliminating the expensive precision helix support rods and to provide the interaction impedance required to achieve acceptable performance. This approach also has the possibility of simplifying construction of the input and output couplers collector insulator.

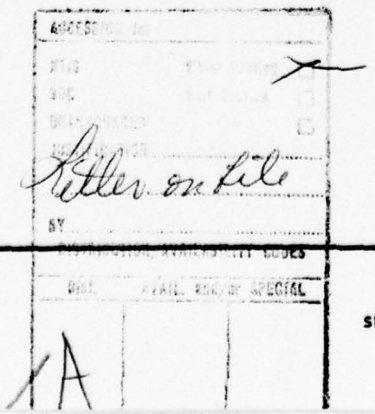

TABLE OF CONTENTS

TABLE OF CONTENTS (CONT)

LIST OF TABLES

LIST OF ILLUSTRATIONS

LIST OF ILLUSTRATIONS (CONT)

LIST OF ILLUSTRATIONS (CONT)

SUMMARY

Preliminary design of the low cost TWT included a cost analysis, which indicated the division of approximately 50% for material and 50% for labor at the manufacturing cost level was appropriate to medium power TWT's. It was observed during this analysis that a significant percentage of the labor was devoted to alignment and testing of the tube. Thus, in addition to reducing the cost of material in assembly labor going in tube construction, consideration must be given to the realization of design which would minimize alignment and test time. Mechanical and electrical designs for the electron gun and focusing structure were considered in detail. Alternative designs were studied to determine which would yield the lowest cost, without compromising shelf life and performance. This study led to a stacked metal ceramic electron gun construction capable of withstanding the high bake-out temperature required to obtain the shelf life. The study of the metal-to-ceramic vacuum seal was confined to a beaded header utilizing Hybralox, a new inexpensive material capable of withstanding high temperatures. The PPM focusing structure constructed independent of the vacuum envelope was shown to be the lowest cost focusing method which could be realized with reasonable weight and efficiency.

A detailed trade-off study on the methods of fabrication for the major cost items in the gun and focusing structure was considered. The parts cost for the gun and focusing system was shown to be approximately $30.00 for quantities in the 2000 to 5000 range. Some initial estimates of construction of the circuit and body indicated that it would be feasible to realize a $250.00 tube manufactured in those quantities. The estimates were exclusive of tooling and packaging of the completed tube, although estimates of parts fabrication tooling are included in the report.

Alignment or shimming of the PPM focusing structure to obtain satisfactory performance and beam focusing over the operational range of the tube contributes several hours to the manufacturing labor. Study of non-ideal PPM focusing was conducted to determine the means and degree of control required on the dimensions, alignment, and magnetic field to reduce this alignment time to a minimum. The study utilized both analytical techniques and numerical studies utilizing a digital computer programmed for the analysis of electron beam forming and focusing.

A beam tester was also constructed, which enabled observation of electron beam behavior inside of a PPM focusing field. Initial test results obtained were limited due to reduced beam current and voltage, but were consistent with analytical study. Further verification of the analytical results by the beam tester will enable the specification of electron gun alignment and concentricity as well as the tolerances on the dimensions of the PPM stack and the magnetic field amplitude.

Preliminary investigation of means of constructing the interaction circuit and tube and body, RF seals, and collector were conducted preparatory to determining the work required to complete a low cost TWT design. A "T" shaped helix wire locked into a dielectric barrel was shown to have the possibility of eliminating the expensive precision helix support rods and to provide the interaction impedance required to achieve acceptable performance. This approach also has the possibility of simplifying construction of the input and output couplers and collector insulator.

I. INTRODUCTION

The aim of the study is the development of a low-cost expendable TWT with the following characteristics:

RF Output Power	50 Watts
Bandwidth	4-8 GHz
Temperature	
Non-operative	-55 to +120°C
Operative*	-20 to +80°C
Efficiency	Maximum
Life	30 minutes

*Assumed to be temperature of body

Moreover, the tube must be operative even after a shelf life of 10 years with a short warm-up time and no further processing.

The principal consideration in this development is the reduction of cost, so that the ultimate selling price will be consistent with application to expendables. The initial design goal is a selling price of $250.

In order to approach the design goal, the following guidelines have been established:

(1) Use components which are in large production for commercial devices, if the tolerances are acceptable. For example:*

Magnets: Strontium or barium ferrites and Alnico 8 are used in millions/year quantities for loud speakers.

Ceramics: Used in large quantities in the automobile industry.

DC Headers: Used for other devices such as triodes.

---

* In a recent article in Countermeasures, October-November, 1975, on "Expendable Jammer", the problem of the "functionability" of the jammer for a shelf life of ten (10) years and the necessity to use commercially available components in non-critical areas is emphasized.

(2) Use techniques for stamping electrodes and/or pole pieces as in CRT's.
(3) Use jigs with sufficient precision to eliminate adjustments of gun and/or the focusing system. The cost of the jigs can be a substantial part of the tooling, and is a function not only of the required tolerances, but also of the life cycle of the jigs.
(4) Limit quality assurance, supervision, engineering and acceptance tests. Poor quality assurance procedures decrease the yield; too severe control increases the cost.*

The main efforts during the first phase of this program were directed to the following:

(1) Design and analysis of the cost of the components of the gun and the PPM focusing system.
(2) Consideration of non-ideal conditions of the PPM focusing and their influence on the beam.
(3) Check of calculated tolerances by means of a real size beam tester, which was developed and fabricated during this phase.

Not much information on the tolerances of the different parameters is known, and the tube designer generally has the tendency to impose the tightest tolerances possible. This leads to expensive tube parts. Moreover, on many parameters, the tolerances achieved in the sub-assembly operations are insufficient, then adjustment of the gun and the PPM stack by shimming becomes necessary, thereby increasing labor cost.

During the engineering phase of many manufacturing contracts, [1][2] "the establishment of tolerance limits on the electrical parameters of subassemblies, which will still yield tubes meeting specification, has to be made."

---

* As an example, many customers require the crossed-fields of a bare magnet to be below about 5 Gauss. The measurements show that the crossed-fields in a PPM stack is determined by misalignment, and not by the crossed-field of a bare magnet, i.e., a quality control on crossed-fields of the bare magnets is not necessary.

However, only very limited information has been obtained by computer or experiments. The establishment of tolerance limits is a complicated and expensive task, and generally cannot be done with the time and the limited funds available. This is also true with the present study described in this report, in spite of the fact that the main work was directed to this item. This is even more difficult if quantitative results, applicable to other designs, have to be established. There is no doubt that such a general study will be extremely effective for cost reduction, not only for low-cost expendable TWT's, for example, but also for more sophisticated tubes.

2. PRE-DESIGN OF LOW-COST TWT

2.1 Previous Cost Experience and Preliminary Analysis

The relative distribution of cost of material and labor required to build a low power TWT at the Electron Tube Section of Northrop were analyzed and compared with cost distribution data from other manufacturers. Some important differences appeared. The labor cost presents about 60-70% of the cost for low power tubes and 40-50% for high power tubes (see Table I).

Table I. Labor and Overhead Costs for Various TWT's Percentage of Total Cost.

Northrop low power tube	61%
MEC low power tube[3]	
For 100	60%
For 1000	62%
For 3000	63%
MEC power tube[4]	40%
Average of 3 Drive Tubes[5]	68%
Average of 2 Power Tubes[5]	53%

The expendable tube with an output power of 50 Watts is at the low end of power tubes, and the expected labor can thus be predicted to be about 50% of the overall cost of the tubes.

Table II shows the labor hours of two production tubes, one made at Northrop and the other at MEC[3]. Both tubes are low power tubes and older models. For the Northrop tube, a large part of the labor is for packaging, which includes shimming of the PPM stack and testing (12.5 hours); for the MEC tube, a large part of the labor is for testing and adjustment (11.5 hours). In more recent tubes, pre-testing is much reduced due to improved control of the alignment of the pole pieces by an integral pole piece structure and by pretreatment of the magnets. Pre-testing of the tube for meeting the specifications of voltage, current, and gain represents about 10% of the labor time. In any case, the required labor for the construction of an actual TWT has been about 30 hours.

Table II. Labor Breakdown for Various TWT's.

WARNECKE:		
VACUUM ENVELOPE:	HOURS	TOTAL
Cathode Assembly	2.3	
Gun	6.5	
Helix	1.6	
Helix & Gun	.9	
Exhaust Assembly	2.	
Exhaust Ageing	3.	
		16.3
PACKAGE:		
Magnet & Coupler	2.4	
Magnet & Tube, with adjustment	12.7	
Housing	.2	
		15.3
		31.6
M.E.C.:		
VACUUM ENVELOPE:		
Sub-assemblies	7.0	
Final Assembly	3.0	
Process	3.0	
Machine Shop	1.0	
		14.0
PACKAGE:		
Magnet	2.0	
Magnet & Tube	2.0	
Housing	1.0	
Adjustment & Testing	11.5	
		16.5
		30.5

Based on the design goal for the low cost TWT of a price of $250, Table III shows the cost breakdown for material and labor. Taking into account profit, G and A, yield and overhead, the cost of the material should be about $72, and the direct labor about $34.

Table III. Cost Breakdown.

Material	$72	Direct Labor	34
Yield Factor - 10%	8	Yield Factor - 15%	5
Material Handling - 7%	5	Labor Overhead - 118%	46
Sub Total Material Cost	$85	Sub Total Labor Cost	85
		Sub Total Manufacturing Cost	$170
		G & A 23%	42
		Sub Total	$212
		Profit 15%	38
		Target Price	$250

2.2 Electrical Design

The electrical parameters of the beam have been calculated under the following assumptions:

Output power	50 Watts
Frequency	4-8 GHz
Beam efficiency	10%
Perveance	0.5×10^{-6}
Beam diameter/average helix diameter	0.4
γa maximum	1.5
(a = helix radius, $\gamma = 2\pi/\Lambda$ where Λ is the wavelength along the helix.)	

Table IV shows the electrical parameters for these conditions.

Table IV.

Electrical Parameters of the Beam

Anode voltage	4,000 Volts
Cathode current	0.125 Amperes
Average helix diameter (0.087 inches)	2.2 mm
Beam diameter (0.035 inches)	0.9 mm
Plasma frequency	1.45 GHz
Plasma wavelength	2.6 cm
Brillouin field	730 Gauss

2.3 Mechanical Design

Figures 1 and 2 show two designs taken into consideration. Figure 1 represents a classical design in which the electrodes are mounted by ceramic spacers. Brazing problems will occur if the electrodes are not made out of Kovar. At the beginning of the contract, molybdenum electrodes were considered, however, test performance showed leaks and/or cracks of the ceramic-molybdenum bond (moly-manganese process). Kovar electrodes must be far enough from the gun so that the induced magnetic fields (crossed-fields) do not perturb the beam forming process. This leads to relatively expensive electrodes.

Figure 2 corresponds to a design commonly used in CRT's. In this design, the electrodes can be made out of stainless steel by stamping. The tolerances can be held by proper jigs. Difficulty exists for high temperature bakeout if glass is used to support the electrodes and/or for the feedthroughs of the header.

Many discussions arose concerning the most reliable design, especially related to leaks and long shelf life. The brazing surfaces of the Figure 1 design are relatively large, so that microleaks have a higher probability of occurring in this design than in the second design, particularly if long shelf life is desired, However, thin pin holes (Figure 2) are difficult to metallize and are one of the main sources of potential leaks.(6)

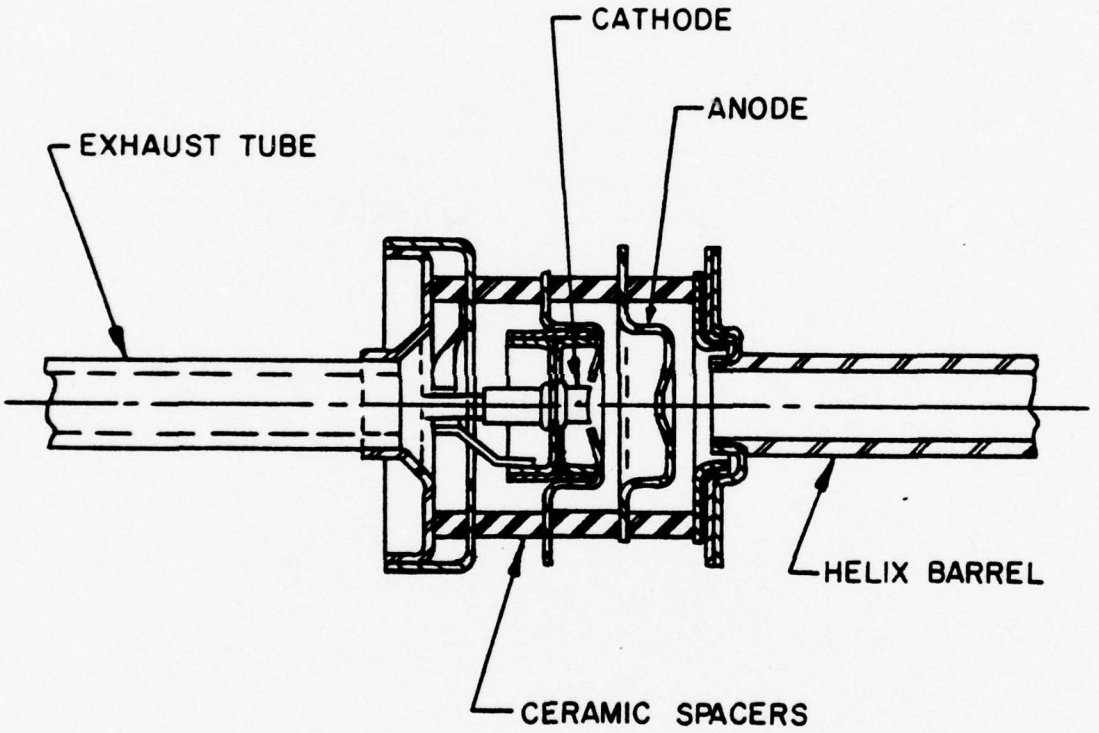

Figure 1. Gun Design TWT Type.

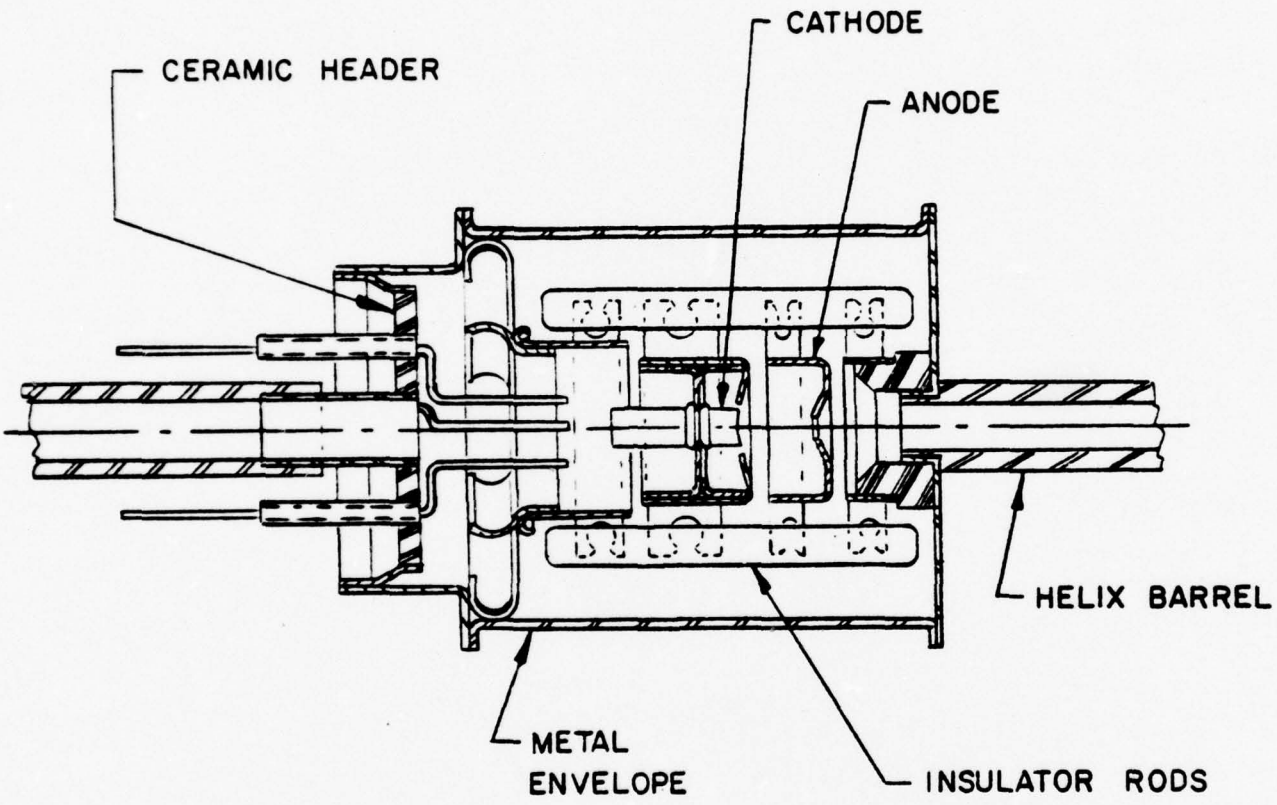

Figure 2. Gun Design CRT Type.

An estimate of the labor and material costs shows that both designs are equivalent. The design of Figure 2 was finally chosen, particularly because a higher probability for shelf life survival is expected with proper headers, using Hybralox (see section 3.5). Figures 3 and 4 show two proposed gun designs. The ceramic spacers for the gun assembly are similar to those produced in large quantities for pumps in the automobile industry; the beam forming electrodes are made by stamping and the alignment between the gun and the helix barrel is obtained by a "snout". The cathode body is made by sintered nickel and held in place by a ceramic disk as in a CRT. The ceramic disk is a good thermal insulator compatible with short "warm-up" times. In Figure 3, the distance between the anode and the cathode is controlled to $\pm$0.0005" by individually selected spacers, a method which is used at Northrop for scan converters and assures a tolerance of $\pm$0.00025". In Figure 4, a cathode body is mounted in a sleeve. Snout, anode, beam-focusing electrode and cathode sleeve are mounted together. The cathode-anode distance is obtained by a jig with tolerances of $\pm$0.0005". The cathode to cathode sleeve fixture is obtained by laser welding. An oxide or "Medicus" cathode and a SAES getter type ST 101[7] will be used. The header insulators are Hybralox, which allows a high bake-out temperature.

In modern TWT's, the vacuum envelope incorporates integral pole pieces, and Alnico 8 or rare earth-cobalt magnets are used. The advantages and disadvantages of this technology are discussed by Burgess and Conquest.[8] If ferrite magnets are used, it is not possible to mount the magnets in halves, and consequently it was decided to mount the pole pieces and magnets by slip fitting them on the external barrel (Figures 5 and 6). The main problems of this design are the input and output connectors which present a serious problem for potential leaks and high labor cost. For this reason, it is proposed to completely change the design of the RF circuit and to study this technology in Phase II of this program. The proposed circuit design is described in Section 7.

2.4 Gun Design

The required short operational life of the expendable TWT presents an advantage to the designer. Since high current densities are required only for a short amount of time, a small beam compression ratio can be used to overcome the divergent lens effect of the anode of the Pierce gun.

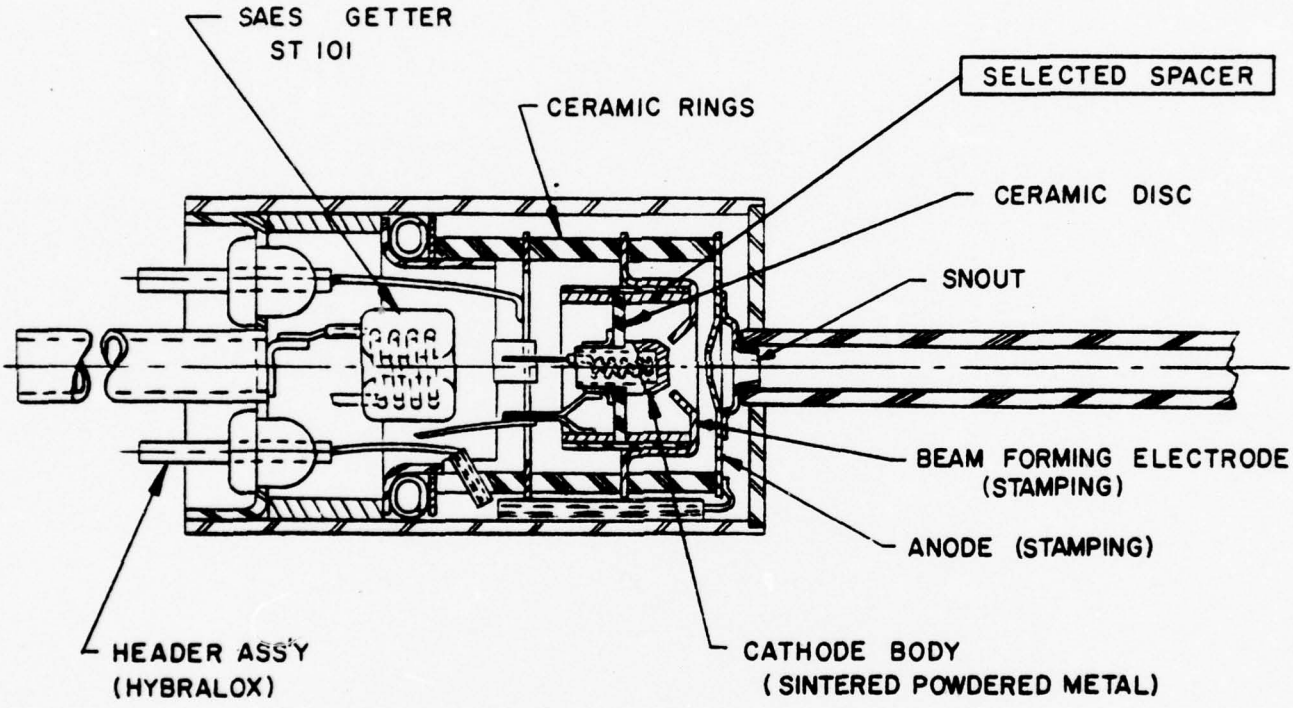

Figure 3. Gun Design.

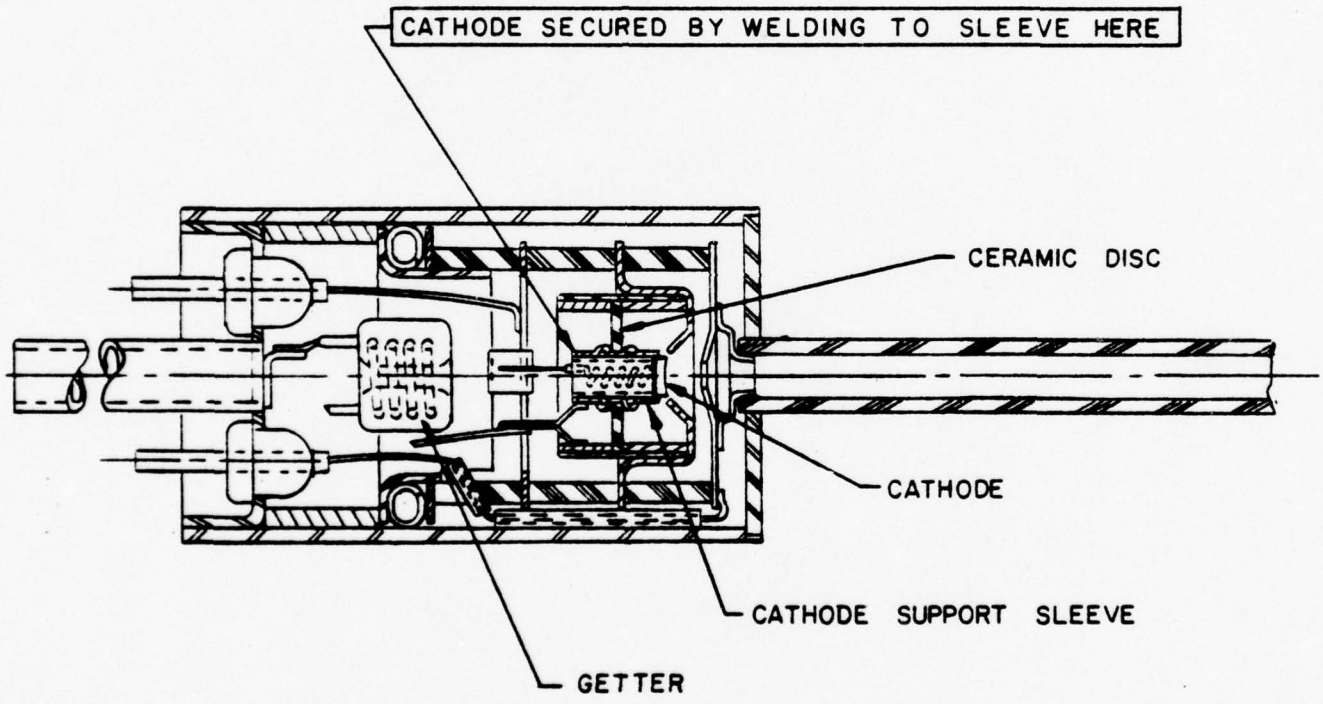

Figure 4. Gun Design (Alternate).

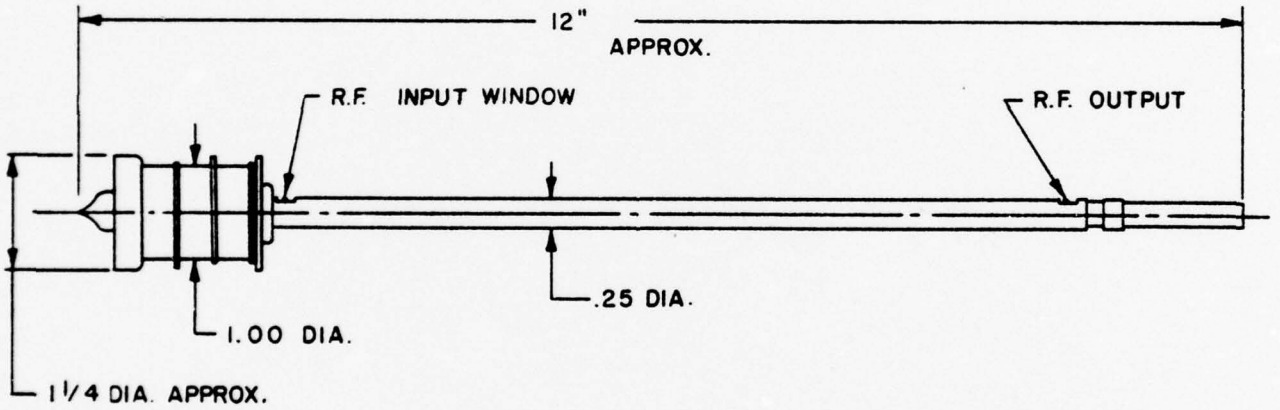

Figure 5. Envelope Outline of Low Cost TWT.

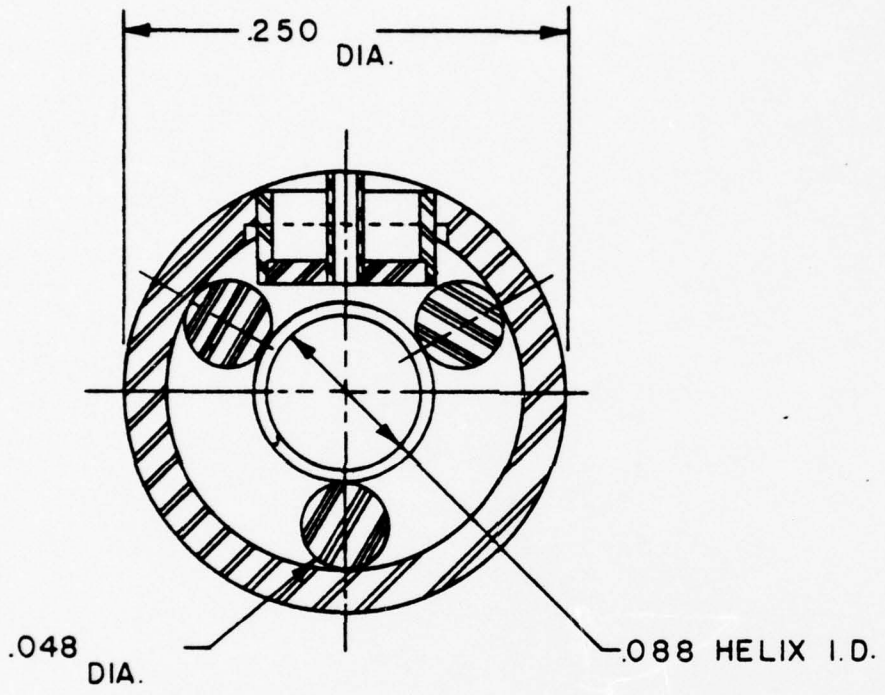

SCALE: 10-1

156-021799-028

Figure 6. Cross-Section of RF Output Window.

The predesign of the Pierce gun was made by following the design procedure described by Pierce[9] and Gittins.[10] The trajectory calculations were made by Shared Applications, Inc. (SAI) with the Rowe program. Figure 7 shows the dimensions of three computed guns. The main objective of the design was the simplicity of the electrode without severe sacrifices in the beam properties. Table V is a summary of the results. Gun No. 1 was also computed by G. Konrad with the Stanford program written by Hermannsfeldt. The SAI and the Stanford program calculate the same perveance. The intercepted current is higher in the SAI program and the variation of the current density larger in the Stanford program. The Stanford program shows a discontinuity of current density at 0.6 of the cathode radius; for the SAI program the current density is a monotonically increasing function of the radius, which seems physically more realistic (Figure 8).

The angle of the Pierce electrode of gun No. 2 was changed from 54^{o} to 45^{o} as proposed by Stevens (SAI). In gun No. 3, no beam interception occurred, the homogenity was good, and the gun has a perveance of 0.49×10^{-6}. Gun No. 2 had a perveance of 0.34×10^{-6} as calculated by following the Pierce procedure.

As of yet only gun No. 1 was mounted in the beam tester. The results were in good agreement with the computation (see Table V, gun No. 1). Gun No. 3 has been constructed, however, it has not been tested due to heater problems of the cathode.

2.5 Focusing

A large number of focusing methods were considered, and the PPM focusing was found to be the best compromise between cost, weight, and tolerances. The Harris flow was used in the spirotron by Tschernov[11] who reported excellent results with efficiencies up to 30% and output power of more than 10 watts between 1.5 and 3 GHz. However, Kirstein, Kino and Waters[12] described the difficulty of the beam launching and the poor stiffness of the flow for the outer electrons of the beam so that high beam interception in high power tubes occurs, which eliminates this type of focusing.

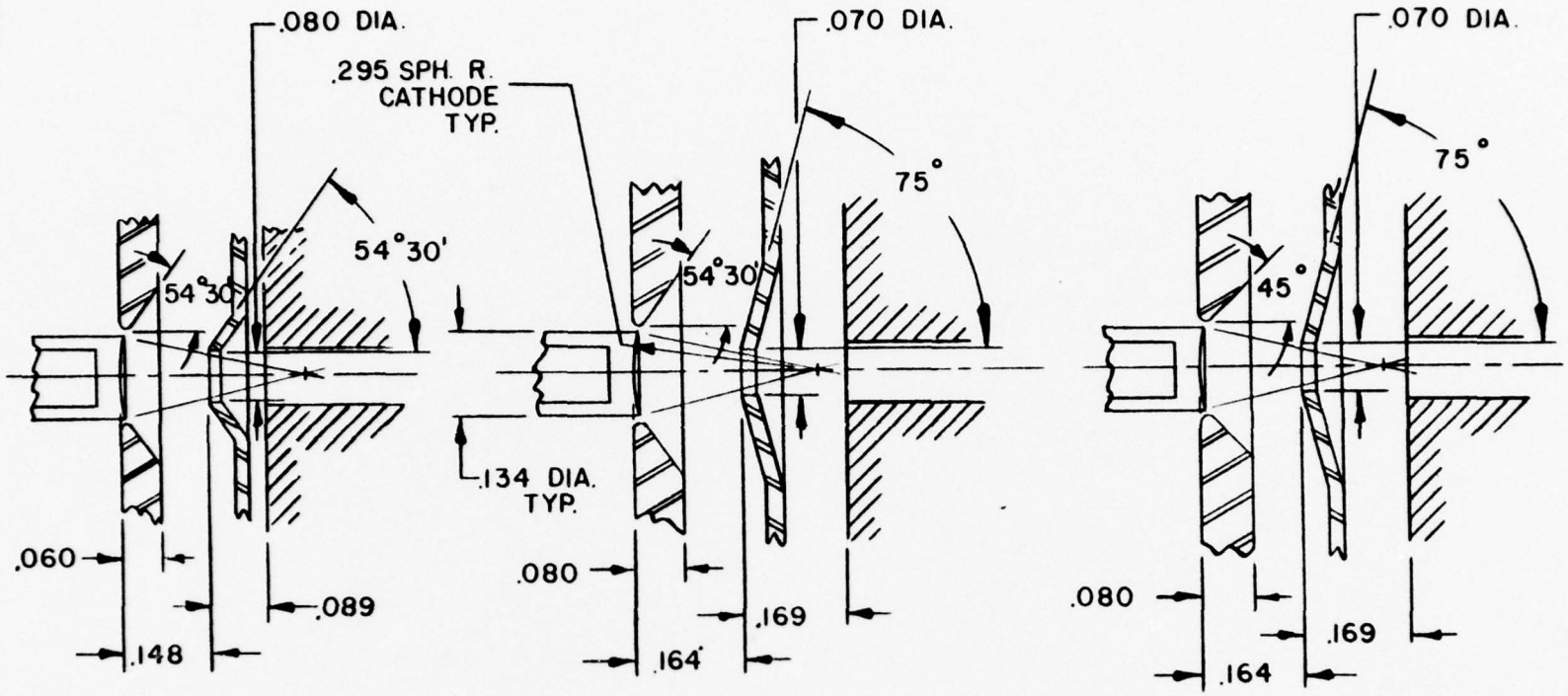

Figure 7. Dimensions of 3 Gun Designs.

Table V. Electron Gun Calculations.

	GUN 1			GUN 2		GUN 3
	SAI	STAN-FORD	OB-SERVED	SAI	STAN-FORD	SAI
TOTAL CURRENT (AMP)	.197	.20	.196	.163	.163	.125
PERVEANCE (10^{-6})	.78	.80	.78	.65	.65	.49
INTERCEPT CURRENT	.039	.020	.050	.050	.32-.48	.00
CATHODE LOADING RATIO $\left(\frac{I_{max/cm^2}}{I_{min/cm^2}}\right)$	1.43	1.65		1.40	1.65	1.09

156-021799-007

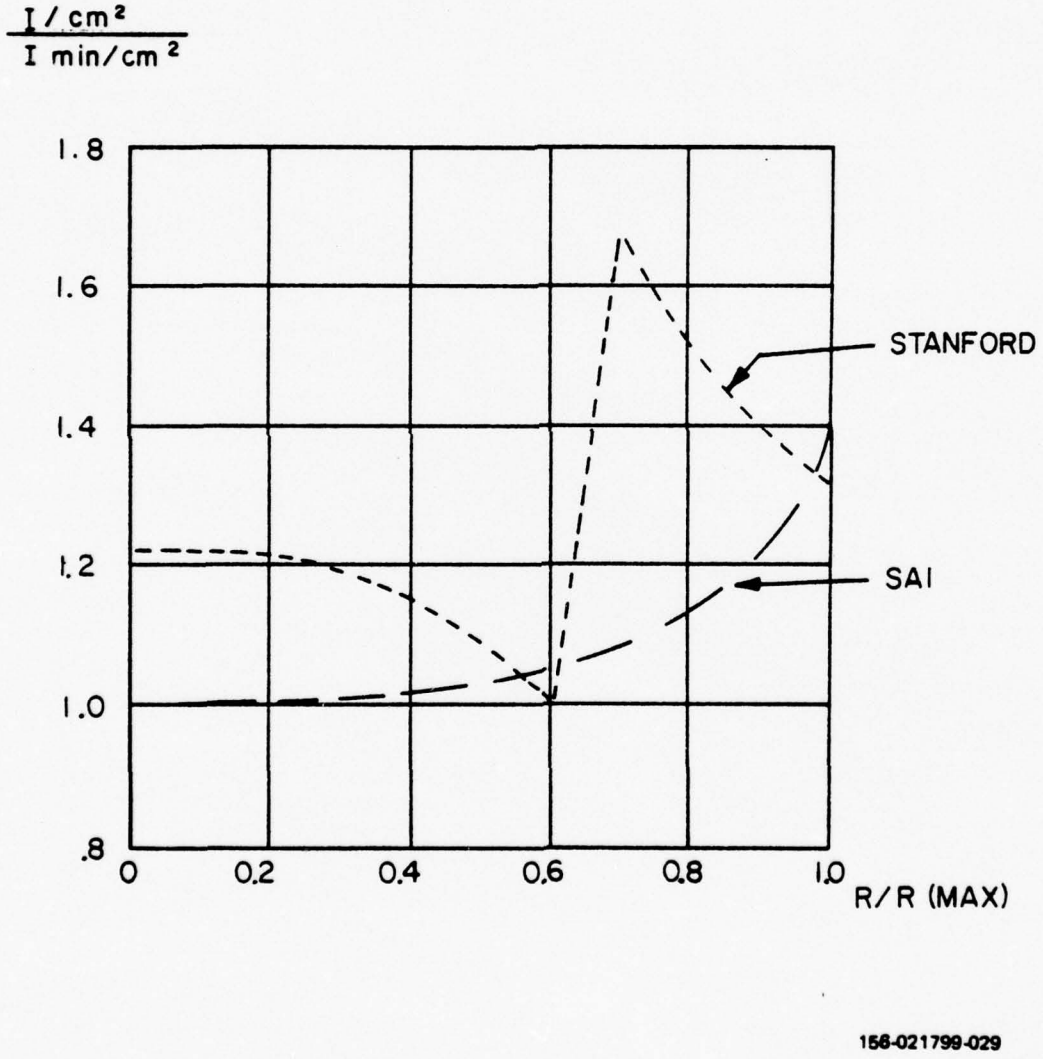

Figure 8. Current Density Distribution of Gun No. 1.

The estiatron [13], an electrostatic focused TWT, uses bifilar helices for focusing. Output power of 20 watts has been obtained. In bifilar helices, two modes exist, with zero and π phase between the two helices, having slightly different phase velocities. Irregularities in the helices and/or asymmetric electron beams will excite the asymmetric mode even if the helices are symmetrical in phase and amplitude at the input. In a broadband TWT, this leads to power holes in the band, and therefore, the yield becomes so low and the required tolerances so high that the tube becomes expensive.

Immersed flow in solenoid focusing systems is the least expensive. However, the DC power for the solenoid leads to too low values of efficiency.

Permanent magnets can be made relatively compact, and with field straighteners, the crossed fields can be reduced to less than 0.2%.[14] The weight and cost eliminate this type of permanent focusing.

Glance[15] studied the quadrupole lens for high perveance beams. Satisfactory beam ripple can be achieved, but the adjustment is critical. This focusing may be interesting if samarium cobalt magnets can be used, however, more theoretical and experimental work is necessary to justify such focusing for low cost TWT's.

Field reversal or multiple field reversal reduces the weight, and is used in coupled cavity TWT's and millimeter wave TWT's.[16] In order to compensate for the influence of the transition region on the trajectories, the magnetic field is slightly decreased (dip compensation) or increased (peak compensation). In this case, the beam ripple is very sensitive to crossed-fields (as in the permanent magnet), and the weight is greater than for the PPM focusing.

3. COST REDUCTION STUDY

In the first phase of this study only the gun and the focusing system have been studied, and the cost analysis was made on these components only.

3.1 Beam Focusing Electrodes

The beam focusing electrodes can be made by machining, by using temporary dies, which limit the production for each die to about 500, or by using permanent dies with which more than 10,000 parts can be produced.

The tolerances achievable with permanent dies are:

Aperture diameter	±0.0005"
Ovality of the aperture	0.0005"
Outside diameter	±0.001"
Tolerances of angle	±1°

Some samples of stainless steel electrodes were heat cycled between room temperature and 1050°C without any measureable permanent deformation.

Table VI shows the quotes obtained from three companies in 1975 dollars. (Note: In this table, and in several others which follow, there are omissions in quantities quoted by various vendors, mainly because the method of manufacture is not suited to the quantities involved).

Table VI. Quoted Prices Each Beam Focusing Electrode.

FOR:	10 PIECES	1,000 PIECES	5,000 PIECES	TOOLING
Machined	$45.00	*	*	-
Temporary Tooling	$15.00	*	*	$ 325
Permanent Tooling	$ .85	$ .14	$ .06	$3,000
(Two Suppliers)	$ 1.29	$ .324	$ .185	$1,590
		ANODE		
Machined	$30.00	*	*	-
Temporary Tooling	$10.00	*	*	$ 250
Permanent Tooling	$ .85	$ .19	$ .05	$1,640
(Two Suppliers)	$ .96	$ .28	$ .133	$1,144

*Not Quoted

3.2 Ceramic Spacers

Table VII shows quotes of different companies for ceramic rings. The cost depends slightly on the tolerances imposed on the thickness, and on the metallization. With moly-manganese metallization, the tolerance given by the vendors is ±0.001" when both sides are metallized.

Table VII. Cost of Ceramic Spacers.

	Tolerances	100	1000	5000	Tooling
Non Metallized:					
	±0.0005"	$4.58	$3.26	$2.84	$360
	±0.0005"	6.65	2.40	1.65	595
	±0.0005"	7.85	2.58	2.17	360
	±0.002"	3.65	2.60	2.30	595
	±0.001"	1.70	.62	.283	710
Metallized:					
	±0.0015	5.83	3.76	3.19	360
	±0.0015"	8.10	3.05	2.15	595
	±0.0020"	4.00	2.75	1.80	-
	±0.0020"	*	1.83	.91	710
	±0.003"	4.90	3.10	2.65	360
	±0.003"	7.65	2.90	2.05	595
Metalization Only:					
	±0.001"	2.30	1.15	.63	200

*Not Quoted

Note: Where multiple rows of data occur corresponding to be same tolerance level, data from more than one vendor is included.

The least expensive ceramics are the rings used in large production. In this case the thickness is fixed at 0.250 inches. The price of the ceramic spacer holding the cathode (See Figures 3 and 4) is less than $0.30. Table VIII shows the measured thickness.

Table VIII. Tolerances of Ceramic Spacers.

Outside diameter	±0.0007"
Ovality outside	0.0002"
Inside diameter	±0.004"
Ovality inside	0.0006"
TIR max.	<0.004"

If a TIR of less than 0.002" is required, the price of the spacer increases:

100 pieces	$3.00
1000 pieces	$1.43
5000 pieces	$1.20

3.3 Cathodes

In modern TWT's, mainly the impregnated tungsten aluminate cathode is used because tight tolerances and high reliability can be achieved, however, the cathode is expensive. Three other cathodes can be envisioned, the classical oxide cathode, the coated powder cathode (CPC) by W. Maurer and C. M. Pleass of the Bell Laboratories, and the Medicus cathode, a nickel matrix cathode invented by Medicus and under study at Northrop. The main parameters are the cost, the reliability and the low getter function of the cold cathode. Unfortunately, the barium is an excellent getter at low temperature and after long storage the cathode in operation will release the absorbed gas. No quantitative measurements of the getter functions of different cathodes in a same environment were available. The choice of the cathode depends on the cathode getter activity compatible with the activity of a cold getter (e.g., ST101 and ST170) and the outgassing process during the processing of the tube. It is expected that quantitative results will soon be made available by NRL.

The proposed cathode-gun assembly is shown in Figures 3 and 4, while Figure 9 shows the cathode structure in detail. An investigation related to the cost of oxide cathodes compatible with the proposed TWT performances was made. The companies contacted are not even interested in the fabrication of such cathodes in small quantities, a small quantity being less than 5,000 pieces. One answer to this problem is to fabricate those cathodes by nickel sintering. Figure 9 also shows the tolerances promised by the manufacturer.

Table IX shows the evaluated cost of the cathodes. No definite prices could be obtained by vendors for the oxide and CPC cathodes. It is expected that the cost of the cathode will not appreciably exceed the cost of the cathode body, since the spraying of the active emissive material is expected to be quite inexpensive. The CPC material is about $50/lb. and the misch-crystal carbonates about $3/lb; thus, CPC cathodes may be slightly more expensive.

Table IX. Cost of Cathodes.

	100	1000	5000	Tooling
Impregnated Cathodes	$20.00	$12.00	$10.00	-
Cathode Body	*	.42	.13	$2000
Heater	1.30	.90	.60	-

* Not Quoted

3.4 Getter

Many glass TWT's are provided with flash getters because the bake-out temperature is limited to about 450°C. Ceramic-metal TWT's are baked out at higher temperatures and there is not enough space for a flash getter. It is proposed to use non-evaporable getters in the low-cost TWT's for the long required shelf life.

Gases from virtual leaks or micro-leaks will be partially absorbed by the barium in the cathode. During warm up time, no increased pressure in the tube can be allowed. Non-evaporable cold getters such as the ST101 or ST171 of SAES are proposed for this purpose. During processing, the getter will be activated, requiring one or two additional feed-throughs. The ST171 getters have a much higher

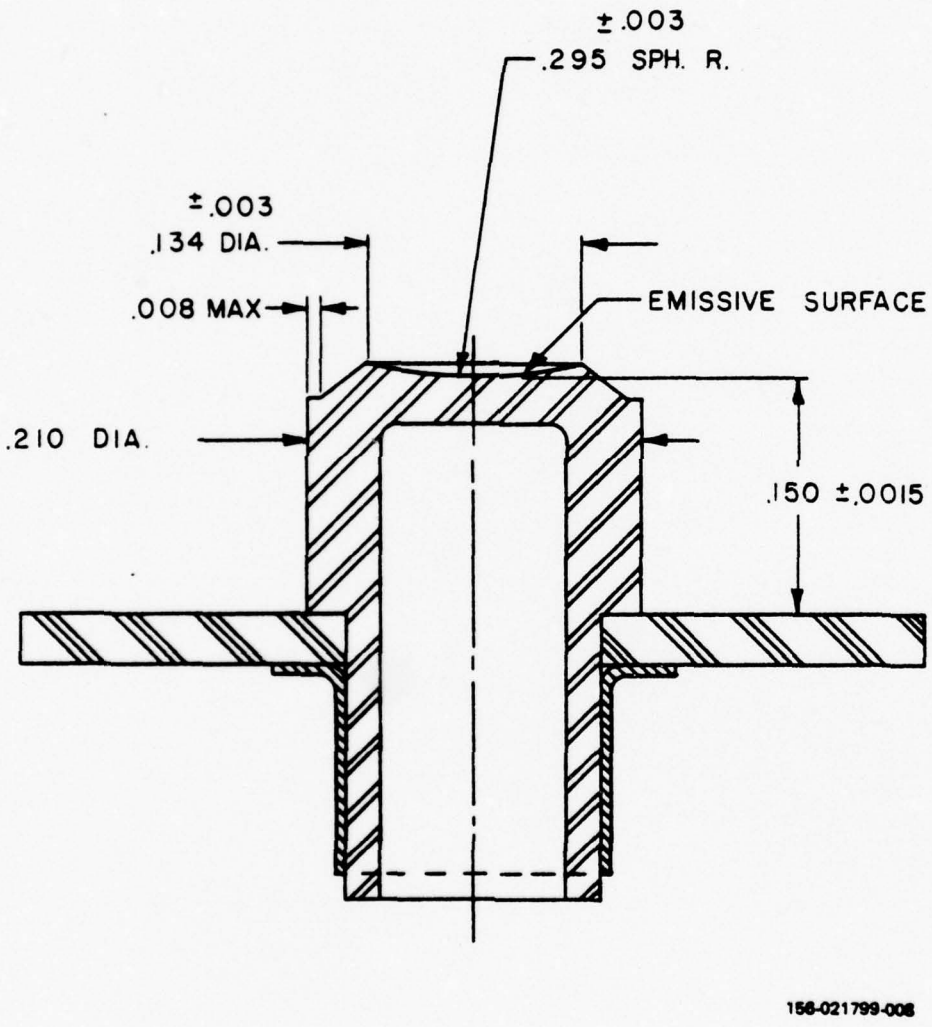

Figure 9. Sintered Nickel Cathode Structure.

absorption capacity than the ST101; however, they are much more expensive ($6 - $35.75 each). The ST101 getter costs $0.40 for quantities above 5000 and $0.51 for small quantities.

3.5 Header

Three different kinds of headers were considered. In Figure 10a, the base is made of ceramic with 3 or 4 feed-throughs and a pumping tube. In Figure 10b, the base is made of metal and the feed-throughs are ceramic with metallic pieces, and Figure 10c shows pins insulated by Hybralox. Hybralox is a hybrid alumina-glass and can be baked-out above 600°C. Figure 11 shows a dummy header. Twenty-seven feed-throughs made by Elecpac, Inc., of Cary, Illinois, were made without leaks. Twelve feed-throughs were fired several times at 600°C without a leak occurring. High voltage arcing occurred at 9 kV.

Table X shows the cost per header for various quantities, and also the cost of the required tooling. Only the Hybralox header seems to be acceptable.

Table X. Cost of Headers.

VENDOR	100	1000	5000	Tooling
Alberlox (Pins)	$15-20	*	$ 5.85	$ 985
Ceramaseal (Pins)	25.81	9.63	7.93	6500
RW-Product (Feedthroughs Only)	(24)	(19.50)	(17.86)	-
Elecpac (Hybralox)	12	2.00	1.75	950

* Not Quoted

3.6 Barrel

To obtain low crossed fields in the PPM stack, the concentricity (TIR) between the PPM stack and the beam center is an important factor. Table XI shows the cost of the barrel for different values of TIR (twice the eccentricity). As can be seen, the cost is much greater for low TIR.

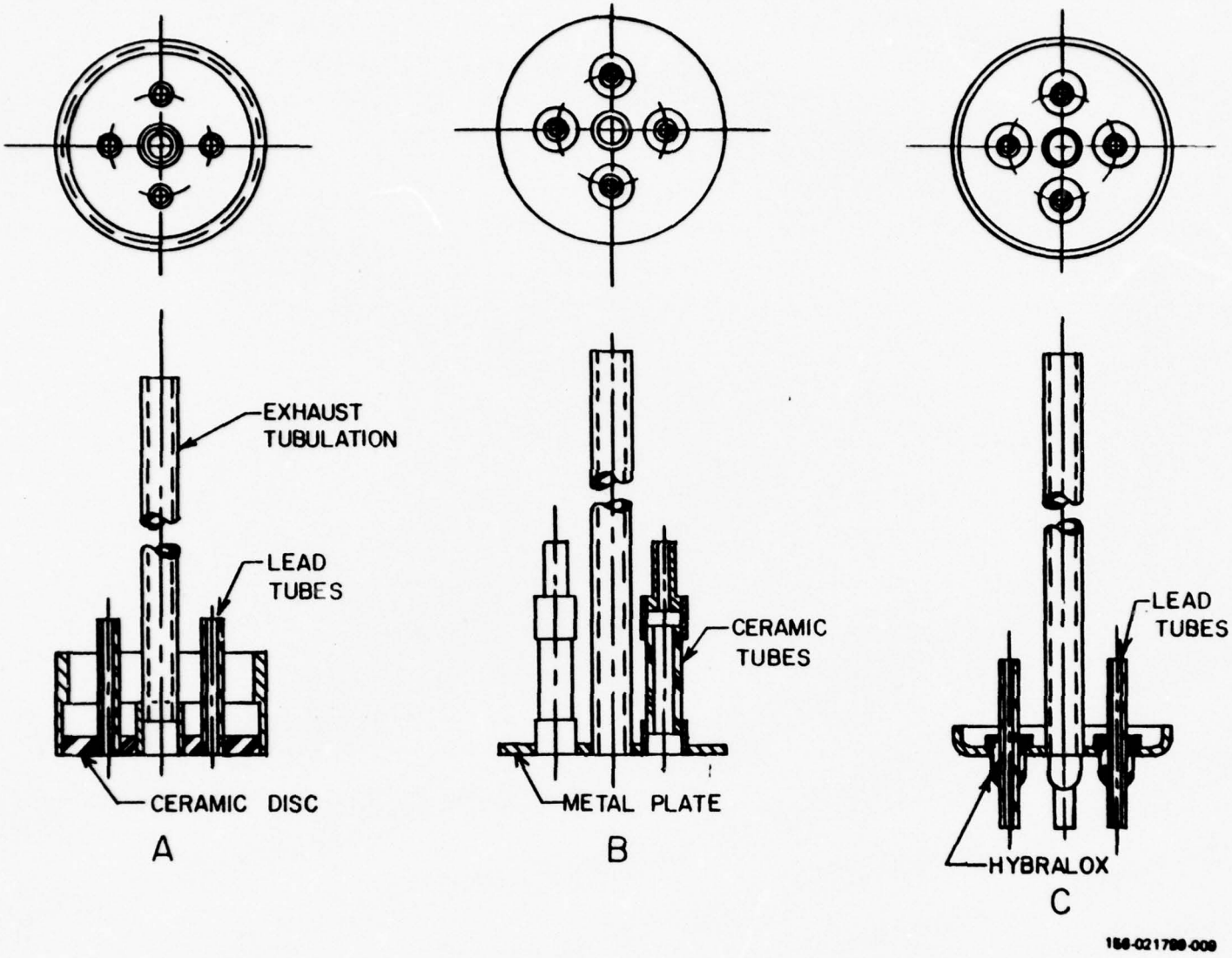

Figure 10. Headers.

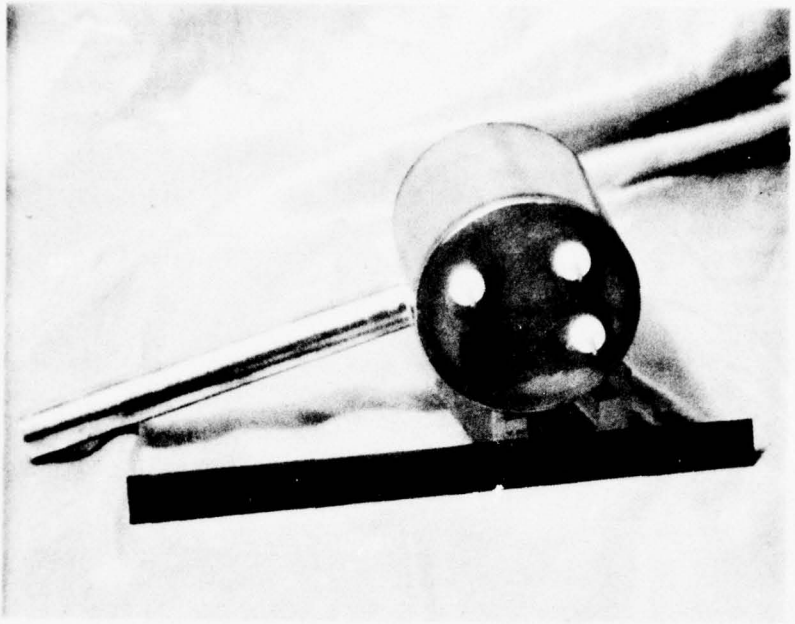

Fig.11 FEEDTHROUGH BY HYBRALOX

Table XI. Cost of Barrel.

	TIR	1	100	1000	5000
Monel	0.0025"	*	$ 3.10	*	$ 1.30
Molybdenum	0.0005"	*	$55.00	*	$22.00
Monel	0.0005"	$390	*	*	*

* Not Quoted

3.7 PPM Stack

Table XII shows the cost of the PPM stack. The tolerances of the thickness of the magnets is ±0.001", which should be sufficient for low beam perturbation. The outer diameter tolerance is 0.020" - 0.030" and the inner diameter is 0.010" -0.015."

The pole pieces are relatively expensive because the inside diameters are honed for a slip fit on the barrel. This is important for obtaining low crossed fields.

As shown in Section 4, high random variation of the peak magnetic field is an important factor in causing poor beam transmission. To reduce variations of the magnetic field, an automatic calibrated magnet charger should be used. The price of this machine is between $3500 and $8500, depending on the required performance, on the speed of operation, and on the manufacturer.

Table XII. Cost of PPM Stack.

	100	1000	5000	Tooling
MAGNETS				
Ferrites	$0.25	$0.25	$0.25	-
(2 Suppliers)	0.42	0.40	0.38	-
Alnico 8	0.80	0.80	0.80	-
POLE PIECES				
Iron Disc	0.137	0.085	0.076	$450.00
Hub	0.050	0.046	0.040	$150.00
Honing	0.350	0.200	0.150	-
SPACER	0.030	0.020	0.015	-

3.8 Conclusion

Table XIII shows the cost breakdown of the components required for the proposed TWT if the lowest price for each item is used (the prices correspond to 1975 dollars). It is not possible to achieve the goal of a sales price of $250 for quantities below 1000 tubes. It seems not impossible to achieve the goal for quantities of 2000-5000. However, tooling and capital investment are not included in this price. The magnet charger should be considered as capital investment. If higher precision and closer tolerances are required on components, a drastic price increase can be expected, e.g., for a barrel with a TIR of 0.0005", the price is $22; for a TIR of 0.0025", it is only $1.30. If more expensive components are required, the net increase of the sales price of the tube will be higher than the cost increases of the component, as shown in the following:

Increase of sales price = increase of component cost:

x material handling	1.08
x G and A	1.23
x profit	1.15
= 1.53 x increase of component price	

Table XIII. Parts Costs.

	100	1000	5000	Tooling
Ceramics (3)	$12.00	$5.50	$2.75	-
Barrel	3.10	2.10	1.30	-
Beam Forming Electrode	1.29	.34	.19	$1640
Anode	.96	.28	.13	1144
PPM Stack				
Magnets (40)	10.00	10.00	10.00	-
Pole Pieces	21.40	13.40	10.50	600
Washer	1.20	.80	.60	-
Cathodes & Heater	7.30	1.84	1.48	3000
Header	12.00	2.00	1.75	950
Getter ST101	.51	.51	.40	-
	69.76	36.77	29.10	7334
Automatic Magnetization & Stabilization				$ 3500-8440
Total Parts Fabrication Tooling				≈ $ 12,000-14,000

4. NON-IDEAL ELECTRON BEAM

4.1 Introduction

The main effort of Phase I was the study of non-ideal forming of the beam. Not much previous work has been done on non-ideal beam forming, and there is almost nothing available in the literature.

All analyses have been made on axialally symmetric beams, and quantitative results which can be applied on new designs are quasi non-existent. Burgess and Conquest[8] calculated the influence of variations of the distance between the cathode and the beam forming electrode and of the distance between the cathode and the anode for the miniature TWT's. However, how the perveance, the position of minimum beam radius and its value, and radius change for different beam compression or current densities of the cathode have not been established as yet.

Hechtel[17] analyzed the non-laminar beam for microwave tubes and he measured the spherical aberration and the transverse velocity components. He defines a laminarity factor F as a ratio of the measured perveance to an apparent perveance, which corresponds to the observed beam spread in the beam minimum. The laminarity decreases rapidly with increasing beam convergence, and considerable variations exist from gun to gun with the same beam convergence. However, two main questions have to be considered:

(1) What is the influence of the beam laminarity on the beam transmission and the RF performance?

(2) What are the parameters which affect the laminarity?

It is only after these questions have been answered that the required tolerances can be determined.

In Section 3, the cost of the components for various tolerances have been given, and it is evident that the tighter the tolerances are, the higher the cost will be. However, the difference in price is not great for axial tolerances, but is extremely large for concentricity tolerances. In the following section, the non-ideal conditions of the PPM stack are discussed. Most of these results are theoretical, based on a modification of the paraxial flow equation assuming a laminar beam of circular cross section. For verification of the calculation and for experimental determination of other non-ideal parameters, a beam tester was built and is discussed in Section 5.

4.2 Non-Ideal PPM Focusing

4.2.1 Introduction

It is the purpose of the calculation methods presented here to evaluate departures from ideal PPM focusing simply and rapidly using a time-sharing computer. The results make it possible to determine many of the dimensional tolerances allowable in TWT construction and in the magnet stack. To reduce cost in a TWT, it is necessary to determine as well as possible what tolerances are acceptable in manufacture of parts and in assembly, and to eliminate or minimize the time-consuming, and therefore costly, procedure of "shimming" the magnet stack, or adjustment of the gun to overcome variations from the ideal.

Those departures from ideal conditions which have been dealt with by these methods of calculation include:

(1) Variation of magnetic field, for example by thermal effects, above and below the optimum value.
(2) Non-ideal beam diameter and convergence or divergence of the beam at the entrance to the PPM stack.
(3) Gun tilted with respect to the axis of the PPM stack.
(4) Random variations of fields from magnet to magnet.
(5) Beam injection eccentric to the axis of the PPM stack.

A general method of approaching this problem has been described by Harker[18] and is based on paraxial flow. He assumed that:

(1) The beam is axially symmetric.
(2) Current density and electron velocity are uniform over the beam cross section.
(3) The PPM stack is periodic and uniform.
(4) The emitted beam at the cathode may be either partially or totally shielded from the magnetic field.
(5) The beam is laminar.

The conditions listed above led to a differential equation which could be expressed in closed form. However, the solution can not be expressed in closed form. Harker[18] used an analog computer to achieve some numerical results. The differential equation is:

$$\sigma'' + a\sigma f^2 - \frac{2\kappa a}{\sigma^3} - \frac{\mathcal{P}}{\sigma} = 0 \qquad (1)$$

In the above:

σ = normalized beam radius r/r_o
r = radius to outside of beam
r_o = radius to outside of beam at beam injection
X = normalized distance along the z-axis = $2\pi z/L$
L = magnet period
a = lens strength parameter = $1/4\ (L/\lambda_H)^2$
λ_H = cyclotron wavelength = $2\pi \dot{z}/\eta B$
η = charge-to-mass ratio of an electron (magnitude)
$\dot{z}$ = electron velocity in the axial direction, assumed uniform
$\hat{B}$ = RMS value of the periodic magnetic field
$\mathcal{P}$ = space charge parameter = $1/2\ (L/\lambda p)^2$
λ_p = plasma wavelength = $2\pi \dot{z}/\omega_p$
ω_p = plasma frequency = $\sqrt{\eta \rho/\epsilon_o}$
ρ = charge density in the beam, assumed uniform
ϵ_o = permittivity of space
κ = cathode shielding factor = $r_c^4\ B_c^2 / 2\hat{B}^2\ r_o^4$
f^2 = magnetic field distribution function
r_c = radius at the outside of the emitter
B_c = magnetic field perpendicular to the emitter surface

The prime denotes d/dX, where X is the axial distance normalized with respect to the period of the magnet. The notations are those used by Kirstein, Kino and Waters.[12]

This differential equation is very easily solved by numerical integration using digital computer equipment, with large numbers of solutions possible at low cost. We have used Equation (1) as it stands to determine results for all but one of the non-ideal conditions listed at the beginning of this section. The last of these, the beam eccentricity with respect to the axis of the PPM stack, requires modification of the expression to take into account radial and circumferential components of magnetic field which exist relative to the frame of reference of the beam (see Appendix I). The conditions applied to the equation to reach an appropriate solution are as follows:

(1) Magnetic field: variation of a
(2) Non-ideal beam diameter and convergence/divergence: variation of initial conditions.
(3) Gun tilt: variation of initial conditions.
(4) Random variation of fields: random variation of a from half-period to half-period (i.e., from magnet to magnet).
(5) Beam eccentric to PPM axis: modify equation per Appendix I.

Any of these conditions may be considered separately or simultaneously in any combination.

An assumption implicit in all of the calculations described here is the definition of the point of entry to the PPM stack. There is always some magnetic field present extending from the stack toward the gun, and there may or may not be a significant field normal to the emitter. Going toward the PPM stack from the gun, the beam encounters a montonically increasing magnetic field which reaches a maximum approximately at the mid-point of the first magnet gap. This point is defined as the entrance to the PPM stack, where $z = 0$, in all calculations discussed here. It is assumed that beyond this point, the magnetic field is described by a cosine function, and then in Equation (1) f^2 becomes equal to $2 \cos^2 X$.

The ideal conditions for injection are considered to be:

(1) At $z = 0$, the beam is neither converging nor diverging; i.e., $dr/dt = 0$ or $d\sigma/dX = \sigma' = 0$.

(2) The relationship between $\mathscr{P}$ and a is such that minimum ripple is produced. The value of $\mathscr{P}$ tends to be slightly less than a. Some representative optimum combinations are:

a :	0.01	0.05	0.10	0.20	0.30
$\mathscr{P}$:	0.00996	0.0491	0.0959	0.184	0.263

As a first step in verifying the computer program, the conditions for which Harker published results were used. All of his results were duplicated.

The calculations reported here are all based on a shielded gun, so that $B_c = 0$ and $\kappa = 0$. However, all of the computer programs written allow for non-zero values of κ.

4.2.2 Comparison with Alternative Method of PPM Focusing Calculation

It is of interest to compare the results achieved by paraxial beam calculations with those based on an entirely different approach. A calculation was made by McGregor of Shared Applications, Inc. (SAI), for the purpose of estimating variations of beam ripple in consequence of $\pm 10\%$ thermal drift of the magnetic field with ferrite magnets. (See Second Quarterly Progress Report on this project.)

The beam input to the PPM stack comes from the output of an electron gun for which SAI already had a program set up. The beam trajectories in the PPM stack were calculated by an iterative process using Lagrange methods and solving Poisson's equation. The beam was simulated by five concentric electron layers, with conditions at the input to the PPM stack ($z = 0$) matched to the result of the gun program. The beam is slightly convergent at this point. The program was in fact a TWT calculation program, with RF power set to zero in this case. Results for one case are shown in Figure 12 for the five layers (solid lines).

For comparison, the results of paraxial beam calculations have been superimposed on the SAI results in Figure 12, and are shown by the broken line. This represents non-optimum radius and beam convergence at the entrance to the stack. To match the SAI entrance conditions $\sigma' = (d\sigma/dX)$ is -0.077, $a = 0.195$, and $\mathscr{P} = 0.0338$, so that the beam is strongly over-focused. It was the original intent in this design to confine the beam with an RMS magnetic field twice the Brillouin value.

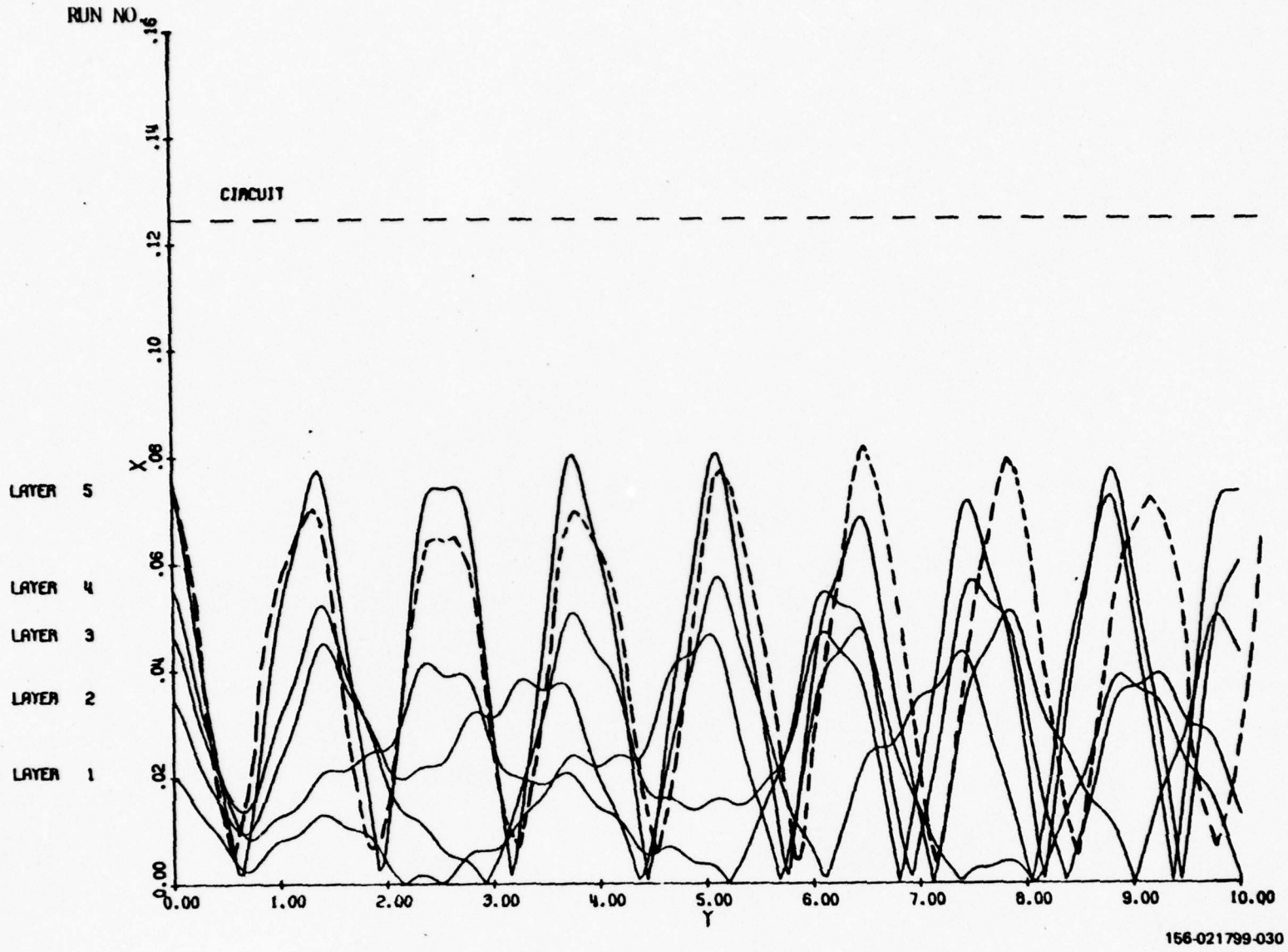

Figure 12. Comparison of Paraxial Beam Calculation with Five-Layer Beam Calculations (Stevens SAI).

(The Brillouin value corresponds to $a \approx \mathscr{P}$; at twice the Brillouin value, $a = 4\mathscr{P}$.) The conditions at the entrance to the PPM stack were more rigorously matched to the beam emerging from the gun in the SAI method than was possible by our simpler method, and SAI takes into account radial space-charge effects upon axial beam velocity. Comparison of the general shapes of the trajectories shows excellent agreement in principle.

4.2.3 Magnetic Field Variations

Figure 13 shows the trajectory patterns obtained with a $\pm$10% variation in magnetic field, assuming ideal beam injection and fully shielded cathode. This amount of field variation corresponds to the extremes foreseen as the result of thermal drift. Assuming $\mathscr{P} = 0.0959$, the optimum value for $a = 0.1$ ($= a_o$), trajectories were calculated for $a = 0.081$, 0.1, and 0.121. The quantities plotted represent normalized radius at the outside of the beam. Figure 14 summarizes the results obtained for maximum and minimum beam diameters with $\pm$10% magnetic field variation for several values of the space charge parameter $\mathscr{P}$. The uppermost curve shows the maxima of σ for low magnetic field, the lowest curve shows the minima of σ for high magnetic field, and the shaded area shows the range of excursion of the outside of the beam for optimum magnetic field. The curve for $a = 0.1$ represents the condition for injection with optimum beam diameter, and the others represent injection with non-optimum beam diameter.

Another view of these calculations is related to optimum beam diameter for the various values of magnetic fields. For minimum ripple when $a = 0.081$, $\mathscr{P}$ should be 0.078 instead of 0.0959; since $\mathscr{P}$ is proportional to I/r_o^2, then the optimum beam radius at injection in Figure 13 would correspond to $\sigma = 1.11$, and this value would correspond to the outermost excursion of beam radius. Similarly, for minimum ripple when $a = 0.121$, $\mathscr{P}$ should be 0.115, and the optimum beam radius at injection would correspond to $\sigma = 0.913$.

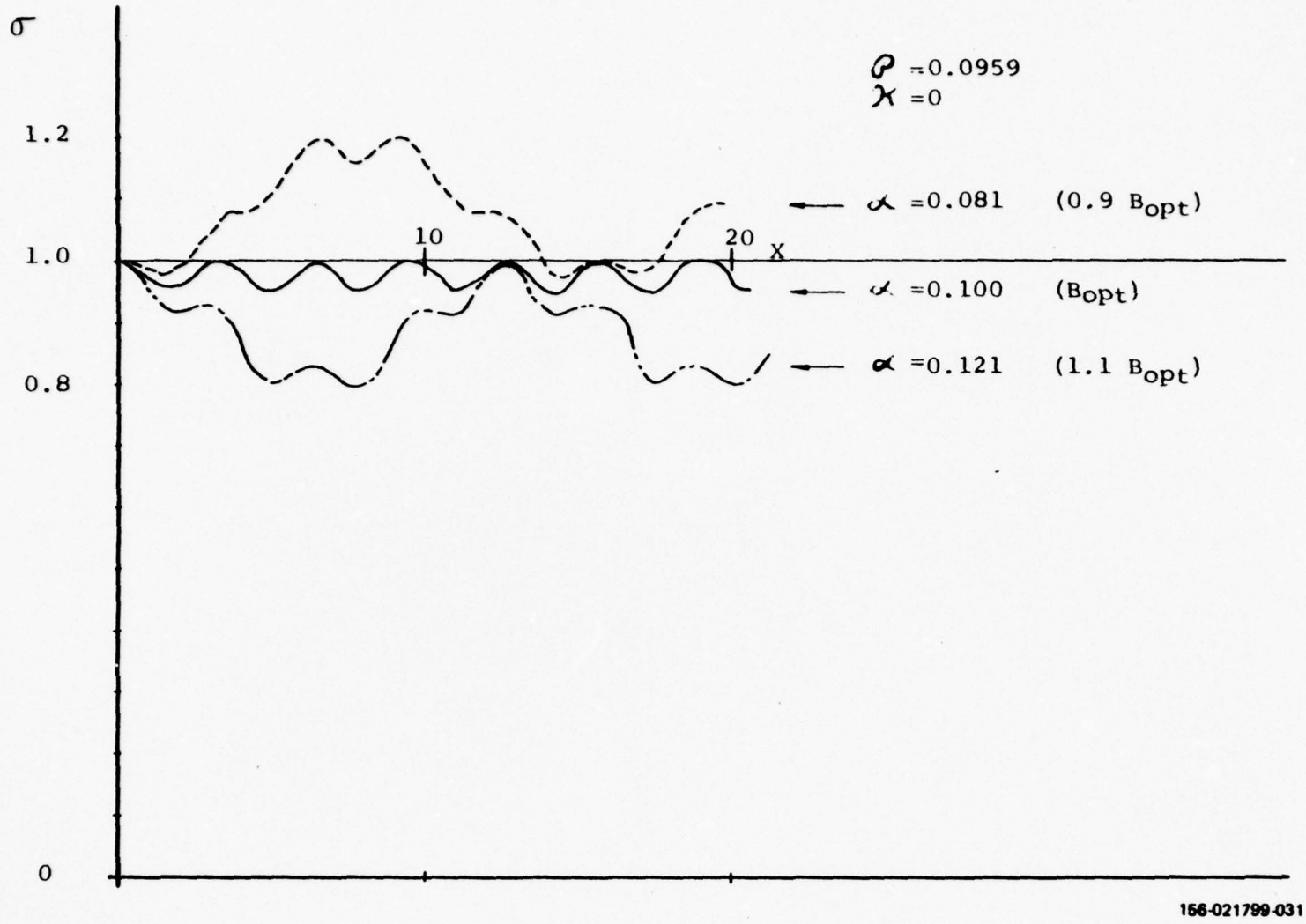

Figure 13. Trajectories for Outside Edge of Beam as Magnetic Field Varies from Optimum Value.

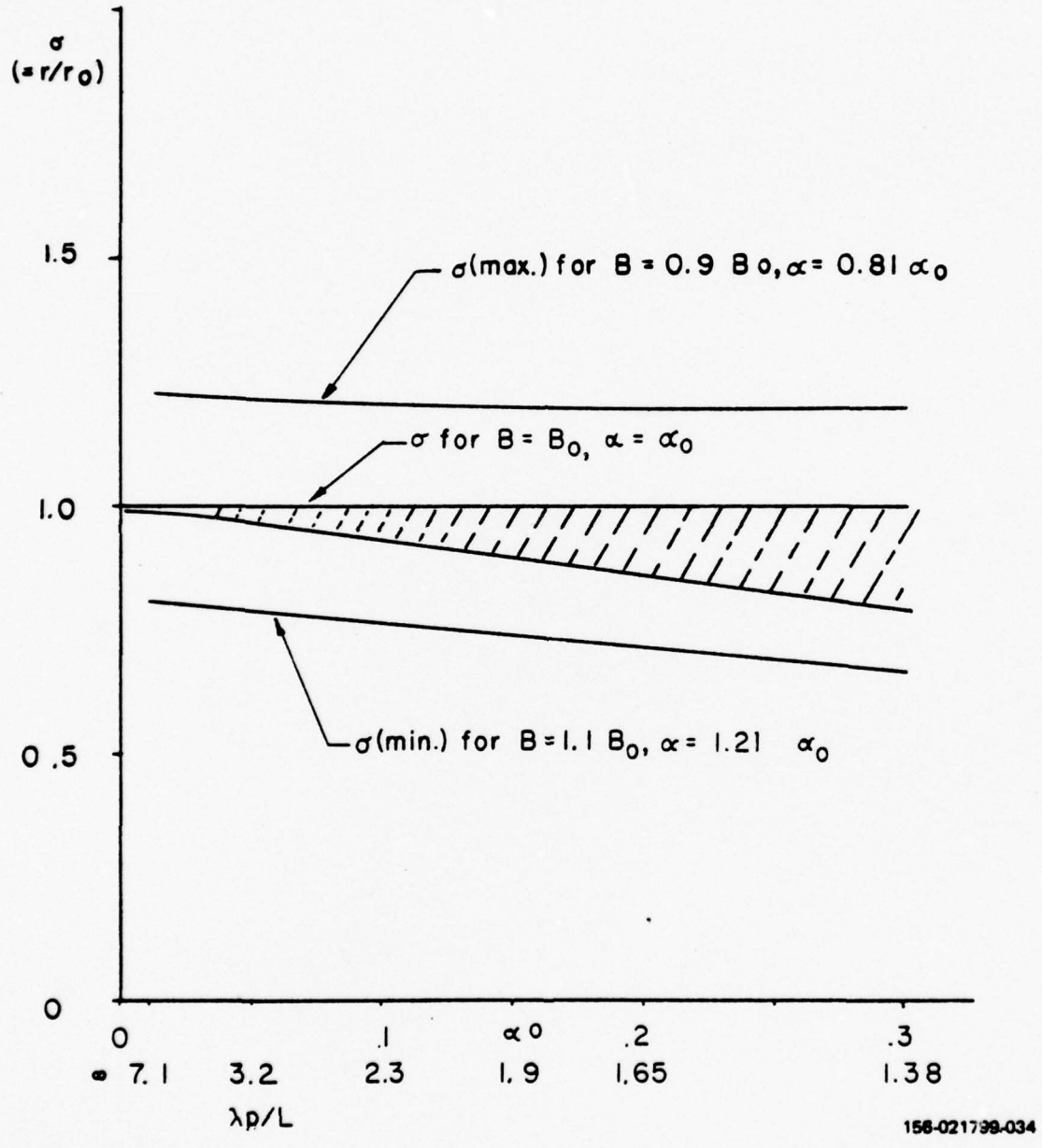

Figure 14. Extremes of Beam Excursion for ±10% Thermal Drift of PPM Magnetic Field. B_0 = Optimum Magnetic Field

4.2.4 Beam Convergence/Divergence

The effect of a diverging or converging beam at the entrance of the PPM stack is quite readily taken into account by setting the initial conditions appropriately. Figure 15 shows a plot of the outer edges of the beam for the conditions of $\mathscr{P}$= 0.0959 (λ_p/L = 2.28), a = 0.10 (optimum) and the initial values of $d\sigma/dX$ are equal to $\pm$0.0876. It is observed here, and for other cases as well, that for the same initial magnitude of $d\sigma/dX$, the maxima and minima of the beam edge excursions are equal for either the diverging or converging case. To compare the effects of different magnet periods, it is necessary to introduce a new reduced variable for the rate of convergence or divergence which does not depend on the magnet period. We have chosen to normalize with respect to plasma wavelength instead. The new reduced variable in the axial direction is defined according to:

$$W = 2\pi z/\lambda_p$$

Based on this reduced variable, $d\sigma/dW = \pm 0.20$ in Figure 16. In Figure 16 are plotted the maximum and minimum excursions of σ for a variety of conditions. The effects of beam convergence or divergence at the entry to the PPM stack are only slightly sensitive to magnet period when a is less than 0.2.

4.2.5 Beam Injection at an Angle (Tilt)

The effects of a gun slightly tilted are calculated by using one value of σ' on one side of the beam at the entrance to the stack, and the negative of that value on the other side. Figure 17 shows the effect of beam injection at angles of 1^o and 3^o. The upper curves and the lower curves show respectively the opposite sides of the same beam. The maximum excursion of the outside of the beam as a function of the angle of injection is shown in Figure 18 for three different values of beam perveance. Although the maximum excursion appears less for greater perveance, the differences between the curves is accounted for by the fact that the higher perveance beam is relatively larger to start with; i.e., for the same charge density, the perveance is proportional to the beam radius. The curves shown here are for a = 0.15 and λ_p/L = 1.9. The results for other values of a (and corresponding optimum λ_p/L) are not significantly different from these.

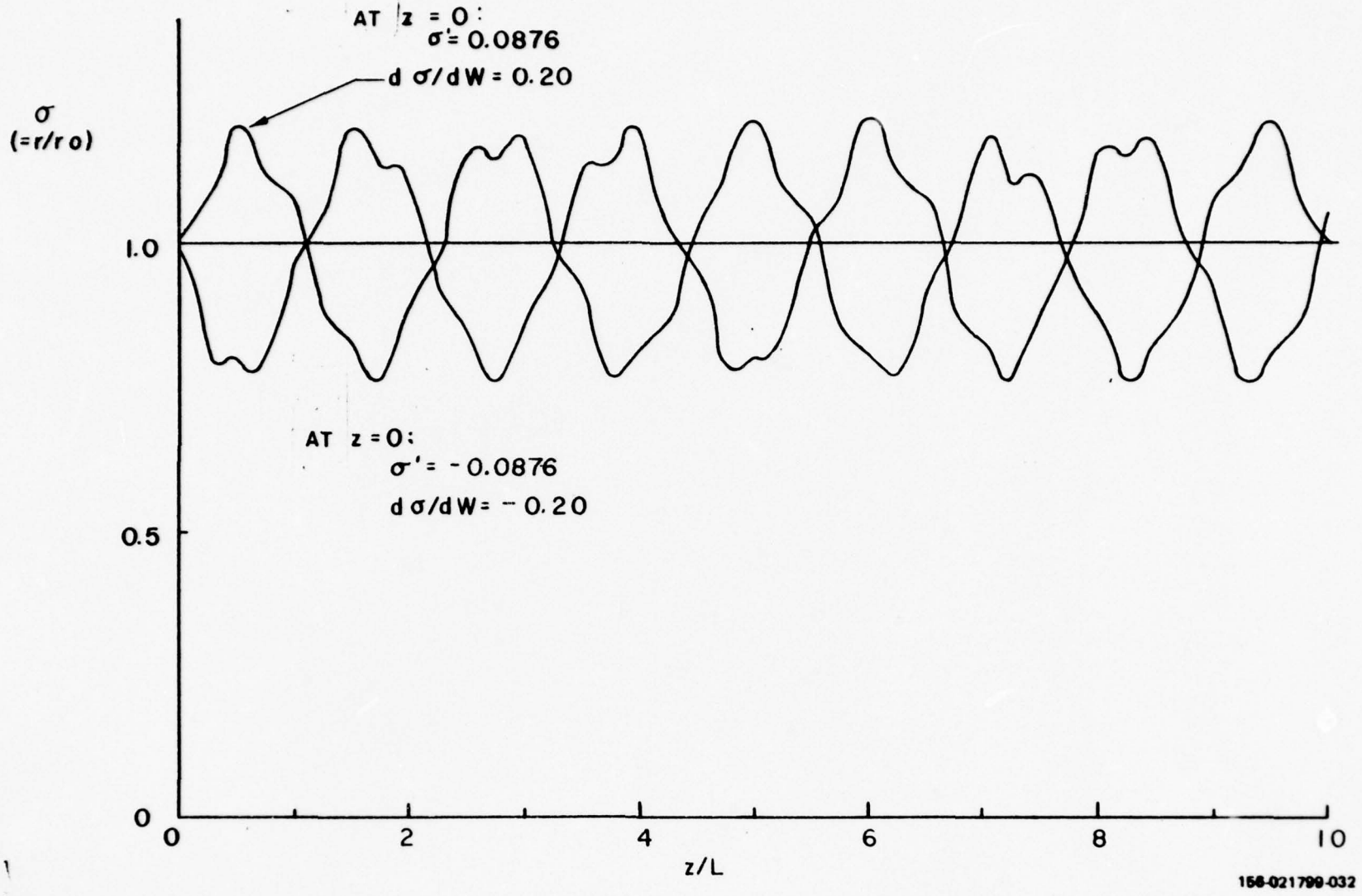

Figure 15. Excursions of Outside Edge at Beam Converging/Diverging at Entrance to PPM Stack.

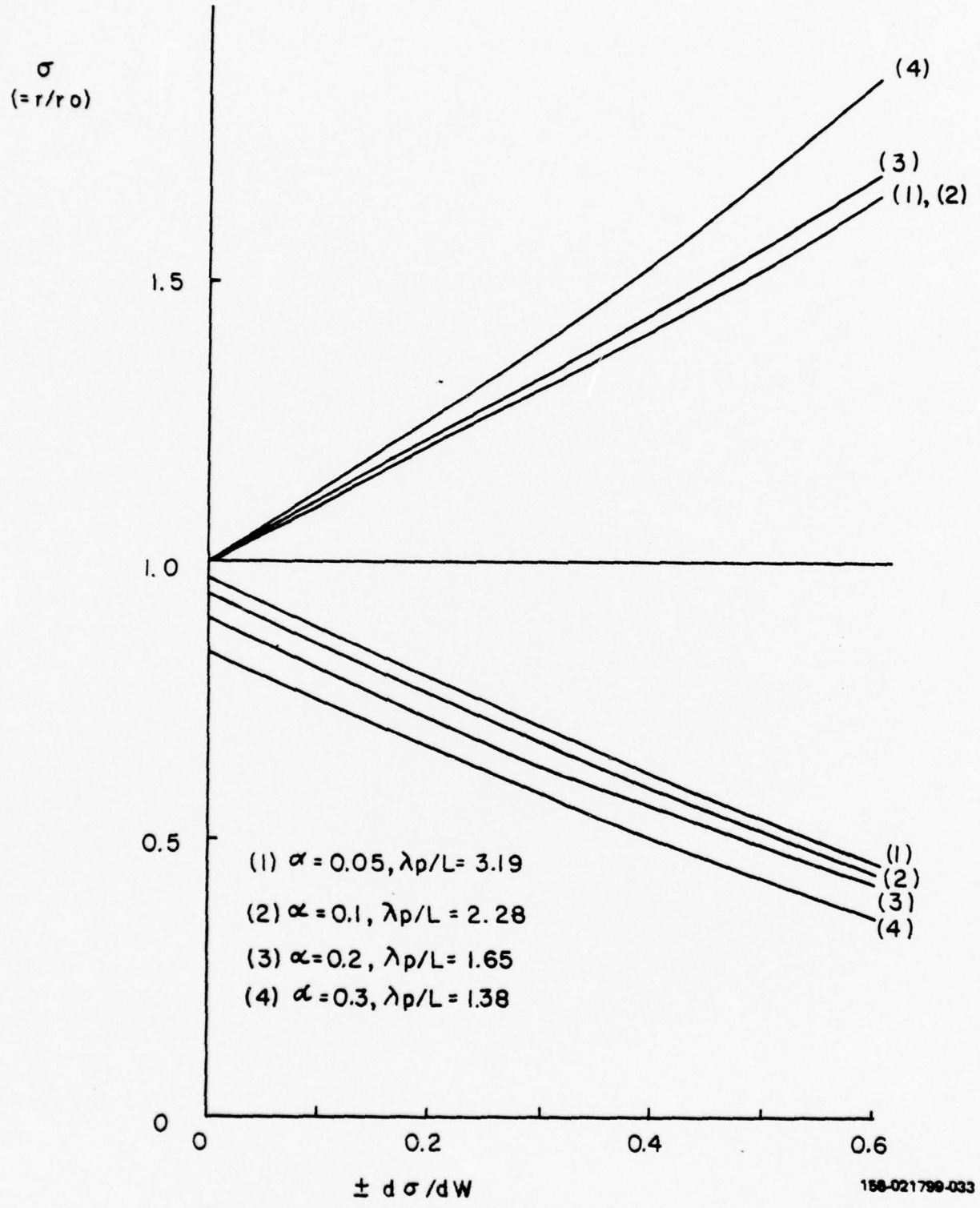

Figure 16. Effect of Convergence/Divergence at Entry to PPM Stack Upon Beam Excursions.

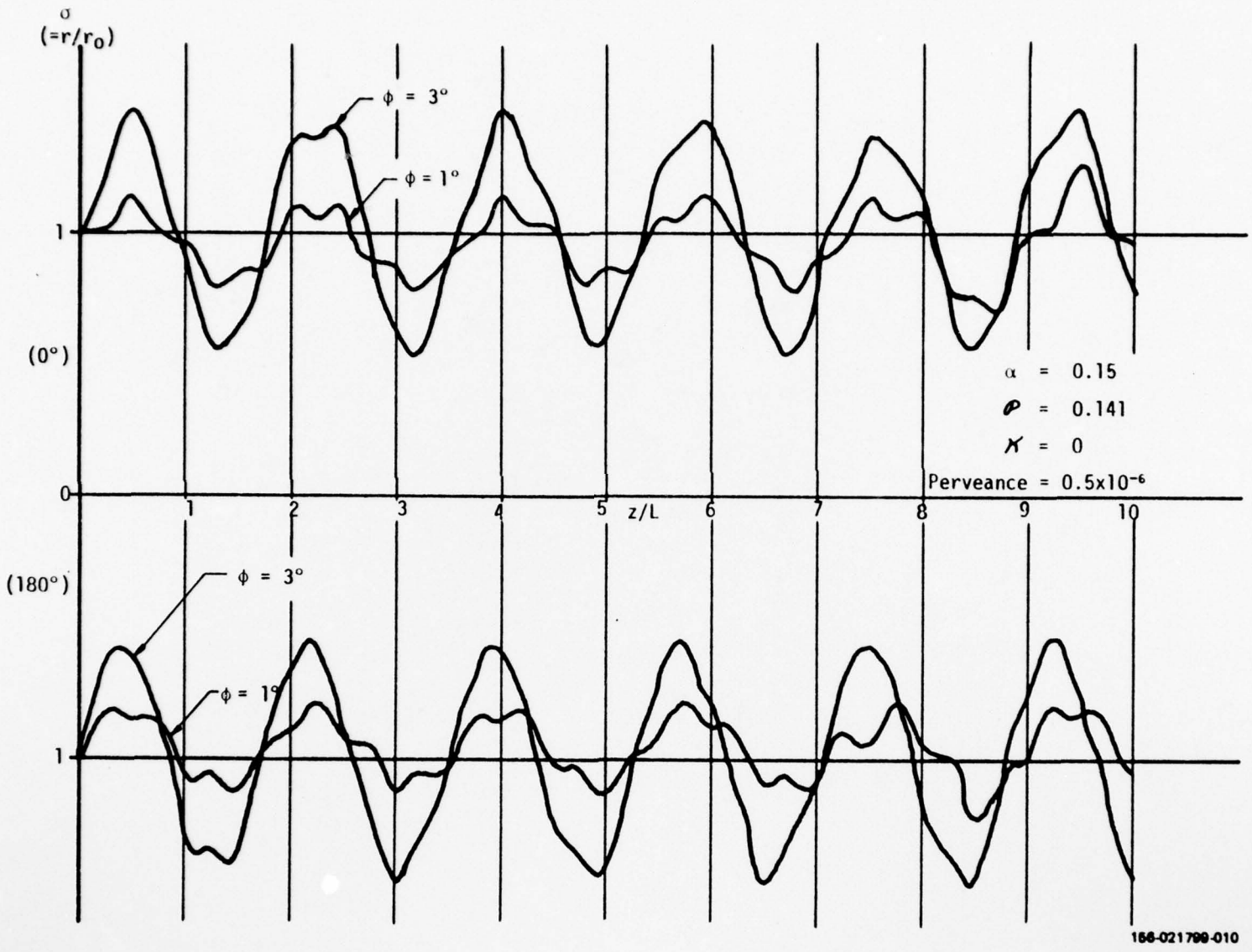

Figure 17. Beam Trajectories in PPM TWT for Injection at Angle ϕ.

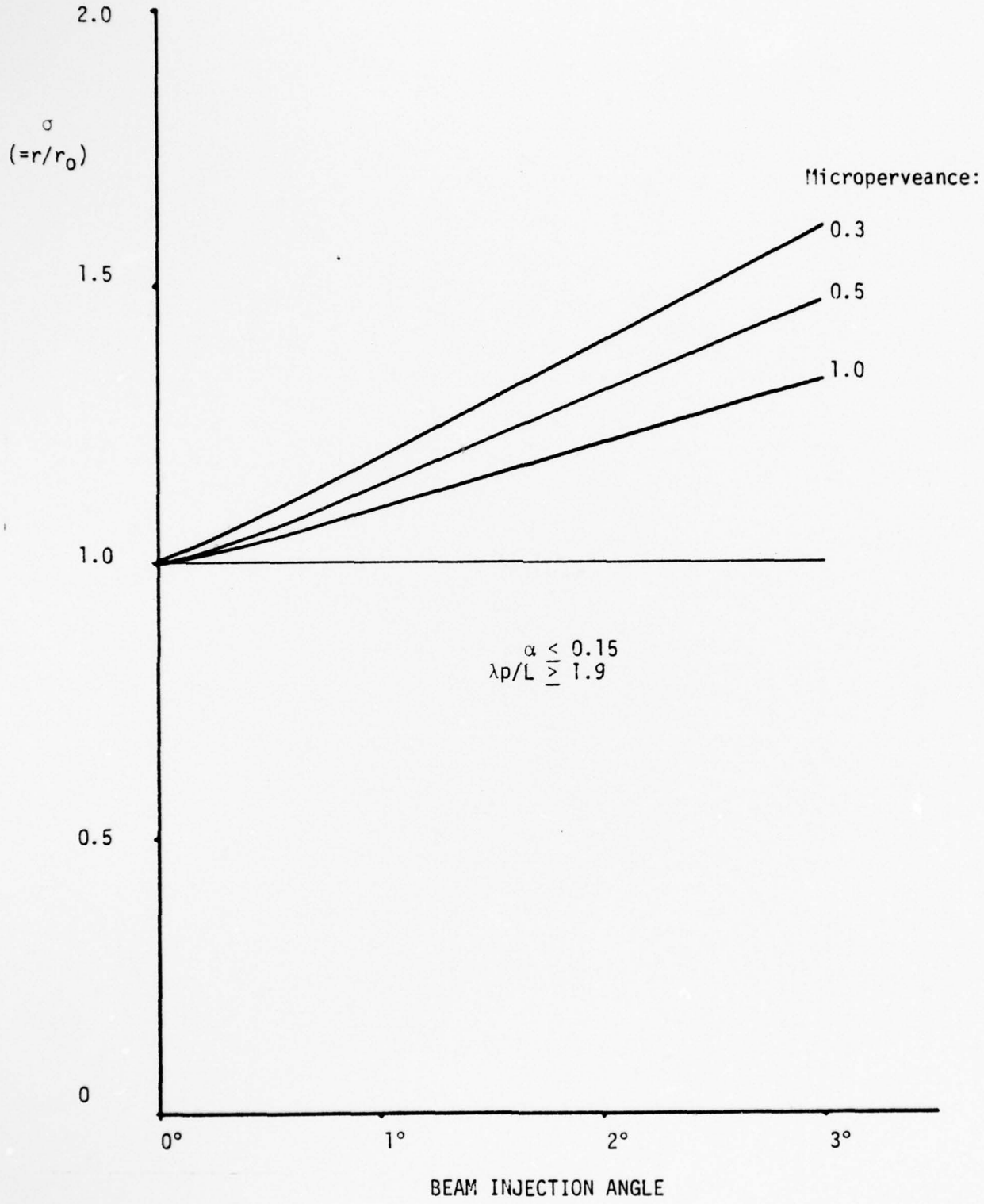

Figure 18. Maximum Peaks of Beam Excursion for Beam Injected at an Angle.

4.2.6 Random Variations of Fields

Figure 19 shows three curves of beam trajectories in which the magnetic field varies randomly in a range of $\pm$ 5% from magnet to magnet, each curve representing a different set of random variations. The distribution of random values was uniform over the $\pm$ 5% range. The value of $a_0 = 0.15$ corresponds to the average magnetic field, and the broken line corresponds to the trajectories for the ideal case of uniform magnetic field. The pattern shown in Figure 19 appears to indicate a gradually increasing divergence of the beam. Accordingly, calculations were carried out for a length of 25 magnet periods, a length more representative of a useful traveling-wave tube. Figure 20 shows the maximum peaks of the outside beam radius over 25 periods for random variations of magnetic fields uniformly distributed over a $\pm$ 5% range. There are five different curves, each representing a different set of random numbers. The following parameters were assumed:

Lens-strength parameter (mean) $= a_0 = 0.100$
Space-charge parameter = $\mathscr{P} = 0.0959$; $\lambda_p/L = 2.28$

To study the beam divergence pattern further, curve No. 1 of Figure 21 was extended to 70 magnet periods. The results are shown in Figure 21. An effort was made to find a mathematical pattern which best fit these points. Of the several functions tried, the best fit was obtained using a curve of the form $y = ax^b$, where $y = \sigma - 1$. Fitting the 24 points plotted in Figure 21 by least-squares method led to:

$a = 0.0865$
$b = 0.520$

The latter curve is also plotted in Figure 21. These results show that the beam diverges approximately in proportion to the square root of the distance it travels along its length. This is the kind of result which might be expected intuitively.

Based on these results, a random variation in magnetic field values of $\pm$ 5% is clearly not acceptable for a useful beam. The calculations were repeated for $\pm$ 3%, $\pm$ 1.5%, and $\pm$1% for 10 sets of random numbers in each case, and for several combinations of a_0 and $\mathscr{P}$. The appearance of the trajectory curves does not differ

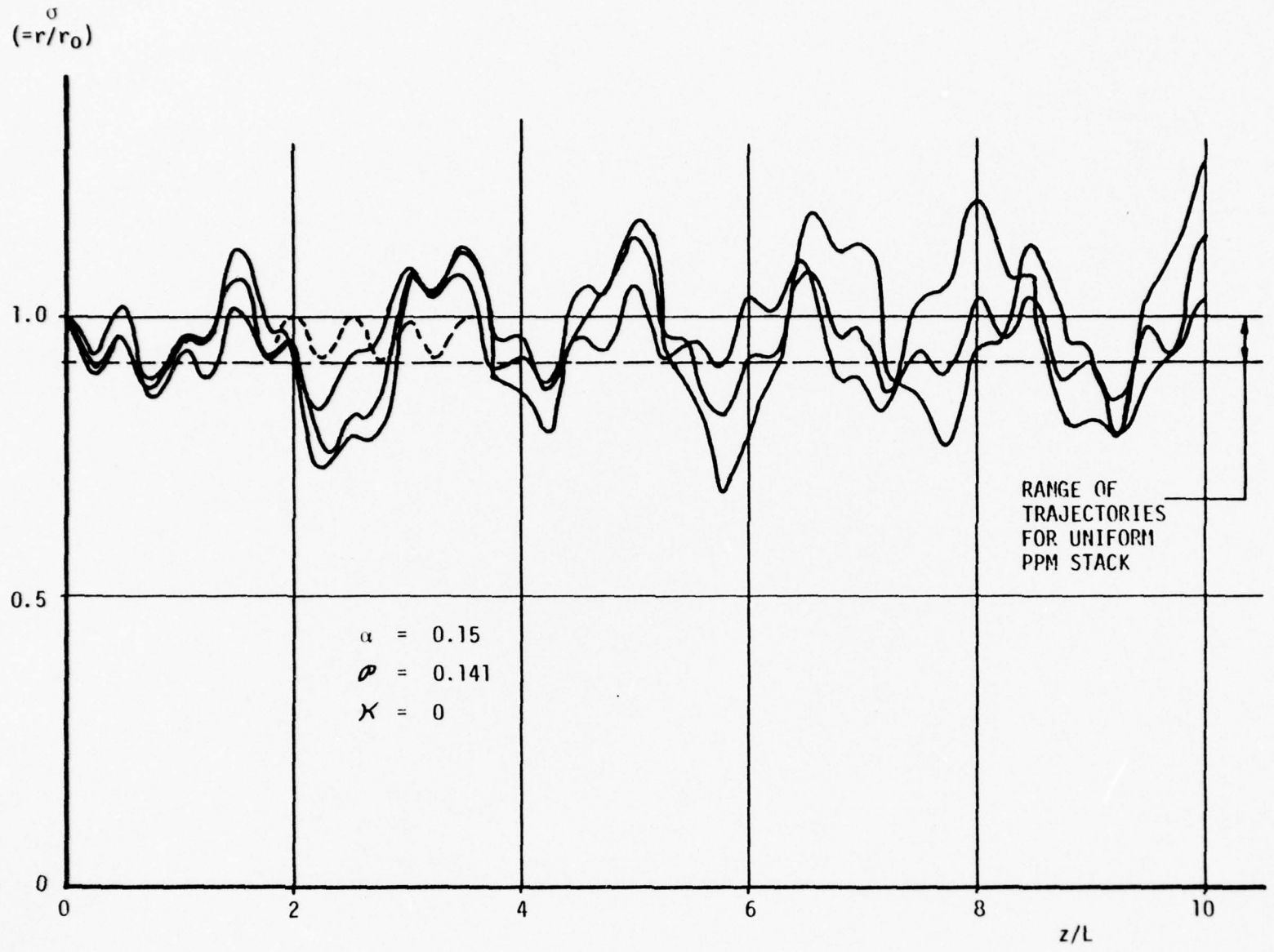

156-021799-036

Figure 19. Trajectories for ±5% Random Variation of Magnets.

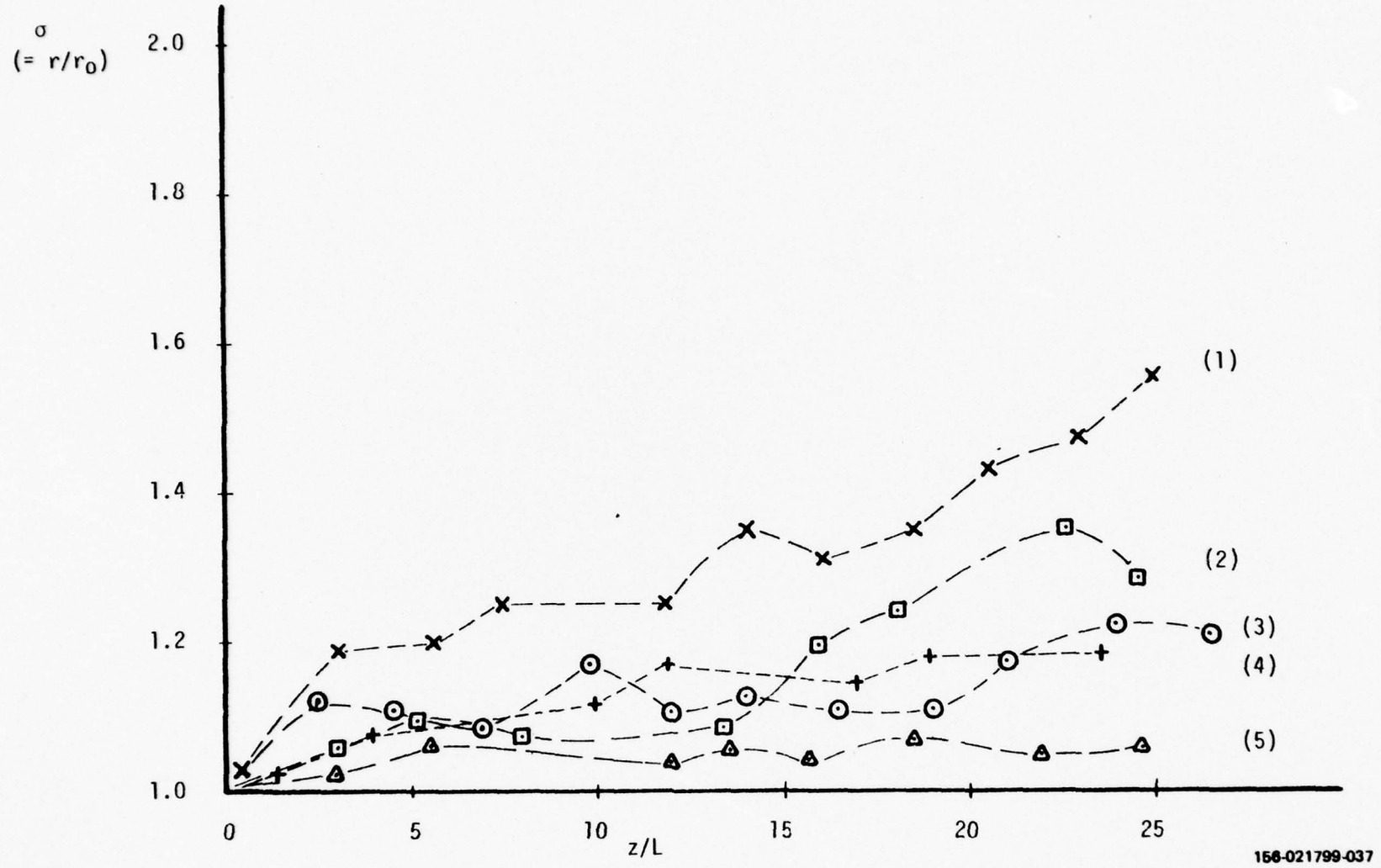

Figure 20. Maximum Peaks of Trajectories for Random Variation of Periodic Magnetic Field by ±5%: a(mean) = 0.1, $\mathscr{P}$ = 0.0959. Five Different Sets of Random Numbers are Shown.

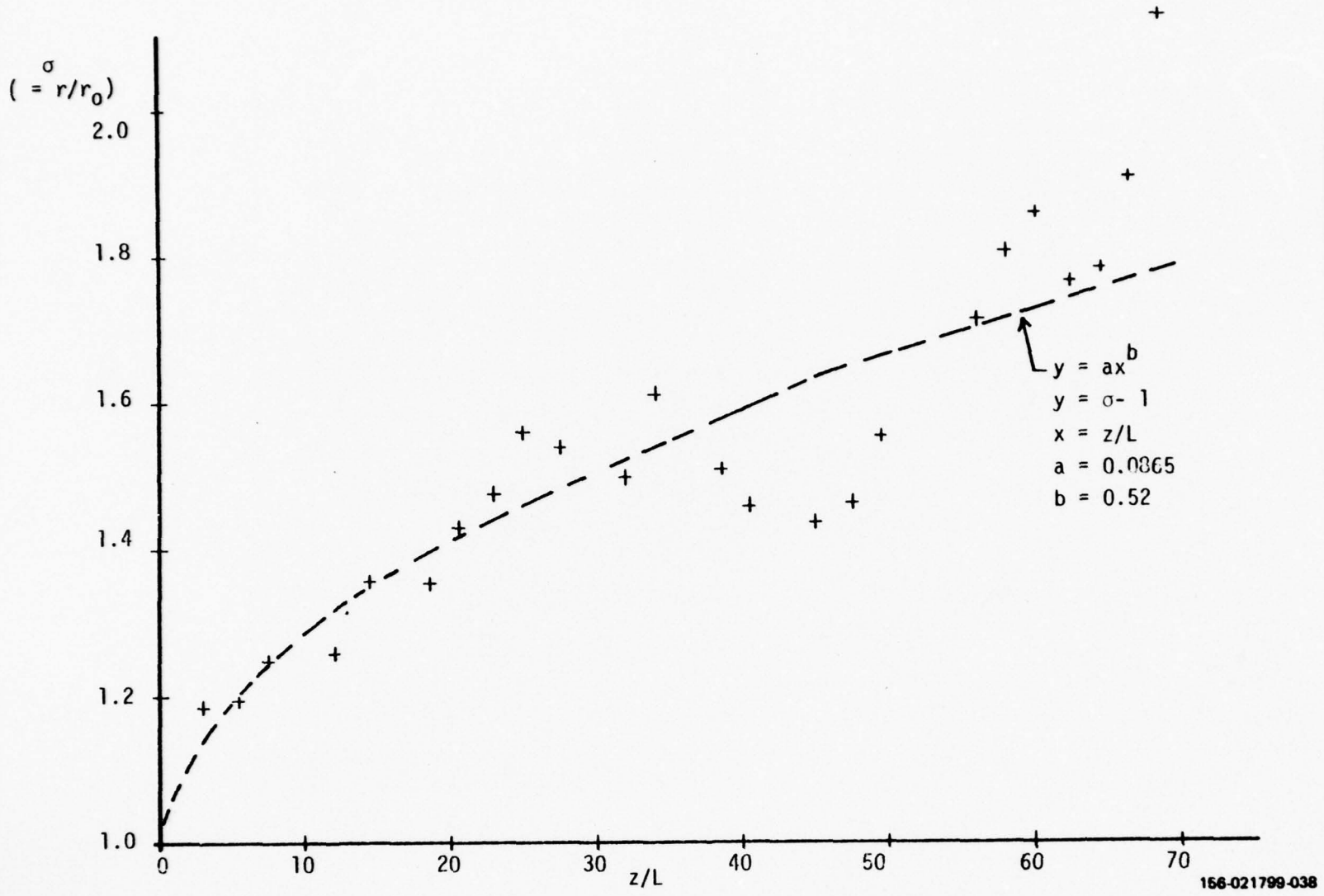

Figure 21. Maximum Peaks of Trajectory for Random Variation of Periodic Magnetic Field by +5%: a (mean) = 0.1, $\mathscr{P}$ = 0.0959. "Best Fit" Mathematical Expression is also shown. (Cf Curve No. 1 of Figure 20)

significantly from Figure 19, except the divergence of the beam is less. Results are summarized in Table XIV, in each case over a length of 12 plasma wavelengths for 10 different runs.

Table XIV. Effect of Random Magnetic Fields.

Magnetic Field Random Variation	Maximum Excursion of a_o = 0.01	0.05	0.10	0.15	0.20	0.30
	λ_p/L = 7.09	3.19	2.28	1.88	1.65	1.38
± 1%	1.050	1.087	1.090	1.137	1.143	1.111
± 1.5%	1.060	1.124	1.153	1.177	1.138	1.137
± 3%	1.171	1.209	1.245	1.431	1.372	1.513
± 5%	1.174	1.568	1.470	1.622	1.489	1.852

The maximum deviation appears to vary approximately in linear fashion with the amount of magnetic field variation. The trend appears to be toward greater deviation with increasing $_o$, but from $_o$ = 0.05 to $_o$ = 0.2, the range of greatest practical interest, there is little significance to the variations of maximum with $_o$. In general, these calculations suggest that random magnetic field variations should be limited to ± 1% (or ± 1.5% at the most) to avoid a large contribution to beam scalloping. Uniformity of ± 1% or better is within the state of the art for conventional magnets (e.g., ferrites, Alnico), and uniformity of ± 1.7% for samarium-cobalt magnets appears to be the limit of the present state of the art.

Similar calculations were made in which the magnet thickness and, therefore, the magnetic half-period, was varied in random fashion. If it is assumed that each magnet is stabilized to produce the same magnetic field in the gap, small variations in pitch were found to have negligible effects. If instead, the variations in thickness generate corresponding variations in magnetic field, then the results are substantially equivalent to those described above for variations from magnet to magnet with constant pitch.

Some calculations for random values of magnets were made previously by Minakovic[19], using the same method of analysis described here. His calculations were limited to 15 half-periods. The greater computing power which is now readily available makes possible the much more extensive set of results we have presented here.

4.2.7 Off-Center Beam Injection

When the beam is injected off center, it is subjected to significant periodic crossed magnetic field components, B_r and B_θ. Figure 22 shows three trajectories for a beam injected off axis by an amount δ, indicating how significant an eccentricity of the magnetic field with respect to the beam may be. The results of calculations are summarized in Figure 23, where the maximum deviation of the outside of the beam as a function of relative eccentricity, δ/r_o, is plotted for a number of beam conditions. If a is less than 0.2, the amount of excursion is relatively insensitive to the value of a. If a is greater than 0.3, the beam becomes unstable very rapidly, even for small values of δ/r_o. The conclusion to be drawn is that it is most desirable to keep δ/r_o no greater than 0.1.

4.2.8 Summary and Conclusions

This kind of analysis may be extended to take into account magnetic field patterns other than simple sinusoids. The random distribution of fields may be made gaussian rather than linear. The effect of RF field on trajectories is obviously beyond the scope of this method. Examination of the detailed results has shown that a more sophisticated treatment of the effect of space charge (the term $\mathscr{P}/\sigma$) is desirable when the beam is off the magnetic axis.

The results clearly provide some very useful indications as to what conditions and tolerances are acceptable in designing a PPM focusing system which will require little or no adjustment at test. For example, the summaries of calculations of magnetic field variations, of beam tilted when injected, of random variations of magnetic field, and of converging or diverging beam at entrance to the PPM stack, all show that for a value of a less than 0.15, there is little to be gained by reducing a further, or in other words, further reducing the magnet period.

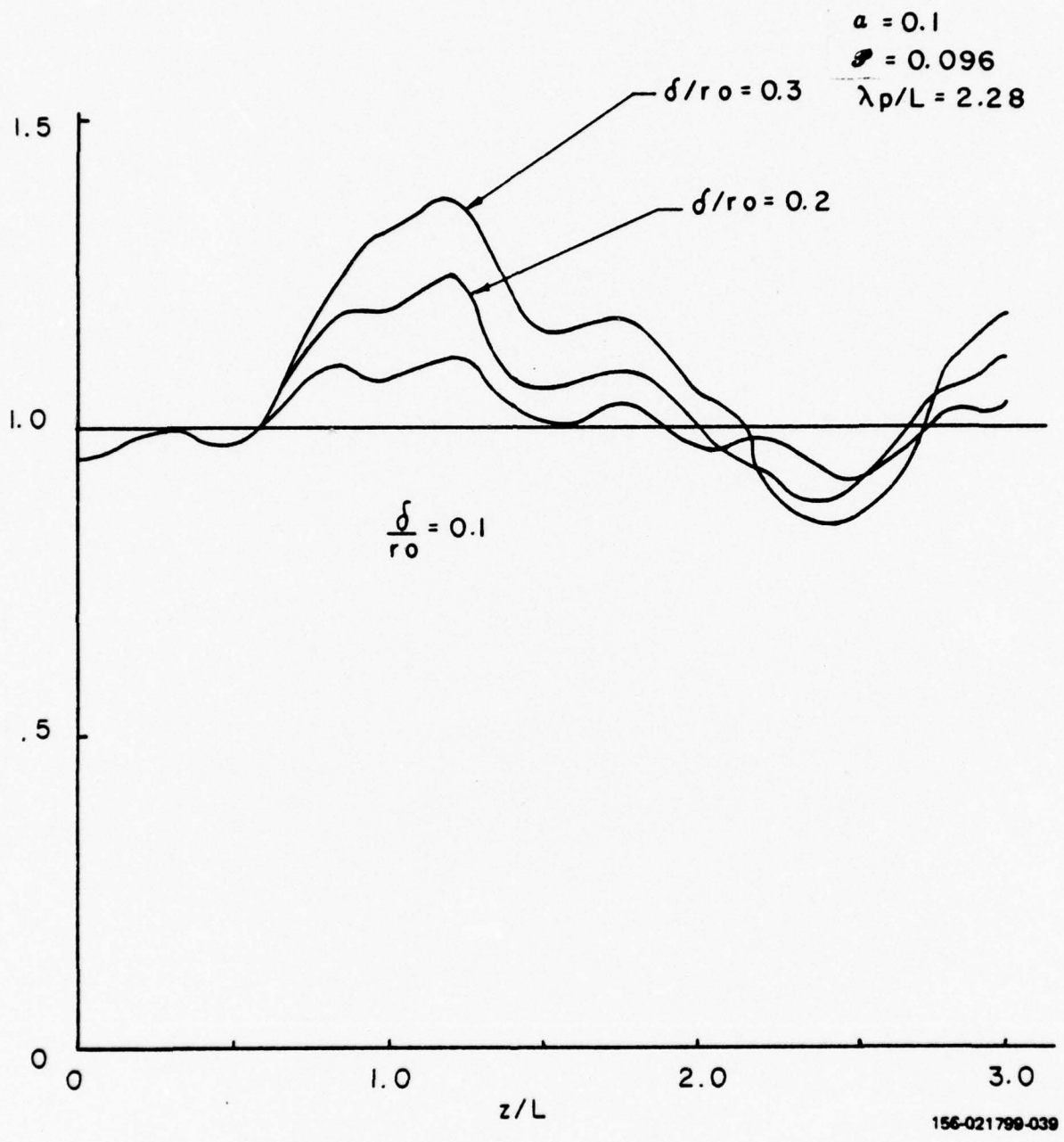

Figure 22. Trajectories-Beam Off Center with Respect to Magnetic Field δ

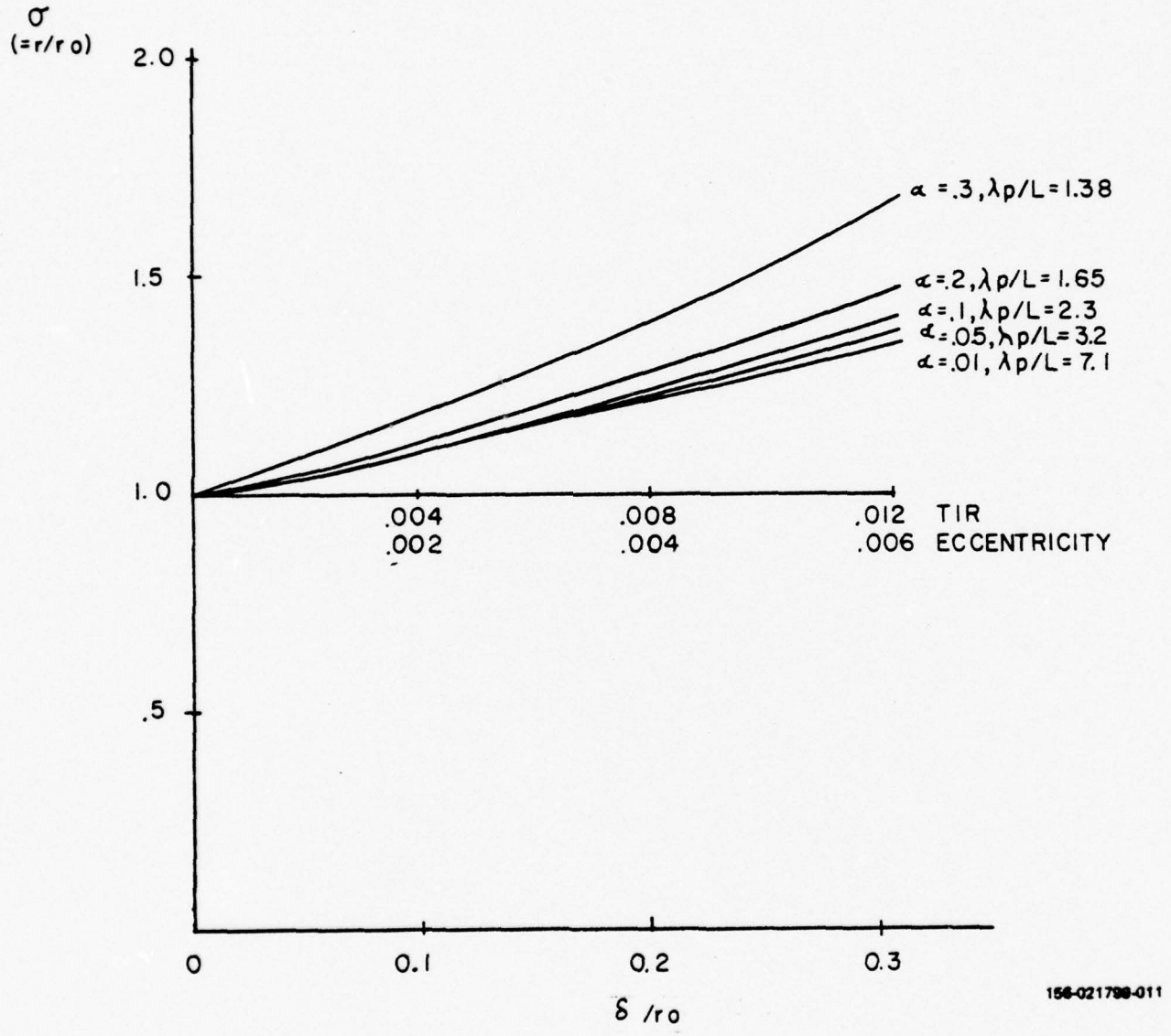

Figure 23. Maximum Peaks of Beam Excursion for Beam Off Center with Respect to PPM Magnetic Field by δ/r_o.

4.3 FERRITE MAGNETS

Ferrite magnets have the advantages of high coercive force and low cost, since they are produced in large quantities for loud-speakers. The main disadvantage is the thermal drift of the magnetization. The first PPM focused tubes were made with ferrites and the thermal drift was compensated by magnetic shunts. Since the shunt absorbs part of the flux, the efficiency of the magnet is decreased and therefore the cost of the magnet is increased at least by a factor of two.

4.3.1 Irreversible Effects

Ferrites have both an irreversible and a reversible drift. Irreversible thermal effects are important only at low temperatures. They are relatively small for magnets with linear demagnetization curves like Arnox 7 or Indox 7 (which are used in the low cost TWT's). These effects are more severe in a magnet configuration in which B/H is low, which is the case for a PPM stack. M.A. Bohlmann* of Indiana General has measured the irreversible effects of Indox ferrite rings and blocks. The rings were tested by exposing them to -20°C and the +80°C temperature, and measuring the axial flux and density with a Hall probe centered in the hole. A block was cut from one of the rings and temperature effects were measured by pulling a search coil off the sample:

	Irreversible effects	
	-20°C	+80°C
Rings	5.5 - 7.1%	0 %
Block	0 %	0 %

Measurements in the laboratory on a PPM stack has shown that the irreversible effects are less than 1% after one thermal cycle between -55°C and room temperature.

* We thank Mr. Bohlmann for this information

4.3.2 Reversible Effects

Vendors specify a reversible thermal drift of the ferrites as follows:

$$\Delta B/B < -0.2\%/^{o}C$$

M.A. Bohlmann of Indiana General communicated to Northrop a thermal drift of Indox given by:

$$\Delta B/B = -0.19\%/^{o}C \pm 0.003\%$$

On a large number of measurements made in the laboratory on Arnox 7 on several different stacks and several thermal cycles, maximum variations were obtained:

$$-0.158\%/^{o}C < \Delta B/B < -0.192\%/^{o}C$$

This means that the statistical variation is much higher than the values obtained by Bohlmann. This strong variation may be due to unreliable measurements. Although possible, this hypothesis is not very probable because similar measurements made on Alnico 8 show good agreement with the figures published by vendors.

Table XV is a summary of the thermal effects of the ferrites.

4.3.3 Random Variation of the Magnetic Field

The calculations of the influence of the random variation on the peak magnetic field (see Section 4.2) indicates that the random variation should be less than $\pm 3\%$ if an acceptable small beam ripple is desired. The ferrites meet these specifications if the stabilization resistance has a tolerance of $\pm 1\%$.

Table XVI shows the random variation of PPM stacks found in the literature or measured in the laboratory. Only the first PPM stack from Mendel and Quate meets the tolerance requirements for random variation.

Table XV. Ferrite Magnets.

ABSOLUTE VARIATION:	$\pm$ 10% FOR -20°C TO +80°C
THERMAL RANDOM VARIATION:	$\pm$ 1.7% FOR -20°C TO +80°C
STABILIZATION MACHINE:	$\pm$ 1.0%
TOTAL RANDOM VARIATION:	$\pm$ 2.7% BETWEEN -20°C TO +80°C

Table XVI. Random Magnetic Field Variations.

MENDEL AND QUATE[20]	< $\pm$3%		
R C A	< $\pm$7.5%		
20 WATT "S" BAND	< $\pm$7.5%	α = .11	14 PERIODS
100 WATT "S" BAND	TAPERED	α = .076	
	FIELD	α = .15	17 PERIODS
200 WATT "S" BAND	< $\pm$12%	α = .15	14 PERIODS
300 WATT "S" BAND DUAL MODE	WITHOUT SHIMS $\pm$11%	α = .3	22 PERIODS
	WITH SHIMS $\pm$5%		

In the 100 watt "S" band tube, the magnetic field is increased from the gun to the collector. Figure 24 shows the measured magnetic field distribution and figure 25 the corresponding calculated trajectories. The average beam radius is smaller near the collector and compensates for the increase of the beam radius by the RF.

Figure 26 shows the electron trajectories of the 200-watt tube calculated by the method of section 4.2 for the measured magnetic field pattern. All measured tubes needed more or less shims; more shims were used for the 200 watt "C" band tube.

In the 300 watt CW 600-watt pulsed tube, a large amount of shimming was used to reduce the random variation from $\pm$11% to $\pm$5%.

In conclusion, the random peak field distribution is a very sensitive factor for the beam transmission. In many commercial tubes, the variation of random peak field distribution is greater than $\pm$ 3 %, the value which we have calculated to be a desirable upper limit.

4.3.4 Crossed Fields

It is generally assumed that crossed fields are a major obstacle to achieving good beam focusing. However, very little by way of theoretical or experimental results on the influence of crossed fields on the focusing of the beam in O-type devices is found in the literature.

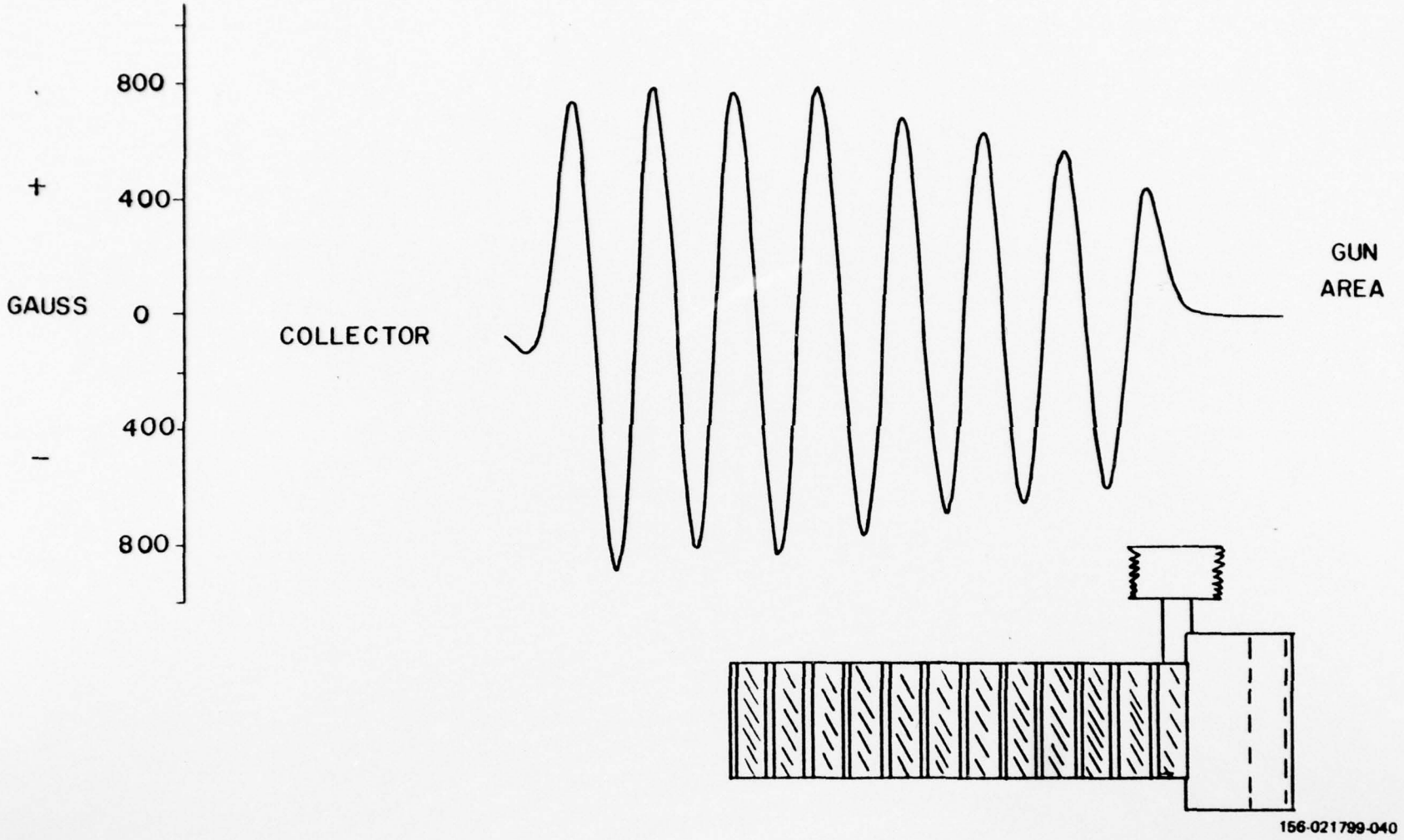

Figure 24. Magnetic Field Measured Off a 100-Watt "S" Band Tube.

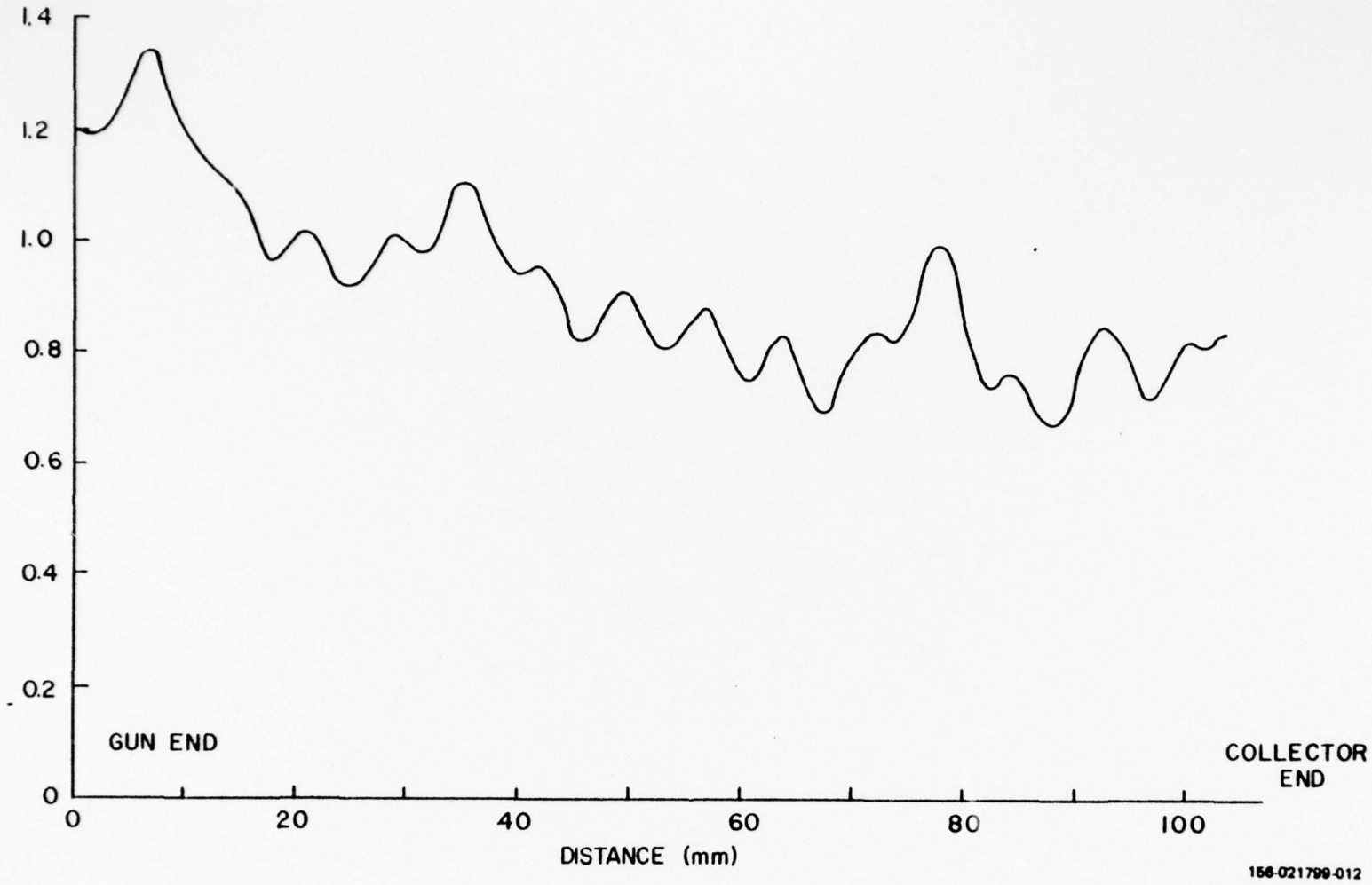

Figure 25. Calculated Trajectories of the "S" Band 100 Watt Tube for the Measurement for Magnetic Field Distribution.

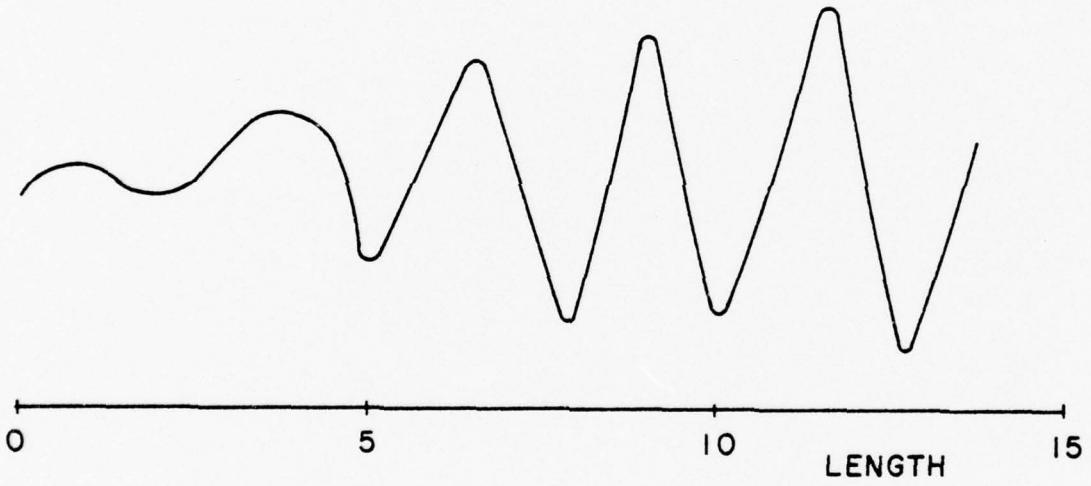

156-021799-041

Figure 26. Ripple of the Beam Vs Length with the Measured PPM Profile. Beam Radius = 0.5 X Helix Radius. Fine Structure of the Beam Ripple Neglected.

There are two reasons for crossed fields:

(a) The magnetization of the ring magnets is not homogeneous over their cross section. As an approximation, the crossed field can be considered as a dipole field (Figure 27). The crossed fields are in one direction. Figure 28 shows the crossed fields of the ferrite magnets without pole pieces along the axis of the magnet*. The crossed fields on the axis are in one direction and are of the order of 5 to 10 Gauss for a maximum field of 800 Gauss. The crossed fields are of the order of about 1%.

(b) In the stack of magnets with pole pieces, one pole piece may be off center with respect to another. The crossed field changes in sign as the probe moves axially through the magnet.

* The crossed fields were measured by mounting a probe to measure the field perpendicular to the axis, and the magnet was rotated on the head of a high precision lathe. If the field measured at 0^0 is B_0 and the field at 180^0 is B_{180}, the symmetric field B_S and the crossed field B_C can be calculated by:

$$B_S + B_C = B_0, \; B_S - B_C = B_{180}$$

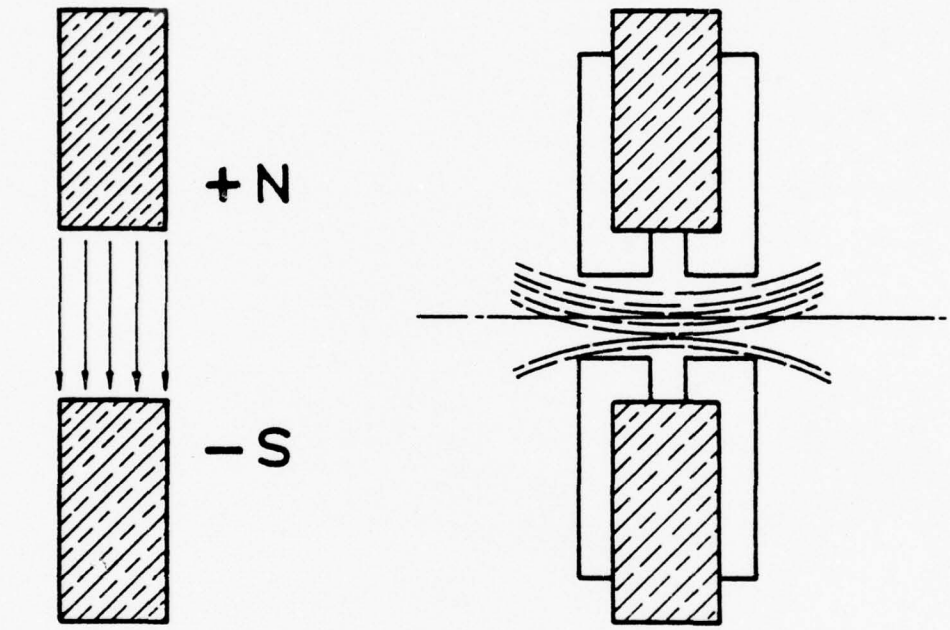

Figure 27. Crossed-Field Configurations.

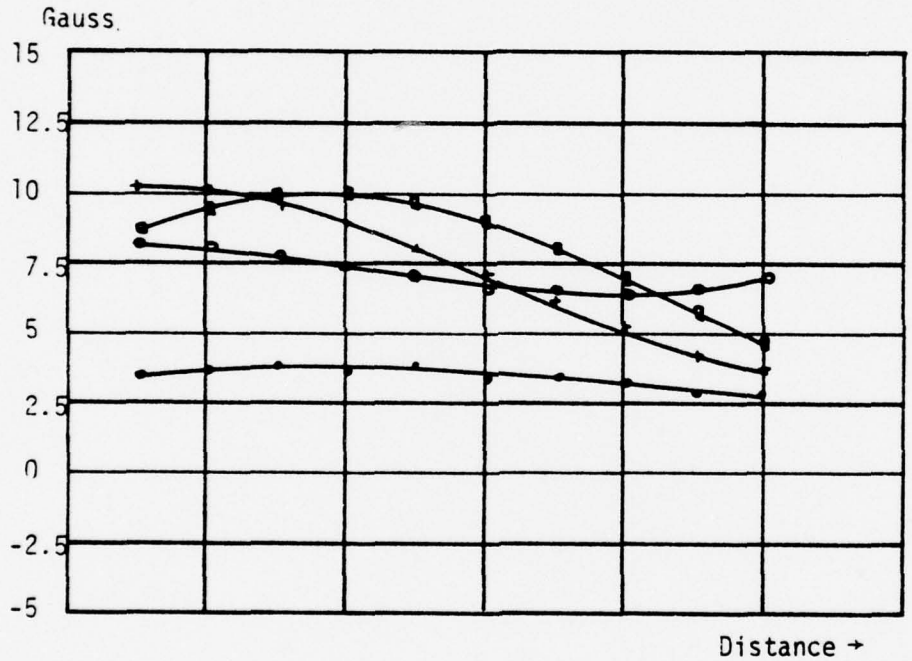

Figure 28. Crossed-Fields of Four Ferrite Magnets Without Pole Pieces.

In Figure 29, the magnetic field of the magnet with pole pieces is shown for different angles of the probe. There are no crossed fields in the center of the magnet. All inherent crossed fields of the bare magnet are short-circuited by the pole pieces and the crossed fields are due only to the eccentricity of one pole piece with respect to the next. The crossed fields due to eccentricity are given by:

$$B_c = B_{om} \; I_1 \left(\frac{2\pi\delta}{L}\right) \approx B_{om} \; \frac{\pi\delta}{L}$$

where:

δ = eccentricity

L = period of the magnetic field

I_1 = modified Bessel function

B_{om} = maximum field on the axis

For the case of Figure 29, the measured crossed field corresponds to a value of TIR (two times δ) = 0.0008 inches. If the crossed fields are not completely shunted by the pole pieces or if the magnets are tilted, then the magnetic field distribution is no longer symmetrical. The crossed field measured in the center of the magnet is the crossed field due to tilt.

Figures 30 and 31 show the field variation perpendicular to the axis of a stack of 3 magnets, measured along the axis. The parameter is the rotation angle of the stack with respect to the fixed Hall probe. For any given value of distance, the maximum crossed field is the difference of the minimum and maximum field divided by 2. In Figure 30, the alignment of the stack was poor and a maximum crossed field of 32 Gauss was measured. In Figure 31, the alignment of the magnet was improved and the maximum crossed field was measured to be 7 Gauss. In both cases, the peak magnetic field was 1400 Gauss.

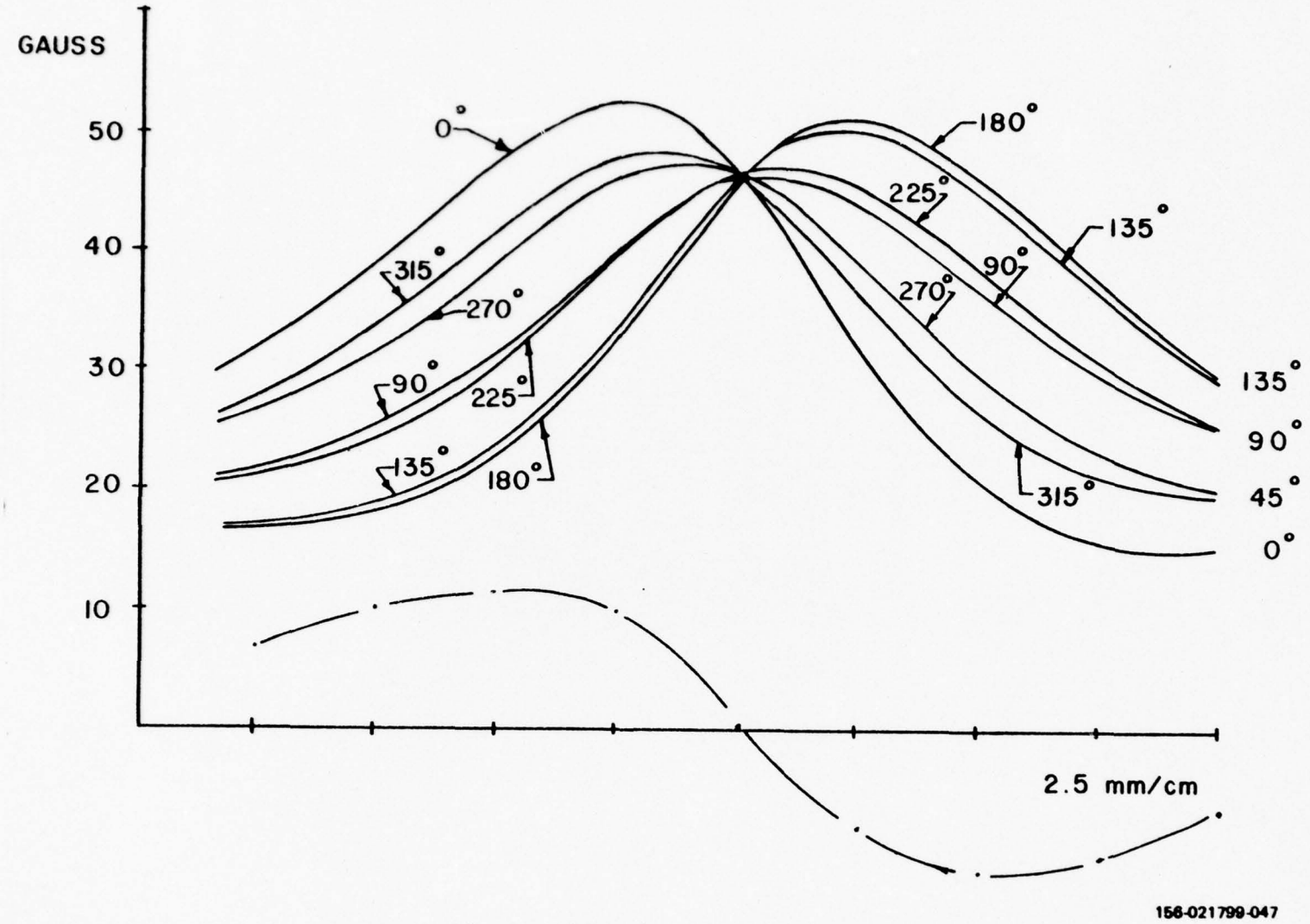

Figure 29. Crossed-Fields in Ferrite Magnets
Upper Curves Measured Crossed-Field Along the Axis
Lower Antisymmetric Crossed-Field $B_c = \left|\frac{Bo-B}{2}\right| 180$

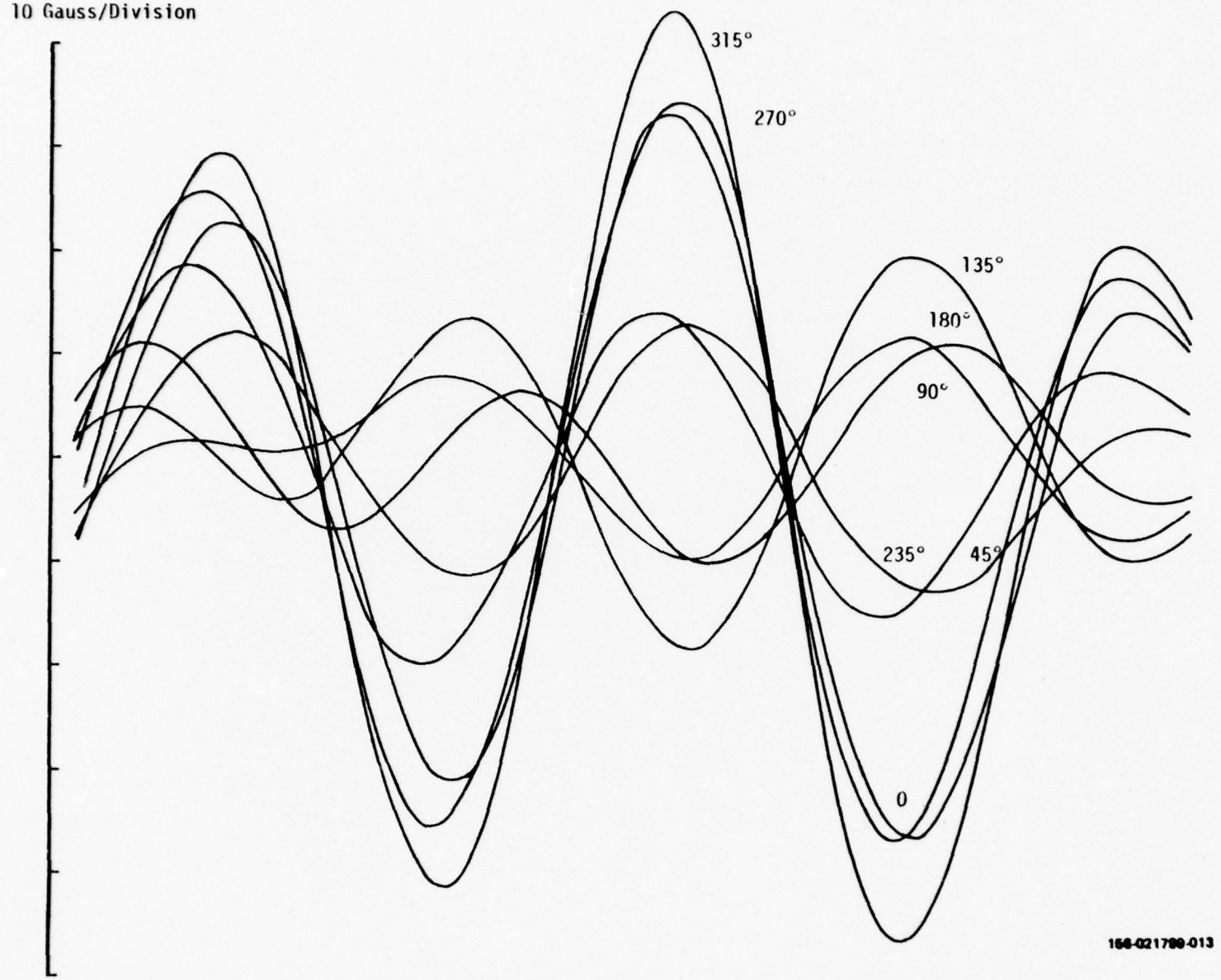

Figure 30. Crossed-Field for Three Ferrite Magnets in Series (Poor Alignment).

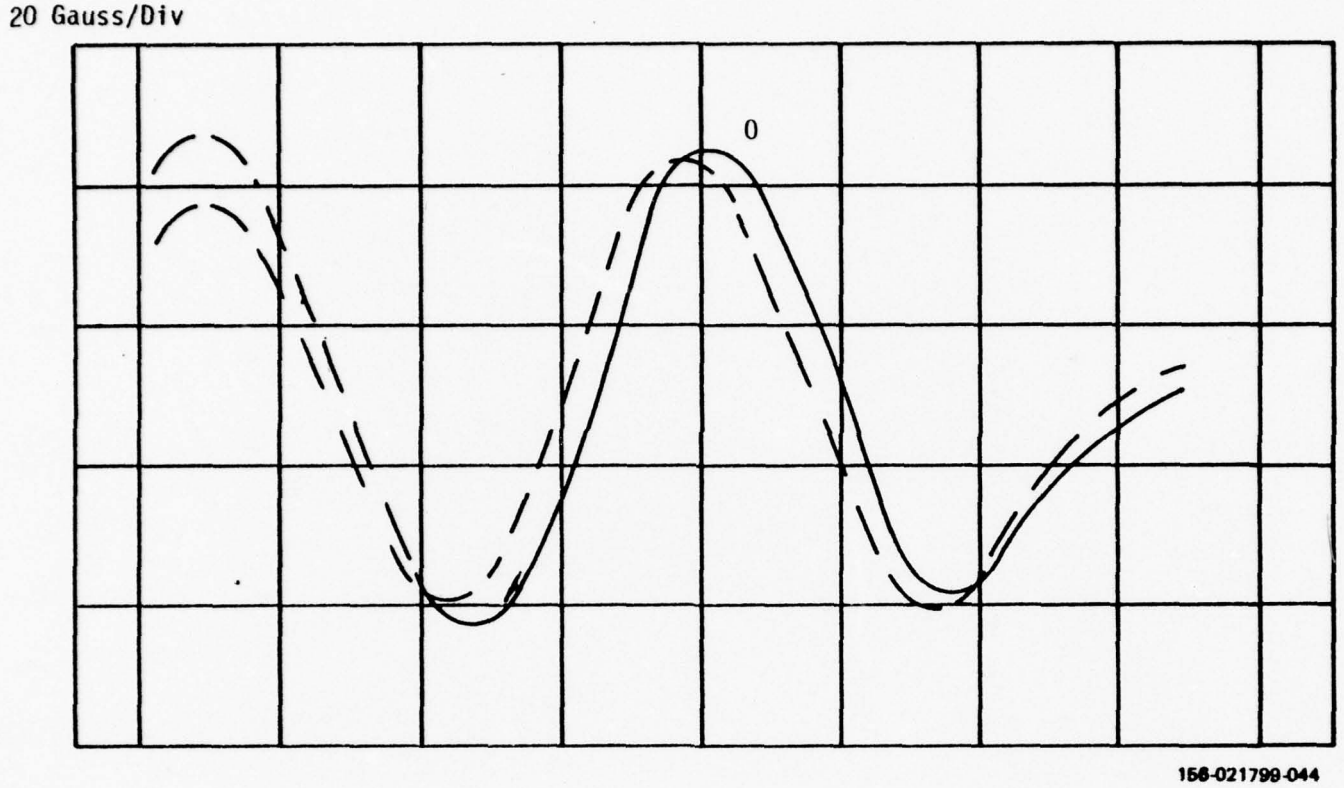

Figure 31. Crossed-Fields of Three Ferrite Magnets in Series (Good Alignment).

Because the crossed fields are strongly influenced by the misalignment of the magnets and by tilting, a slip-fit PPM stack is necessary. Therefore, the cost of the pole pieces is relatively high (see Section 3).

In Section 4.2.7, the influence of the eccentricity on the ripple of the beam has been calculated. For the proposed tube, the average beam radius, 0.018 inches, and the variation of the beam ripple as a function of the TIR of the barrel for various values of beam "stiffness", λ_p/L, or for corresponding values of σ, is shown in Figure 23. For a TIR of 0.0025 inches, a value which can generally be held by suppliers of drawn tubing, the ripple is relatively small and can be accepted.

4.3.5 Crossed Fields in the Gun Area

Most TWT's have a shielded gun with no magnetic flux through the cathode, and the magnetic field distribution in the gun area is a critical factor for good injection. Some measurements were described by Villotte[21]. He found a dissymmetry of 5 Gauss in the gun area near the cathode for a peak field of 1300 Gauss. He obtained a beam transmission of 66%. After shimming, the crossed fields were reduced and a beam transmission of 85% was obtained.

On a magnet stack for a PPM focussed TWT made at Northrop, the longitudinal field and the crossed field for the pole piece shield were measured without shims and with the shims introduced to meet performance specifications. Figure 32 shows the longitudinal field near the cathode area with and without shims. The difference between the fields is less than 1 Gauss. In Figure 33, the crossed fields are shown for different rotation angles of the magnet plus the shielding barrel. In the center of the cathode surface, the crossed fields are 1.5 Gauss without shims and 0.75 Gauss with shims. These measurements show the extreme sensitivity of the crossed fields for beam transmission.

A calculation of the influence of a crossed field on the deviation of electrons in a spherical space-charge limited diode discharge was made. The deviation from the radial trajectory in the presence of a crossed field is given by

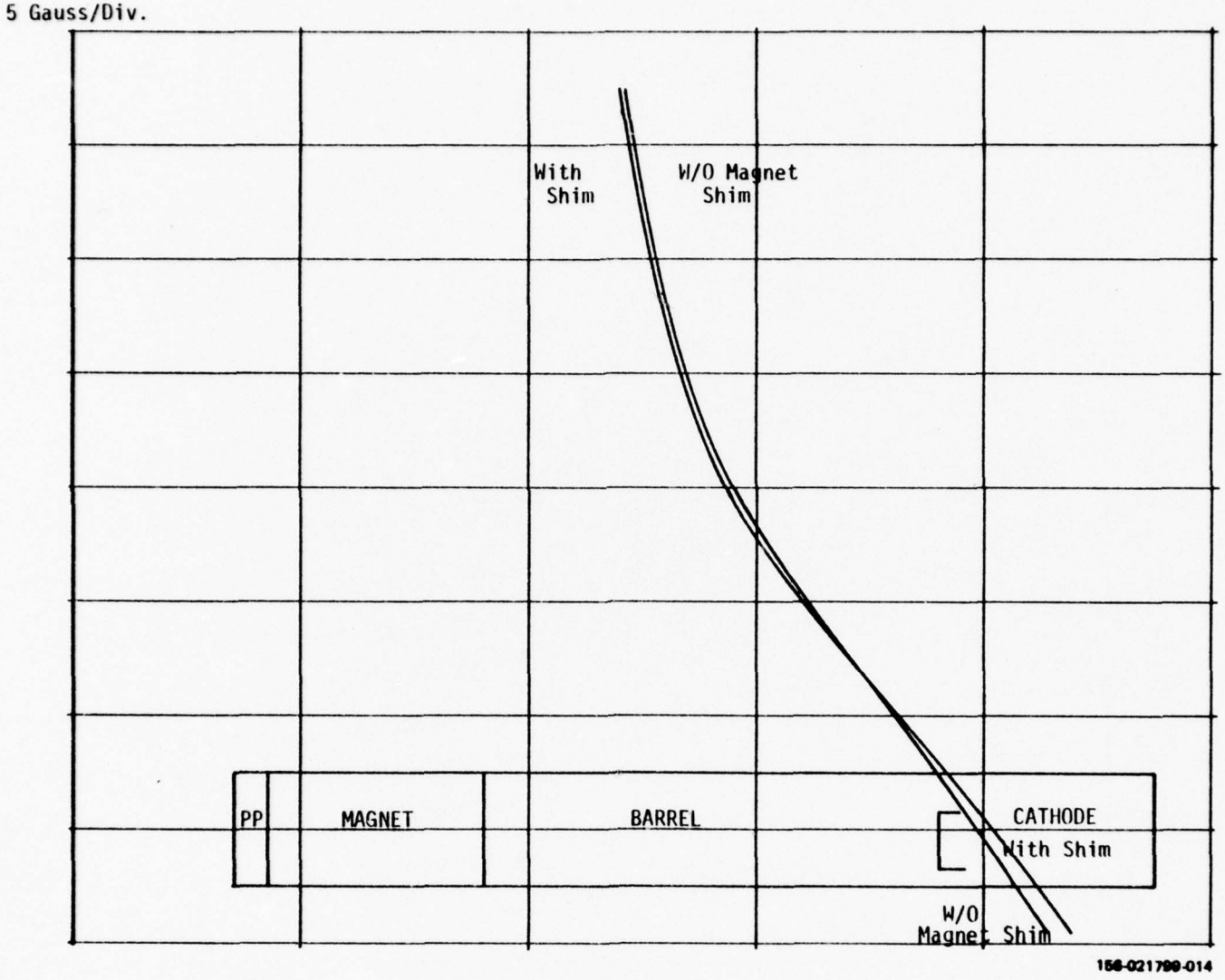

Figure 32. Axial Field in Gun Area With and Without Shims.

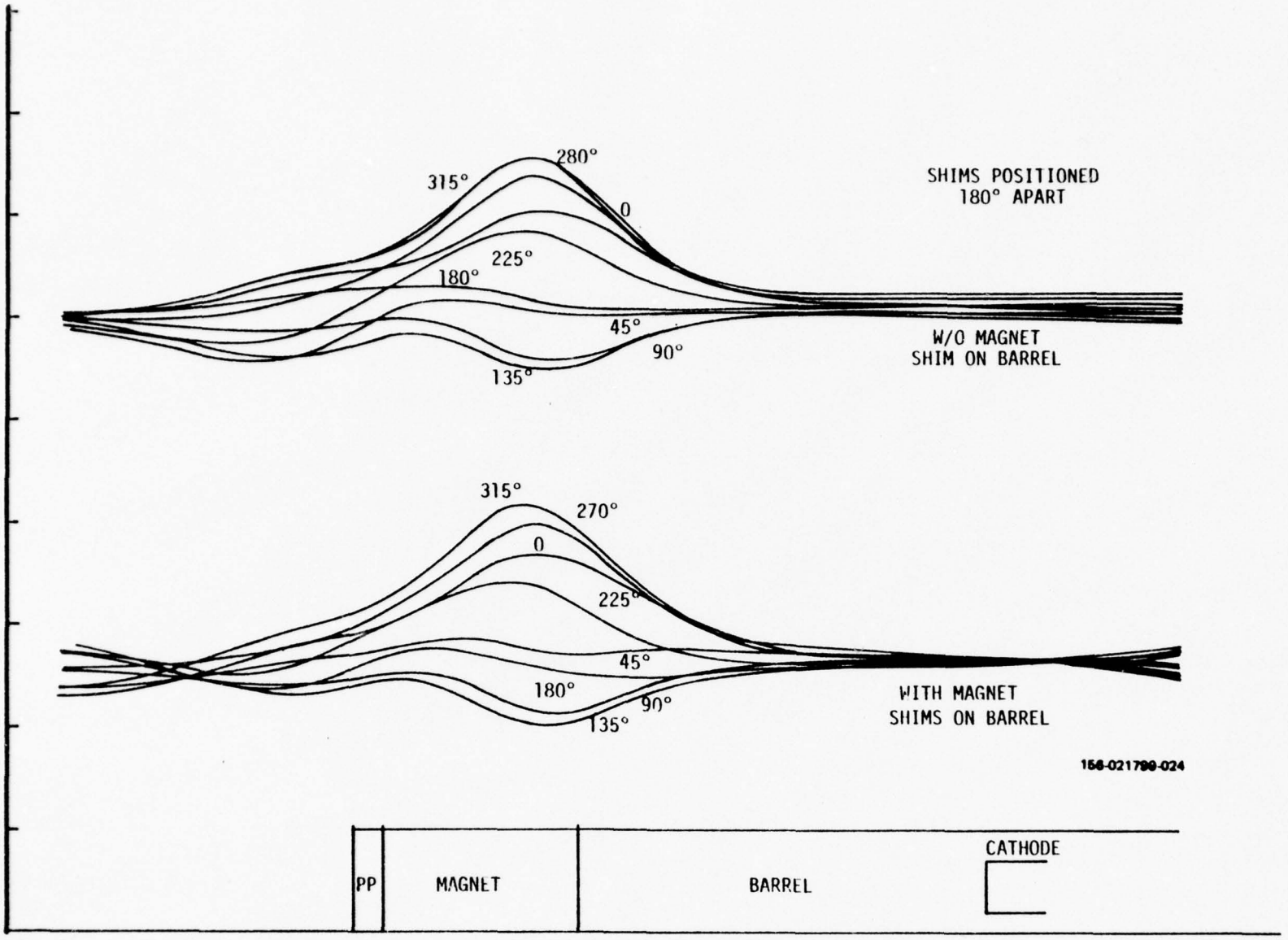

Figure 33. Crossed-Fields in Gun Area With and Without Shims.

$$x = \frac{0.3 r_c^2 B}{\sqrt{V}} \int_1^{r_a/r_c} \frac{(1-r/r_c)\left[-a^2(r_a/r_c)\right]^{2/3}}{\left[-\frac{2}{a}(r/r_c)\right]^{2/3}} \left(d\frac{r}{r_c}\right)$$

V = Voltage between the two spherical electrodes

B = Magnetic field in gauss

σ_x = Deviation at the inner sphere in cm

r_a = Radius of the anode sphere

r_c = Radius of the cathode sphere

The $(-a^2)$ functions for spherical diodes are presented by Kirstein, Kino and Waters[12]; for $r_c/r_a = 2$, the integral is 0.25.

In the Northrop tube, using the magnetic field distribution shown in Figures 32 and 33, r_c = 1.8 cm and V = 1300 volts. For a constant crossed field B, the deviation is x = 0.0037 inches, a value quite high. In all recent TWT's, the measured crossed fields are 0.2 to 0.5 Gauss or less.

Section 4.4 Conclusions

The following conclusions can be drawn:

(1) The random variation of the peak magnetic field is the principal reason for variation of performance characteristics from tube to tube, and shimming is necessary to obtain the required performance. The random variations must be less than $\pm$3%, and values of $\pm$1.5% or less are desirable.

(2) Variation of the pitch of stacks is not critical if the peak field does not change.

(3) Variation of the magnetic field of the ferrites with temperature change between -20° and +80°C can probably be tolerated. In the design of the proposed tube, Brillouin

beam diameter is 0.4 time the average helix diameter. Due to the thermal drift between -20° and +80°C, the average beam diameter relative to the helix diameter changes from 0.36 at -20°C to 0.45 at +80°C and the ripple is ± 0.1. Therefore, the maximum diameter is 0.5 of the average helix diameter at 80°C and the minimum diameter is 0.32 at -20°. Calculations by L. Winslow* show that only slight changes in efficiency occur for a variation of the average beam diameter between 0.36 and 0.45 times the helix diameter.

(4) The crossed fields in the PPM stack for either ferrite or Alnico 8 magnets are caused mainly by misalignment of the PPM stack with respect to the axis of the beam. For a slip-fit assembly of the PPM stack, the TIR of the barrel of 0.0025-0.003", commonly available on the market, is adequate for experimental tubes to be built.**

(5) Crossed fields in a shielded gun have a large in-influence on the injection of the beam into the PPM stack. All modern tubes have crossed fields of less than 0.2 to 0.5 Gauss in the gun area.

(6) Calculations with the paraxial flow equations and the calculation of the trajectories for a gun and PPM stack by SAI using 5 layers of electron charge show comparable results in terms of beam variations for the same set of conditions.

All of these conclusions are primarily based on calculations. Additional experimental verification is necessary.

* We thank L. Winslow of the Naval Research Laboratory for computing the efficiency of the proposed tube under these extreme conditions.

** In Figure 23, the TIR or eccentricity of the proposed tube is indicated.

5. BEAM TESTER

5.1 Introduction

Most companies fabricating linear beam devices use more or less sophisticated and complex beam testers which evaluate the beam behavior accurately in the gun region, but which have very limited usefulness in evaluating the beam in the PPM stack. Generally these beam testers are many times oversize so that the required tolerances within the electron gun are easily achieved. The results are then scaled to the real-size tube dimensions by using experimentally and theoretically determined design factors. Such beam testers can be used and sometimes are used to determine the required tolerances of the gun design for the required beam perveance, the beam minimum position, and the beam diameter tolerances. However, the beam testers do not answer two problems which are inherent in a PPM focusing system:

- What are the tolerances necessary and sufficient for the beam transmission in the PPM stack and for the RF efficiency, i.e., tolerances of the random peak magnetic field, of the pitch of the PPM stack, of the crossed fields, of the eccentricity, of the injection conditions into the PPM stack, of the thermal drift, etc.?
- Is the technology used in the real size focusing system precise enough to obtain reliable and reproducible beam transmission and efficiency without any supplementary adjustment or with minimum labor for the adjustment? If the measurements of the beam structure are consistent and repeatable, but not reproducible from one gun to another where the gun and PPM stack are of the same design, the technology used is not adequate for the construction of the TWT.

An alternative approach using this same type of beam tester is to build a large scale model and intentionally vary the critical dimensions from one test to the next. This approach also will aid in determing the required tolerances.

The beam tester developed under this program is of real size and has the capability of examining the electron beam within the PPM structure. Experimental results obtained with such a beam tester thus allow the determination of the quality of the electron gun and the PPM focusing stack and their combined effect on the

current distribution in all three dimensions (r, ϕ, and z) in the interaction space. Furthermore, the determination of all critical tolerances for real tubes can be established.

5.2 Construction

Figure 34 shows the cross section of the beam tester and Figure 35 is a photograph of the beam tester as actually constructed. A movable probe assembly consisting of 5 individual current probes can be freely rotated (angle ϕ) and displaced in the z direction. The measurement of the individual probe currents as a function of ϕ and z determines the current distribution in the interaction space. Measurement of current distribution in radial dimension, r, depends on the fact that each individual probe is set at a different radius.

Care has been exercised in the construction of the beam tester to insure that the dimensional accuracy is sufficient for the repeatability of the data. The probe assembly has been made very precise so that the rotation is concentric and the displacement along the z-axis can be achieved with negligible backlash.

Figure 36 shows the probe electrode assembly. The collector was made of alumina, and small holes were drilled with a laser beam with a little ellipticity, the diameter varying from 0.004" to 0.005". Nickel wires of 0.003" diameter, insulated by glass tubes of about 0.004" inside diameter, were melted at the head to form a ball of about 0.008 to 0.010" diameter to serve as the current probes. The ceramic collector disc was metallized by evaporation of aluminum to suppress charges on the ceramic. During evaporation, the areas to be behind the probes were masked. Several difficulties were encountered:

- Short circuits between the probes and the metallized collector.
- Evaporation of the aluminum during operation with a duty of 10^{-5} to 10^{-3}.
- Difficulty with the activation of the cathode because the bake-out temperature was limited to 100^{o}C by the O-rings.

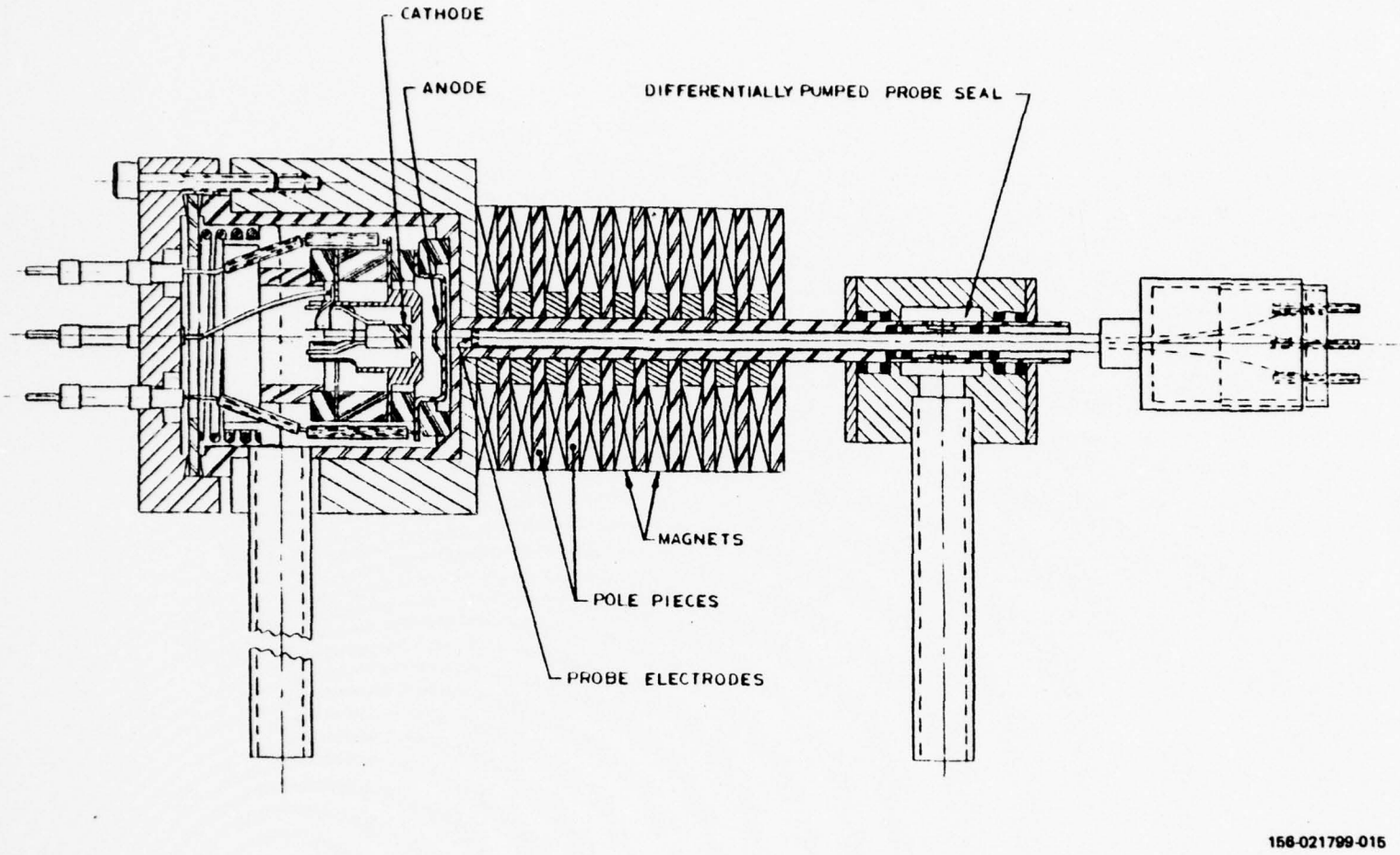

Figure 34. Cross-Section of Beam Test.

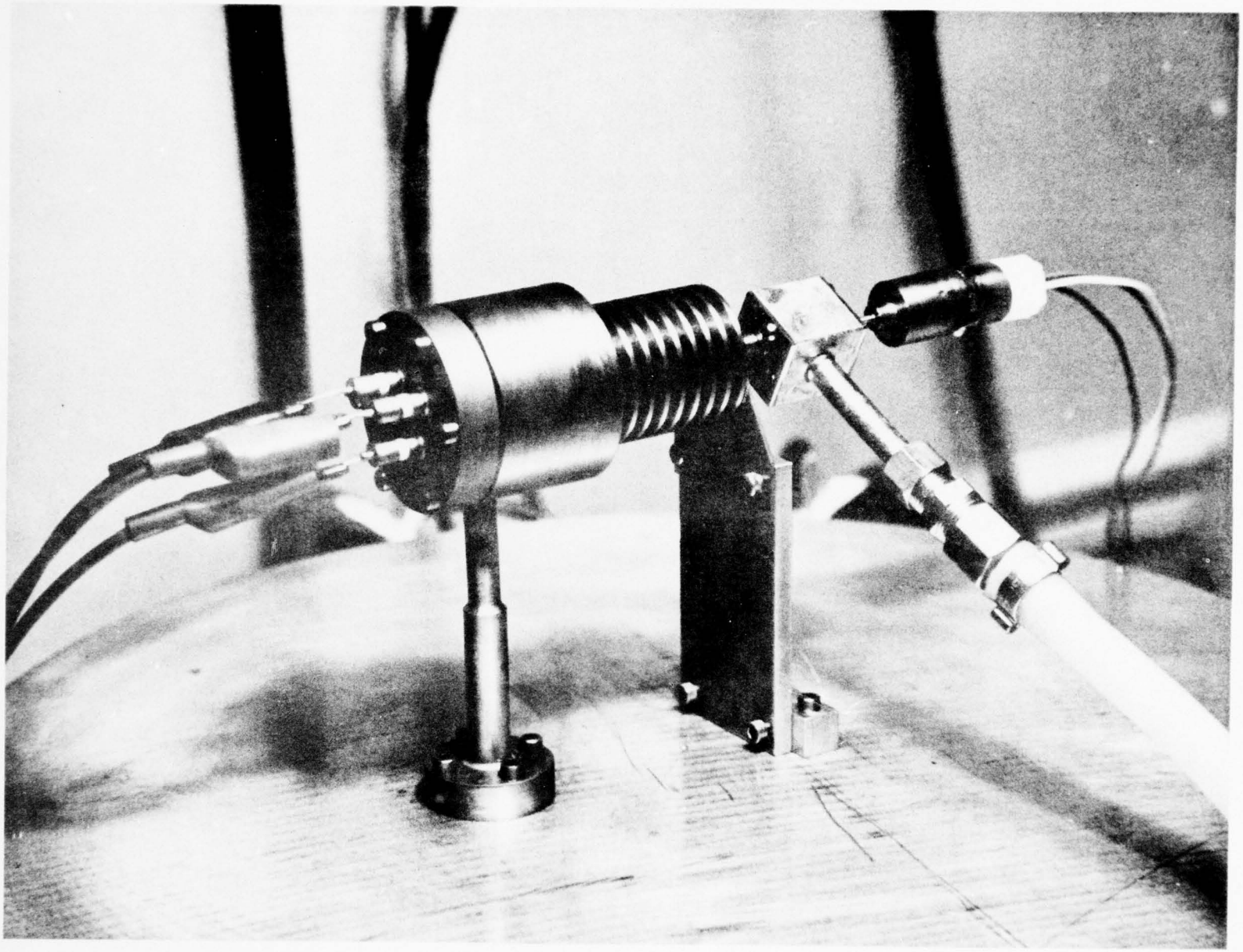

Fig. 35 PHOTO OF THE BEAM TESTER

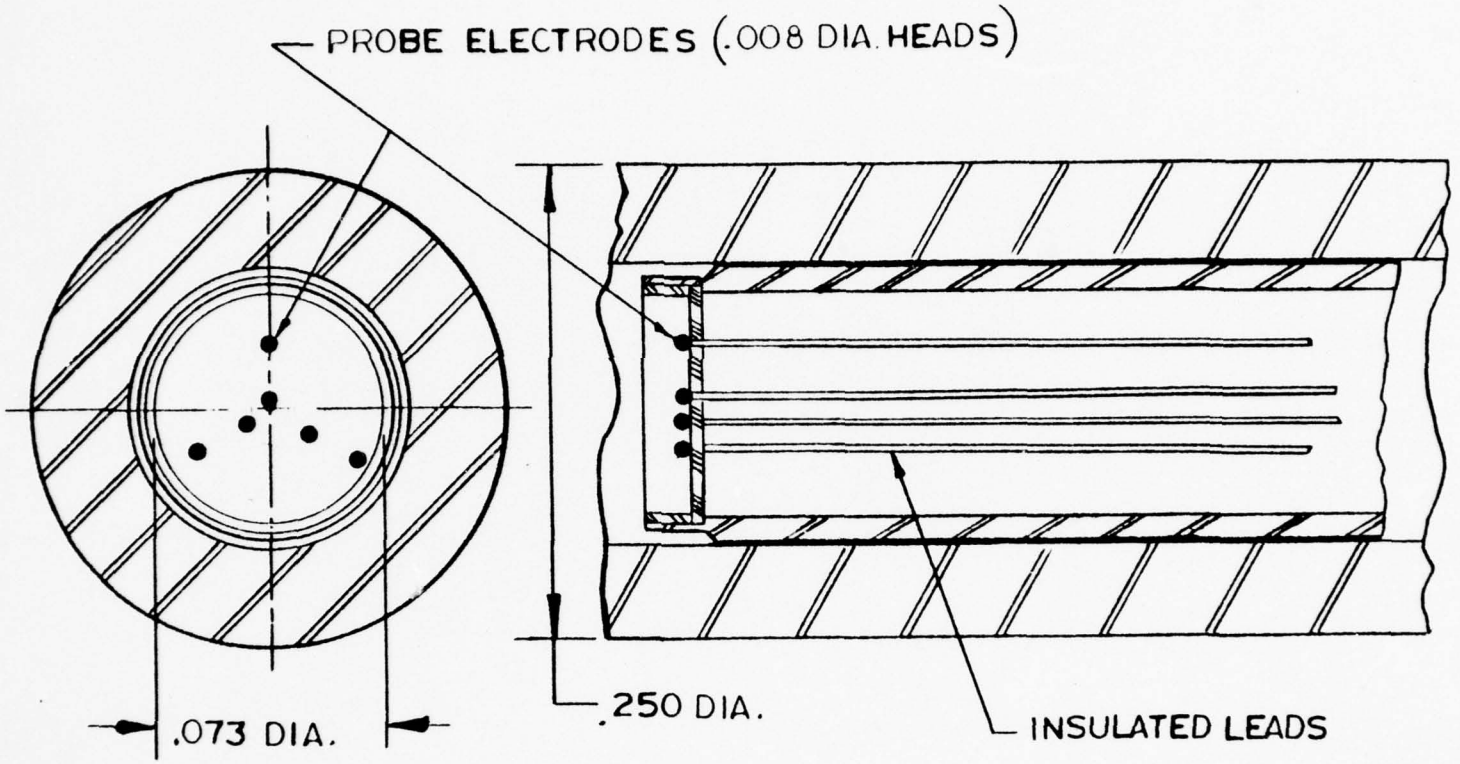

Figure 36. Probe Electrode Assembly.

A redesign has been made, as shown in Figure 37. The collector is a metallic cap with holes, and behind it is a ceramic disc on which the probes are to be deposited as in the beam tester actually built. "Viton" O-rings will be used to allow a bake-out temperature of 200°C.

In case that a leak in the O-ring assembly occurs during the rotation and displacement of the collector, differential pumping as shown in Figure 38 protects the cathode from contamination by poor vacuum. No problem with respect to leaks in the O-ring assembly was found.

5.3 Experimental Results

Only a few measurements could be made because of the difficulties described in 5.2. The operating conditions under which measurements were made were as follows:

Cathode Voltage:	1 kV
Cathode Current:	28.7 mA
Collector Current:	17 mA
Peak Magnetic Field:	1120 Gauss
Beam Radius for Brillouin Beam (calculated using RMS magnetic field):	.248 mm
Magnetic Field at Probe Position:	600 Gauss

The eccentricity of the PPM stack was less than 0.001" TIR. In the first test, only three probes were operable. The probe wires used in this test were platinum, coated with aluminum oxide, and the aluminum oxide flaked off because of brittleness. Figure 39 shows the position of the three probes and their tolerances, measured after the operation of the tester. Table XVII summarizes some of the results obtained, the values indicated having been averaged over three different experimental runs.

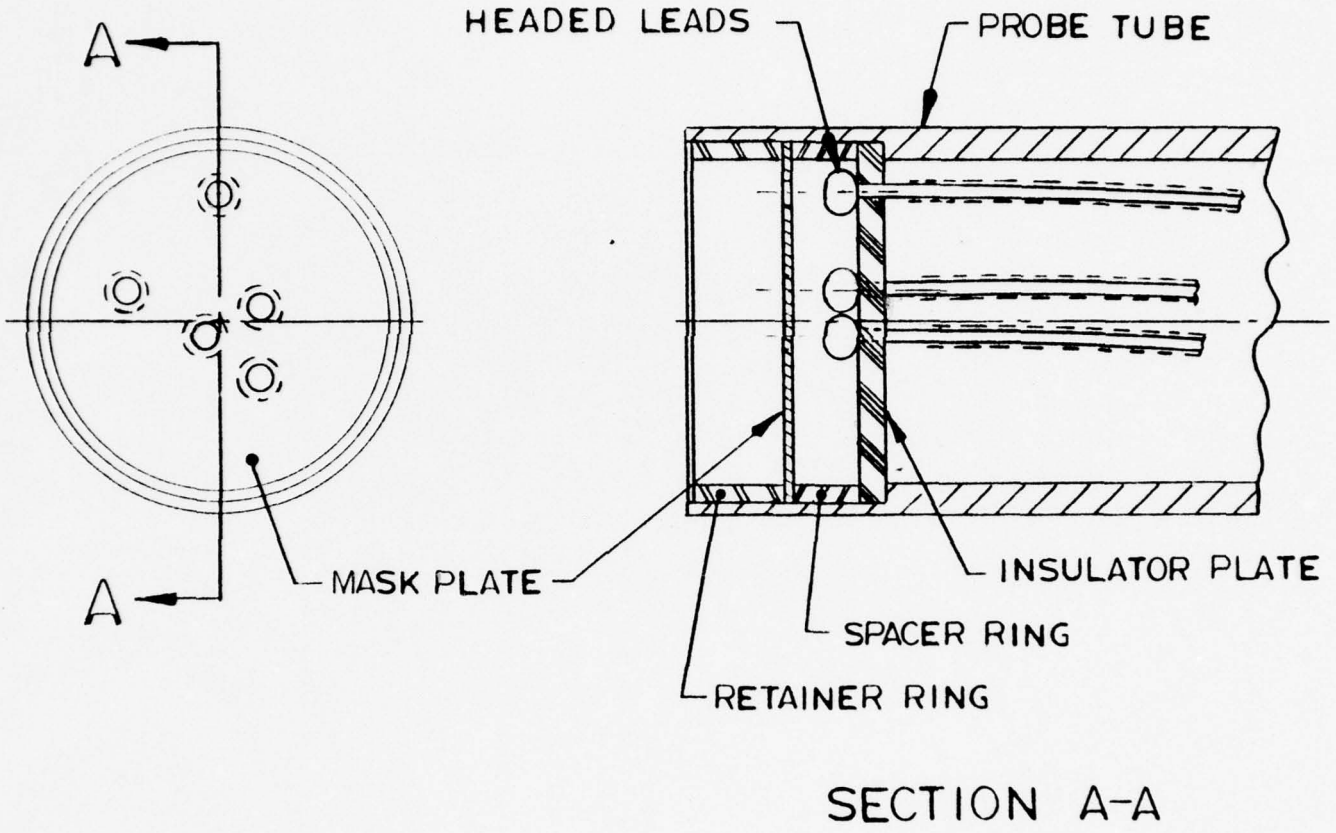

Figure 37. Redesign of the Probe.

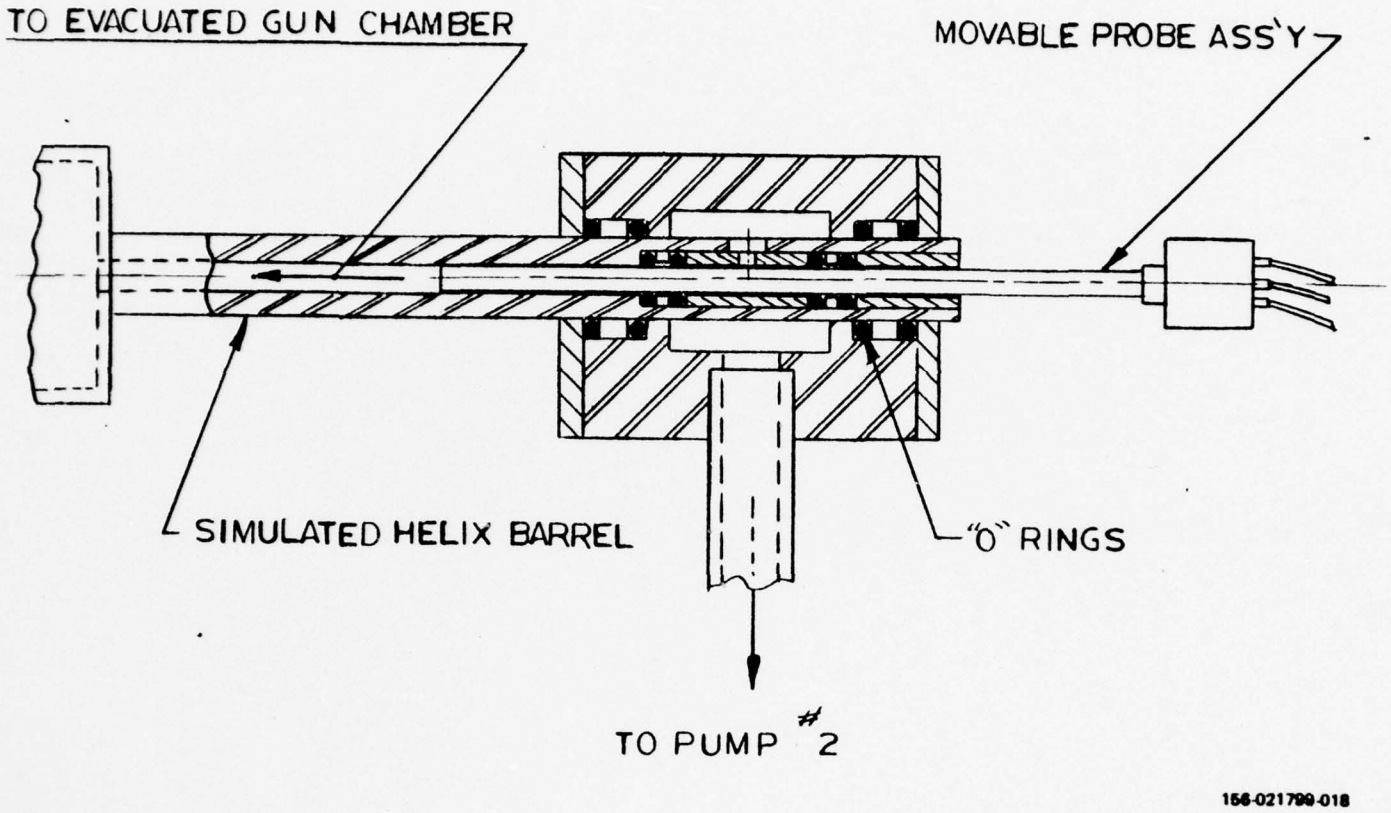

Figure 38. Probe Movement Seal (Differentially Pumped).

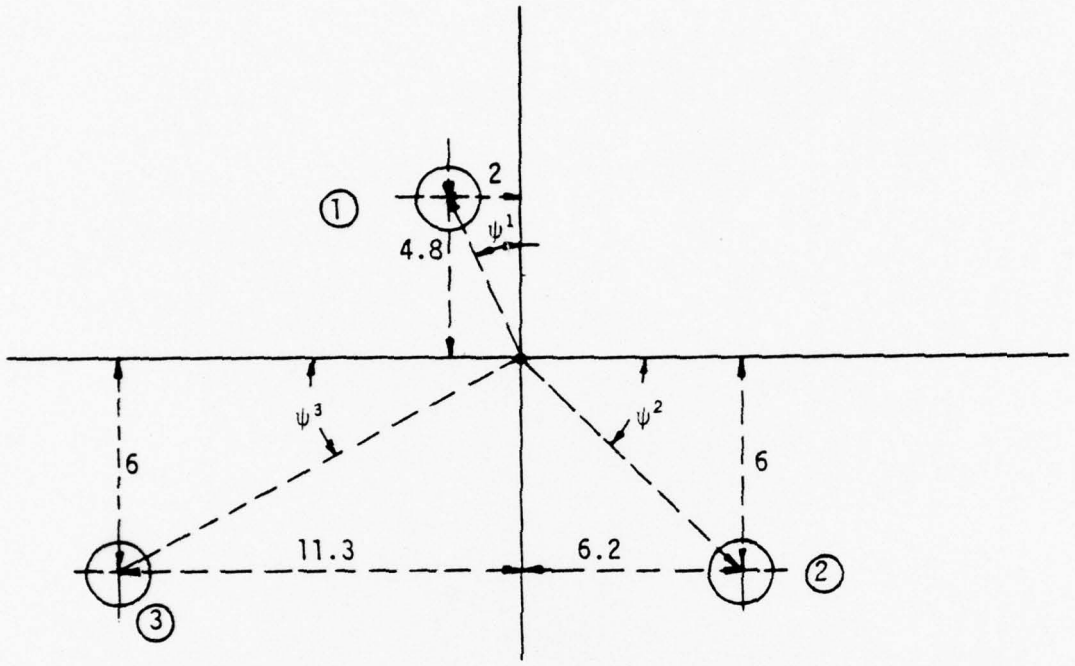

158-021799-045

THE ACTUAL DISTANCES ρ_i CAN BE CALCULATED AND ARE:

PROBE 1: $\rho_1 = 5.20$

PROBE 2: $\rho_2 = 8.63$

PROBE 3: $\rho_3 = 12.8$

THE ANGLES ARE AS FOLLOWS:

$\phi_{12} = 90° + \psi^1 + \psi^2 = 157°$ $(\psi^1 = 22.6°)$

$\phi_{32} = 180° - (\psi^2 + \psi^3) = 108°$ $(\psi^2 = 44°)$

$\phi_{31} = 90° - \psi^1 + \psi^3 = 95°$ $(\psi^3 = 27.9°)$

Figure 39. Measured Locations of the Probes as Referenced to Center Point C. The Center Point C is Referenced to Outside Diameter of Tubing Holding the Probe Assembly. Dimensions are Given in MILS.

Table XVII. Experimental Results Beam Tester.

Angle of Rotation ϕ	0^o	90^o	180^o	270^o
Measured I (mA) on 1	2.4	3.5	5.2	2
Measured I (mA) on 2	2.4	1.3	.8	4.45
Measured I (mA) on 3	1.1	1.4	.4	.25
Total Current (mA)	5.85	6.3	6.35	6.60

Under ideal conditions, (i.e., the current distribution having cylindrical symmetry and both the current distribution and the current probe assembly being perfectly centered) the current measured by each probe should be constant as a function of the rotation angle ϕ. Obviously, this is not the case. The first probe is about 5.2 mils away from the center. The mechanical eccentricity of the probe assembly is less than 1 mil. Therefore, the first probe is always less than 6.2 mils from the center, and yet an appreciable variation of probe current was found.

Let us assume that the beam itself is ideal, i.e., it has cylindrical symmetry, about its center, and that the current varies as a function of the distance R from the axis of symmetry according to the following proportion:

$$I \approx \exp\ -(R/r)^2$$

where r is a measure of the beam size. Let us assume furthermore that the beam is off center with respect to the probe assembly by a distance y_o. The current I; measured by each probe will then be given by:

$$I_j = I_o \exp -\left[y_o^{\,2} + \rho_j^{\,2} - 2y_o \rho_j \cos\ (\phi_j - \phi_i) \right] / r^2 = I_o \exp\ (\eta_{ij}) \quad (1)$$

where ρ_j is the distance of the probe j from the center of the probe assembly, ϕ_i is the ange that the beam center makes with the positive horizontal axis, I_o is the current which would be collected by a probe of the center of the beam, and ϕ_{ij} is the angle of probe j with respect to the positive horizontal axis. The conditions assumed so far are equivalent to the assumption that the probe assembly is perfectly centered and the beam, which although symmetrical, is off center by the distance y_o. It is irrelevant at this point to discuss whether the beam or the probe assembly is off center.

Considering equation (1), it follows that the logarithm of the measured I_i varies sinusoidally as a function of η.

$$\eta_j = \ell n(I_j/I_o) = \frac{2y_o \rho_i}{r^2} \cos(\phi_j - \phi_i) - \frac{\rho_i^2 + y_o^2}{r^2} \qquad (2)$$

For each probe j, 4 data points (as shown in Table XVII) were taken. In fitting the natural logarithm of these measurements by using the least-square law method according to:

$$\eta_j = b_{oj} + b_{ij} \cos \phi_j + a_{ij} \sin \phi_j = \eta_{oj} + \eta_{ij} \cos(\phi_j - \phi_i)$$

one obtains the following results:

$$\text{Probe (1)};\ \eta_1' = 1.12 + .48 \cos(\phi - 143^o)$$

$$\text{Probe (2)}:\ \eta_2' = .60 + .79 \cos(\phi + 52^o) \qquad (3)$$

$$\text{Probe (3)}:\ \eta_3' = .47 + 1.04 \cos(\phi - 55^o)$$

These η's are referenced to an I_o' of 1 mA, which accounts for the positive b_o values. The angle ϕ in the cosine arguments of (3) represents the angle of rotation of the probe assembly with respect to some reference. If for example the probe 1 was started coincident with the positive horizontal axis, which is assumed fixed with respect to the barrel, then the angle of ϕ_i in that frame of reference would be 143^o. Figure 40 shows the current variations as computed from the least squares approximation using:

$$I_j \approx \exp(\eta_j') \qquad (4)$$

for the three probes, as well as the measured experimental results. The fact that the experimental points are above or below the best fitting curve can be attributed to experimental errors and to the finite size of the current probes. For example, if the current probe is close to the center (maximum current), the current density will not vary as much across the probe area as if the current probe is further away from the symmetry axis where the current density varies more rapidly with ρ, i.e., across the probe area.

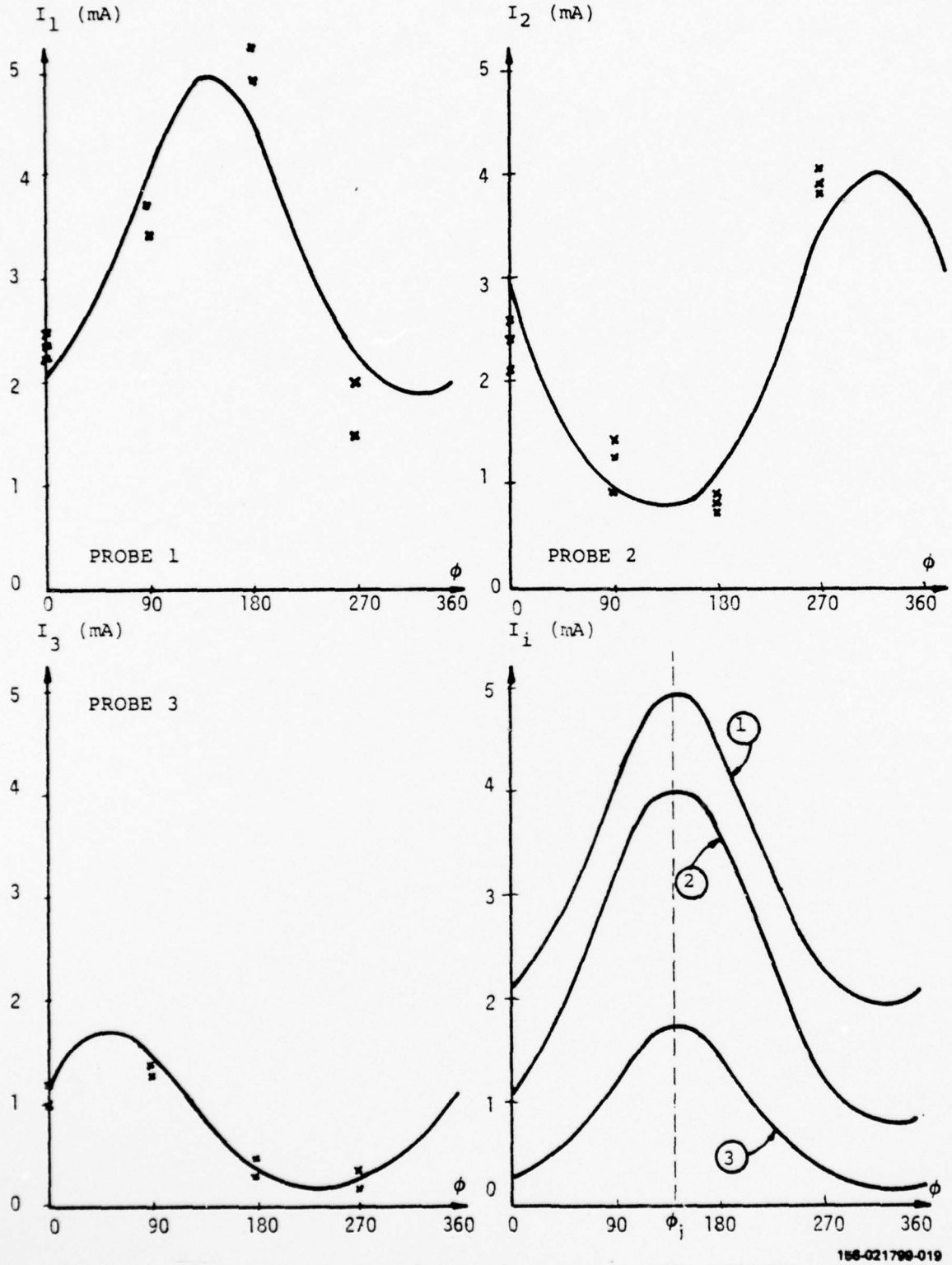

Figure 40. Best Fitting Sine Curves for the 3 Probes.
The lower right graph shows the current distributions referenced to the beam center.

Considering relation (3) it follows that the maxima I_j^m of the currents occur at rotation angles ϕ_j^m given by:

$$\phi_1^m = 143^o; \quad \phi_2^m = 308^o; \quad \phi_3^m = 55^o \tag{5}$$

The difference angles between the probes are:

	evaluated	measured
$\phi_{12} = \phi_2^m - \phi_1^m =$	165^o	157^o
$\phi_{13} = \phi_1^m - \phi_3^m =$	253^o or 107^o	108^o
$\phi_{23} = \phi_3^m - \phi_3^m =$	88^o or 272^o	95^o

Relation (2), shows that the amplitude of η_{ij} is proportional to ρ_j. Figure 41 shows the amplitudes obtained from relation (3) as functions of the three distances ρ_j as obtained from Figure 40. From $\eta_{ij} \approx 2y_o \rho_j / r^2$ the following relation can be determined:

$$r^2 = 23.5\, y_o \tag{6}$$

Relations (1) and (2) furthermore imply that the normalized DC component η_{oj} of η is a function of ρ_j (see relation 3)

$$\eta'_{oj} = \left[- \frac{y_o^2 + \rho_i^2}{r^2} \right] + k = \eta_{oj} + k \tag{7}$$

where k is an arbitrary constant.

Therefore, if one plots the DC-component η_{oj} as a function of ρ_j^2, a straight line should be obtained, and from the slope, the value of r can be determined. This has been done in Figure 42 with the result:

$$r = 9.3 \text{ mils} = 0.24 \text{ mm} \tag{8}$$

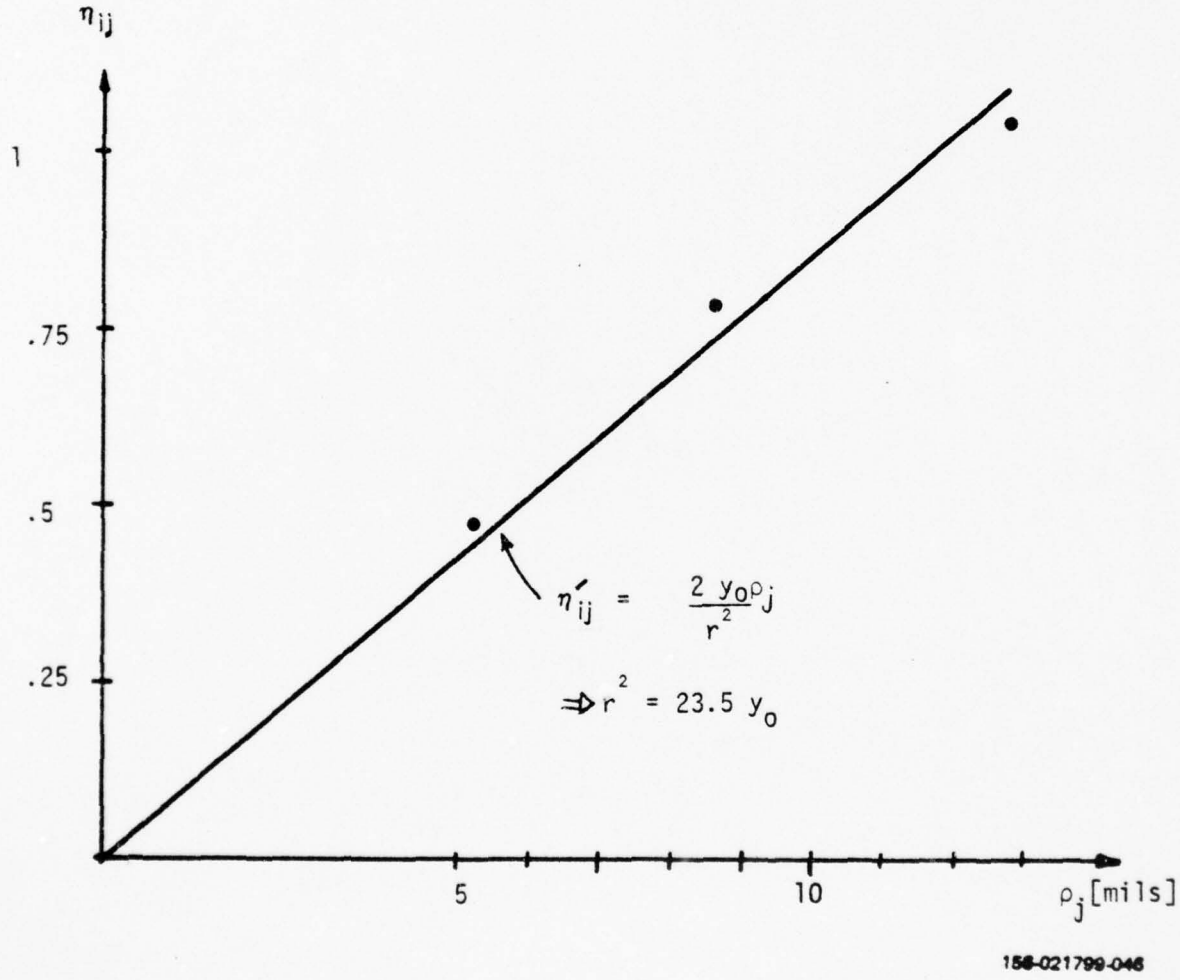

Figure 41. Plot of η_{ij} -Amplitude Versus distance ρ_j.

AD-A033 885 NORTHROP CORP DES PLAINES ILL DEFENSE SYSTEMS DEPT F/G 17/4
LOW COST EXPENDABLE TWT AMPLIFIER FOR ECM.(U)
AUG 76 O DOEHLER, R MOATS N00173-75-C-0464
UNCLASSIFIED 094-007576 NL

2 OF 2
ADA033885

END

DATE
FILMED
2 -77

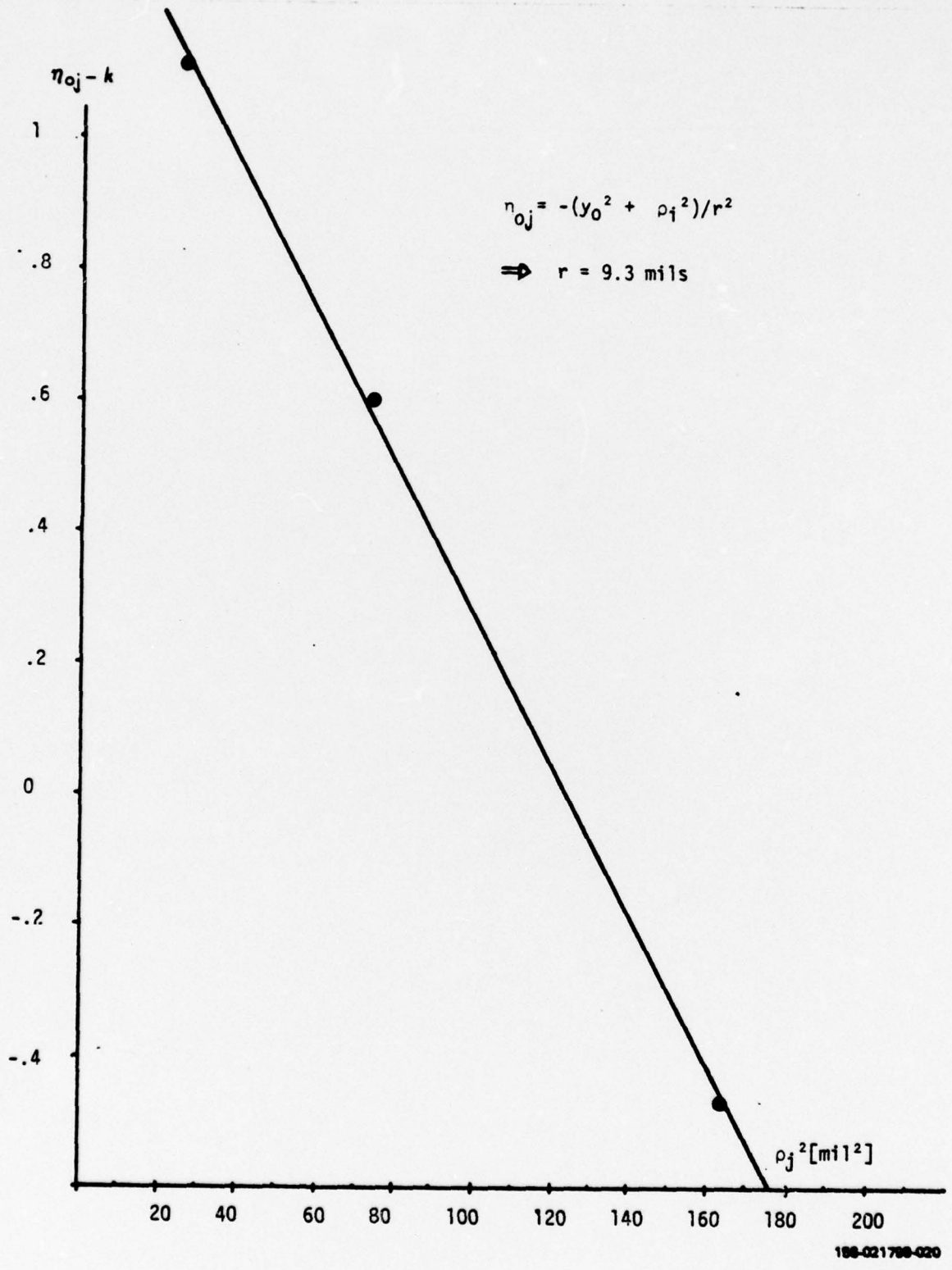

Figure 42. $\eta_{dc} = \eta_{oj} - k$ versus ρ_j^2 - Plot.

compared to a computed Brillouin beam radius of 0.248 mm. It follows now from relation (8) that the eccentricity y_o can be calculated to be:

$$y_o = 3.7 \text{ mils} = 0.095 \text{ mm} \qquad (9)$$

From this evaluation it follows that the current distribution seems to have the cylindrical symmetry assumed and can be represented by the relation $I \approx \exp\left[-(R-r_o)^2/r^2\right]$. The probe radii are about 0.125 mm. The current density at the center of the beam can be evaluated from the probe position and the measured probe current. Using the measured distribution of beam current density and integrating over the cross section of the beam, a total beam current of 21.5 mA is calculated, compared to a measured beam current of 17 mA.

The observation that the beam is off center with respect to the probe under these conditions of beam voltage and current is consistent with the analytic results of Section 4.2.7. In the present case, with reduced beam velocity, exceeds 0.4, and any small deviation from concentric injection is magnified in the PPM stack.

The agreement between the measured beam diameter and the Brillouin beam diameter calculated from voltage current and magnet fields may be valid or may be a coincidence.

More measurements are necessary to determine the flow and the PPM stack under different conditions. It is easy to visualize a computer program to perform the calculations described above, for one set of measurements.

6. SUMMARY OF THE RESULTS ACHIEVED DURING THE FIRST PHASE

6.1 Low Cost Components for the Gun and the PPM Stack

Sources of low cost parts for the gun and PPM stack were systematically explored. The lowest cost parts which have been found are:

- Beam focusing and anode electrodes, made by stamping
- Ceramic rings, as used in the auto industry
- Oxide cathodes, CPC cathodes, or Medicus cathodes made by powder metallurgy
- SAES getter ST101
- Header with Hybralox insulators
- Ferrite magnets, as used in loudspeakers
- Barrel made from drawn tubing with eccentricity no more than 0.0025" TIR

If the above components are used, the cost of the parts for the gun and PPM stack is about $30 each for 5,000 tubes. The main cost driver is the PPM stack. To meet the goal of $72 or less for the total bill of materials for the tube, it will be necessary to demonstrate that ferrite magnets can be used in spite of the thermal drift of the magnetic fields.

If one of these parts has to be replaced by a more expensive one, it is estimated that the selling price of the tube will increase by the price difference multiplied by a factor of 1.53.

6.2 Non-Ideal PPM Focusing

It has been shown experimentally that, for both ferrites and Alnico 8, crossed fields due to inhomogeneous magnetization can be neglected with a proper design and alignment of pole pieces.

Under all of the conditions investigated, paraxial flow equations were used to study the effect of non-ideal beam injection. In addition, calculations were made for one particular case by Shared Applications, Inc. (SAI) using a 5-layer electron beam and iteratively solving Poisson's equation. Comparisons of the paraxial flow calculations with the SAI calculations show that the results are substantially equivalent. The calculations have led to the following conclusions:

- Eccentricity of the beam with respect to the magnetic field introduces crossed-field components which are tolerable for an eccentricity of less than 0.001" (TIR less than 0.002") for λ_p/L greater than 2. (λ_p = plasma wavelength, L = length of the magnet.)
- If crossed fields in the gun area are held below 0.5 Gauss, a value found to be achievable, the beam may be injected properly.
- The angle of injection must be below 1^o, which can be held by the mounting of the gun with a "snout" (Figures 3 and 4).
- The most important factor for good beam transmission is the regularity of the peak magnetic field in the periodic stack.
- The random of the variation must be less than $\pm$3% and most desirably, no more than $\pm$1.5%. The PPM stacks in several commercially available TWT's were measured and none met the $\pm$3% requirement.

6.3 Beam Tests

The real size beam tester showed that the measurements are repeatable and preliminary results appear to be in good agreement with calculations.

A complete analysis of the validity of the computation could not be done because of the difficulty with the cathode heater, which did not allow high enough cathode temperature for full emission.

6.4 Construction

With respect to construction, the principle difficulty is seen in leaks in the RF connectors. It is proposed that in the second phase, a completely different technology of constructing the RF circuit be used as compared with that proposed during the first phase, in order to eliminate this difficulty.

7. PROPOSED WORK FOR THE SECOND PHASE

7.1 Beam Tester

To finish the program outlined in Section 2.3, an estimated time of 4 - 5 months is required.

7.2 Delay Line Technology

A new approach to the technology of the delay line is proposed. Figure 43 shows the new approach to be considered.* The helix tape is T-shaped (Figure 44) and the helix is inserted into a ceramic tube which could be metallized on the outside. The ceramic of the tube can be of BeO, Al_2O_3, glass, or Hybralox (a mixture of glass and Al_2O_3) depending on the RF power requirements. The locking of the helix in the barrel can be achieved by heat shrinkage, by cementing, or by shrinkage of the insulator tube if glass or Hybralox is used as material.

This proposed technique has the advantages of low cost and reliable construction; no supplementary insulators for the collector and for the RF output are needed. The RF output can be either a pin, as in most TWT's, or a coupled helix outside of the tube (Figure 45). The coupling between both helices must be made strong so that matching becomes less critical. The coupled helix system eliminates possible leak failure and reduces the cost of the matching system.

Continuous support of the helix can result in improved helix cooling, which will enable application to higher powered TWT's. It may also eliminate filter effects which produce output power variations in high powered TWT's using rod supported helices.

7.3 Cold Test Study

The main problem related to the proposed type of technology is the dielectric loading of the helix. It is well known that a flat helix inserted into a dielectric cylinder exhibits high dielectric loading. This was confirmed by the low gain measured on printed circuit TWT's.

*The T-Shaped helix was first described by L. Winslow, as an alternative to notching support rods in high power TWT's to increase interactive impedance.

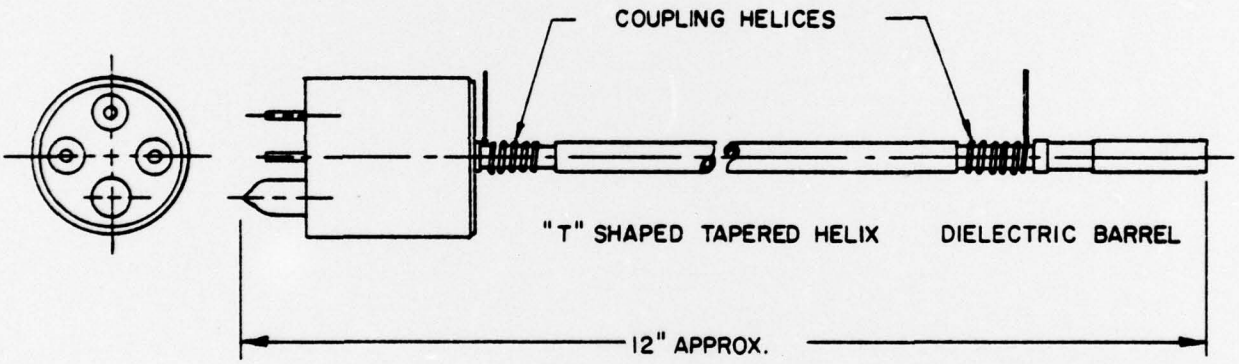

Figure 43. Proposed Low Cost TWT.

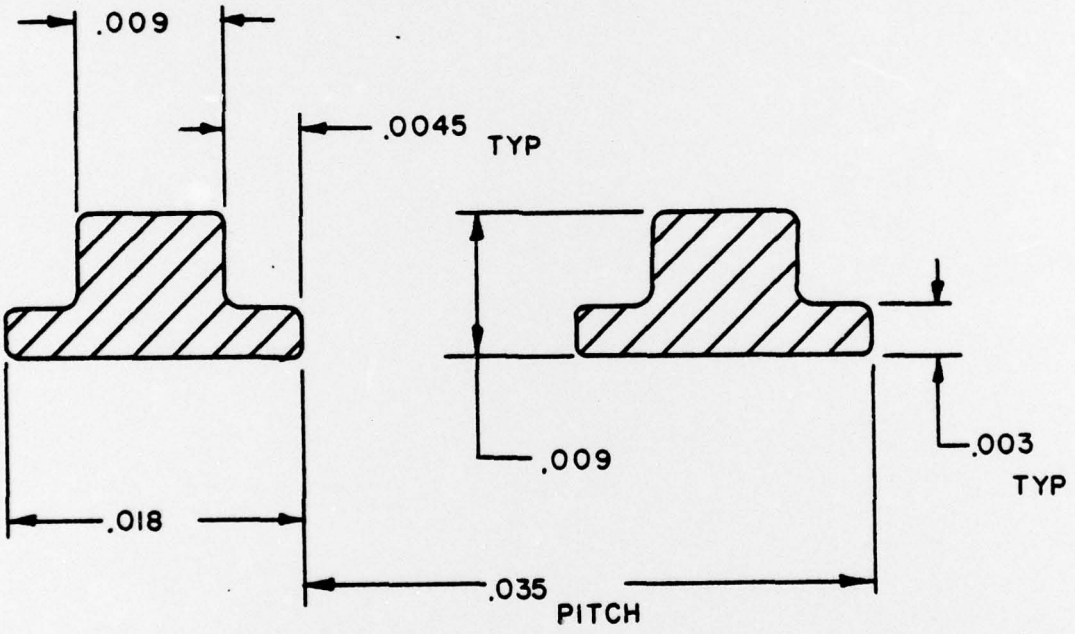

Figure 44. "T" Shaped Tapered Helix.

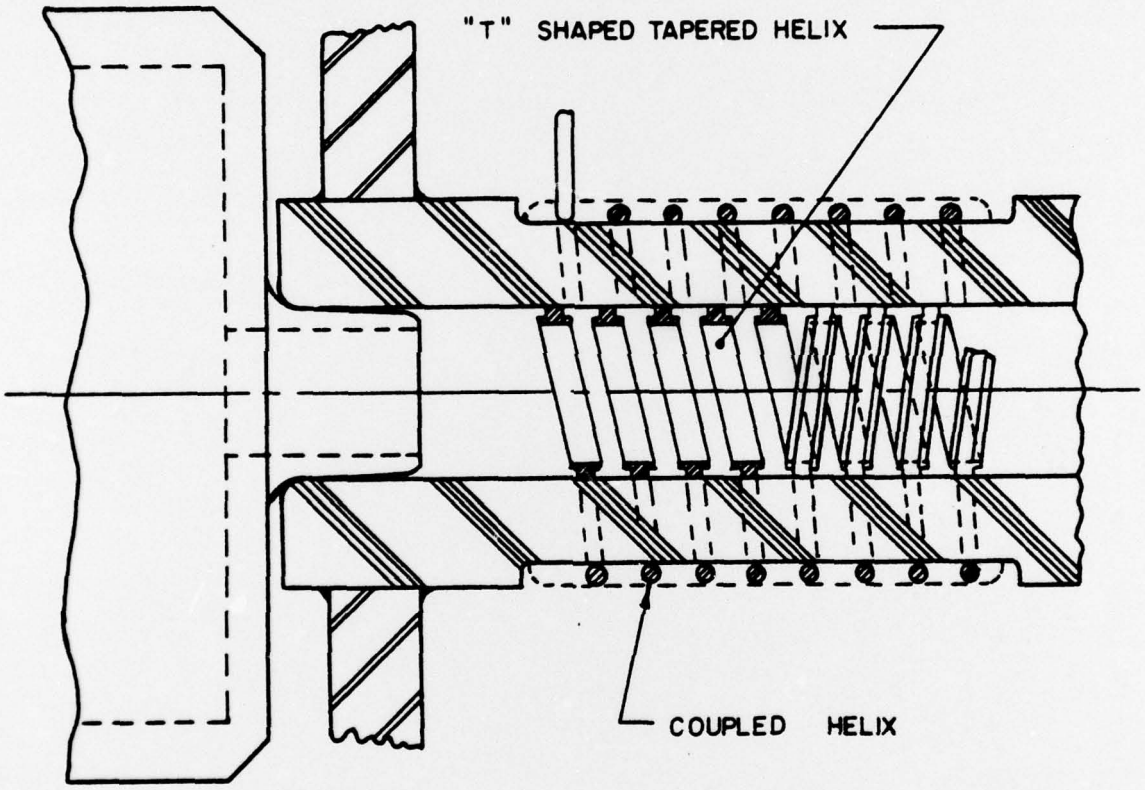

Figure 45. Coupled Helix Input.

To evaluate the dielectric loading by the T-helix, a simple model was built. The simplest possible equivalent circuit of the helix is an L-C filter line (Figure 46). In this schematic, the impedance reduction factor is the square of the dielectric loading factor. Figure 47 shows the exact calculation of Tien (22) of F_2 versus the normalized helix radius $\omega a/c$. As a first approximation, the reduction factors are equivalent.

To evaluate whether the dielectric loading factor of the T-helix is too small, three rings have been mounted on Teflon, which has a low dielectric constant, as shown in Figure 48. The rings simulate three pitches of the helix. In Figure 49b, three rods of stycast 6 ($\epsilon = 6$) were attached to the rings simulating the rods of the classical helix. In Figure 48a, three T-shaped rings were surrounded by a tube of stycast 6. Table XVIII shows the ratio of coupling impedance of the T-shaped helix in a cylindrical barrel to the flat helix with three rods. If the width of the T is about 1/4 of the width of the tape, the two coupling impedances are approximately equal.

TABLE XVIII

Reduction of Coupling Impedance of T-Shaped Helix in Cylindrical Barrel to Flat Helix with Three Rods ($\epsilon = 6$)

Width of T	0.090"	0.045"	0.022"
$\frac{Z_{T\text{-Shaped}}}{Z_{Flat}}$	0.65 0.72	0.84 0.85	0.90 0.91

The dielectric loading increases when the distance between helix and dielectric barrel is increased, i.e., when the T-shaped wire height is increased. However, the technology in fabricating helices with large T-shaped wire height is complicated. The ideal case is to draw the T-shaped wire, but if the height must be relatively great, then two or three taped wires with different widths can be brazed together,

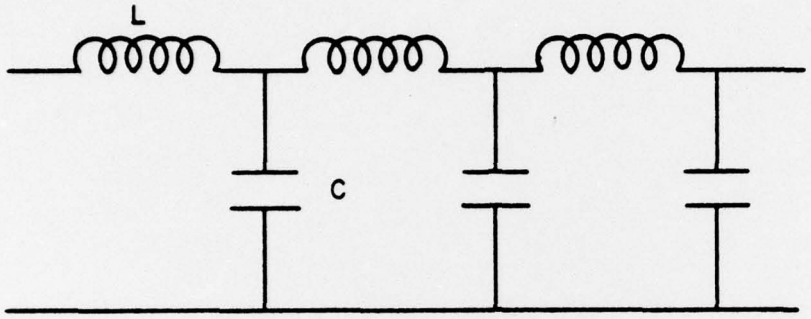

PHASE VELOCITY $v_{ph} = \frac{1}{\sqrt{LC}}$
FOR $\varepsilon = 1$

PHASE VELOCITY $v_{ph} = \frac{1}{\sqrt{LC\,\varepsilon_{eff.}}}$
FOR $\varepsilon = \varepsilon_{eff.}$

FOR $v'_{ph} = v_{ph}$ = DIELECTRIC LOADING FACTOR

$$DLF = \frac{1}{\sqrt{\varepsilon_{eff.}}}$$

CHARACTERISTIC IMPEDANCE $Z_o = \sqrt{\frac{L}{C}} = \frac{1}{vC}$
FOR $\varepsilon = 1$

CHARACTERISTIC IMPEDANCE
FOR $\varepsilon = \varepsilon_{eff.}$ $Z = \sqrt{\frac{L}{C\,\varepsilon_{eff.}}} = \frac{1}{v'C\,\varepsilon_{eff.}}$

$$\frac{Z}{Z_o} = \frac{1}{\varepsilon_{eff.}} = (DLF)^2$$

156-021798-023

Figure 46. Simulated Helix by L-C Circuit.

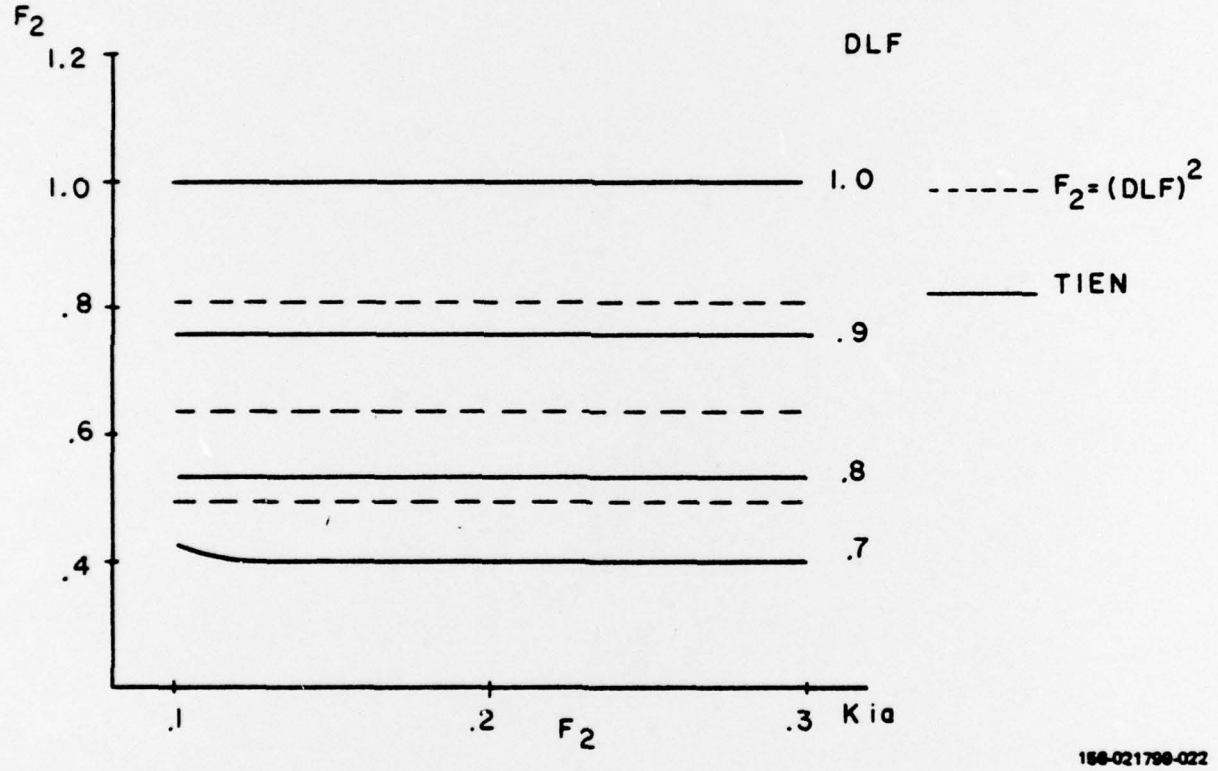

Figure 47. Coupling Reduction Factor for Different "DLF".

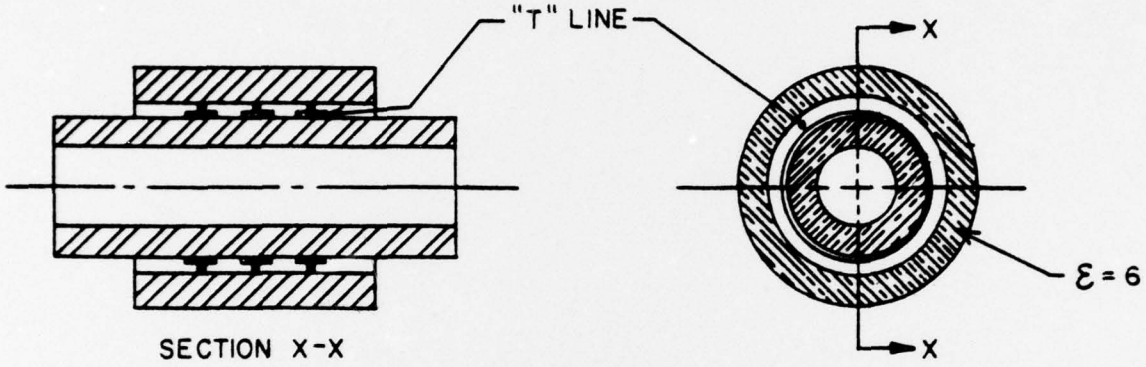

Fig. a

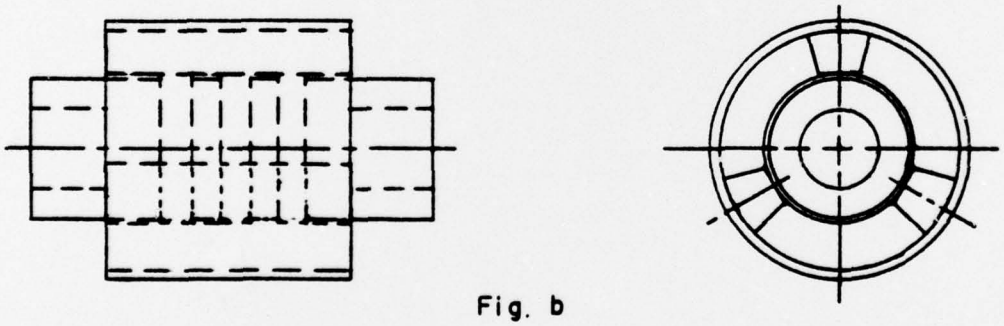

Fig. b

156-021799-025

Figure 48. Simulated Dielectric Loading of "T" Line (Fig. a), Loading of Classical Helix (Fig. b).

one on top of another. The main cold tests, therefore, to be performed are as follows:

- Measure the dielectric loading
- Measure the ω-β diagram
- Measure the coupling impedance
- Measure the tolerances of pitch, diameter and concentricity (mechanical stresses)
- Determine the matching by pins and by coupled helices

7.4 Technology of the Attenuation

The pyrolytic deposition of carbon as commonly used in modern TWT's might be adapted to this technology. It is also proposed to evaluate evaporation of thin film tantalum, as described by Amand and Morris.[23]

7.5 Cost Analysis

The dielectric barrel is one of the most expensive parts. Although a BeO barrel does not appear to be necessary, vendor quotes were obtained from two suppliers on such barrels and are shown in Table XIX.

TABLE XIX

Ceramic Barrel (Two Suppliers)

	100	1000	5000
Length 6" ID .110" ± .002 concentricity TIR 0.002"	$ 7.10	$ 4.96	$4.05
Length 6" ID .110" ± .005	$35	$12	$9.50

In both cases, the inner diameter is not held to sufficiently tight tolerances for a proper fit between the T-helix and the ceramic barrel. However, the TIR seems to be satisfactory. No further investigation of BeO, glass, or Hybralox barrels has been made.

REFERENCES

(1) Statement of Work: Manufacturing Program for Miniature Traveling Wave Tube, Contract Number F33615-73-C-5032, 1973.

(2) Statement of Work: Manufacturing Methods for Dual Mode Traveling Wave Tubes, Contract No. F33615-75-5256, 1975.

(3) Production Technique and Cost Study For Compact Traveling Wave Tube Amplifier, NRL Report, Contract N00014-72-C-0453, 1974.

(4) Presented By M.E.C. on Conference "Lower Cost ECM", 1975.

(5) Lower Cost ECM Conference, February, 1975, File ARS-74-1049.

(6) See e.g., A. T. Raczynski: "Manufacturing Methods for Dual Mode Traveling Wave Tubes," Interim Report No. 1, Contract No. F33615-75-5256, 1975.

(7) TECHNICAL note of SAES Getters, VIA GALLARATA 215, 20151 Milano, Italy, US Representative: 160 Sugg Road, Buffalo, NY 14225.

(8) J. E. BURGESS and E. A. Conquest: Manufacturing Methods Program for Miniature Traveling Wave Tubes, Contract No. F33615-73-C-5032.

(9) J. R. Pierce: Theory and Design of Electron Beams. D. Van Nostrand Co., New York, 1949.

(10) G. F. Gittins: Power Traveling Wave Tubes. American Elevier Publishing Company, Inc., New York, 1964.

(11) C. S. Tschernov: "Interaction of Electromagnetic Waves and Electron Beams with Centrifugal Electrostatic Focusing," Proceedings of the Symposium on Electronic Waveguides, Polytechnic Press, New York, 1958.

(12) P. T. Kirstein, G. S. Kino, W. E. Waters, Space Charge Flow, McGraw-Hill Book Co., New York, 1967.

(13) D. J. Blakner, F. E. Vaccaro, "Electrostatic Focused Traveling Wave Tubes," Electronics, January 2, 1959.

(14) M. S. Glass, "Straight Field Permanent Magnets of Minimum Weight for T.W.T. Focusing; Design and Graphic Aids in Design," Proc. IEEE, vol. 45, p. 1100, 1957.

(15) B. G. Glance, "Focusing of High Perveance Electron Beams by Quadrupole Lenses," Microwave Tubes, Proceedings of the 5th International Congress, Paris, Academic Press, New York, 1964.

(16) W. W. Siekanowicz, J. H. Cash, Jr., "Focusing of Medium - and High-power Electron Beams by Use of Long Period Magnetic Fields: Microwave Tubes, Proceedings of the 5th International Congress, Oarus Academic Press, Academic Press, New York, 1964.

(17) J. R. Hechtel, "Analysis of Non-laminar Electron Beams for High-power Microwave Tubes," Technical Digest, 1974 International Electron Devices Meeting, Washington, D. C., 1974.

(18) K. J. Harker: "Periodic Focusing of Beams from Partially Shielded Cathodes," IRE Transactions on Electron Devices, V. ED-2 p. 13, October, 1955.

(19) B. Mikanovic: "Non-Uniformities in a PPM Focusing Unit," crowave, Proceedings of the 4th International Congress on Microwave Tubes, pps. 605-609, Centrex Publishing Co., Eindhoven, 1963.

(20) J. T. Mendel, C. F. Quate, W. A. Yocom, "Electron Beam Focusing with Periodic Permanent Magnetic Fields," Proc. IRE, vol. 42, p. 800, May, 1954.

(21) F. Villotte: "Etude des dissymetries du champ dans un systeme a focalisation alternee axiale," 5th International Congress on Microwave Tubes, Paris, 1964, p. 45.

(22) Ping King Tien: "Traveling wave tube helix impedance," Proc. IRE, vol. 41, p. 1617, November, 1953.

(23) A. T. Amand, R. S. Morris, "Application of tantalum films as traveling wave tube attenuators," Ninth Conference on Tube Techniques, IEEE, New York, 1968.

APPENDIX I

Beam Trajectories in PPM Focusing

In a magnet stack for PPM focusing, we shall assume a magnetic field in the z direction (axial) of the form:

$$B_z = B_o \cos\left(\frac{2\pi z}{L}\right) I_0\left(\frac{2\pi r}{L}\right) \quad (1)$$

where L is the period of the magnetic field.

The radial component has the form:

$$B_r = B_o \sin\left(\frac{2\pi z}{L}\right) I_1\left(\frac{2\pi r}{L}\right) \quad (2)$$

It is convenient to replace $2\pi z/L$ by X. The rms field, $\hat{B}$, is equal to $B_o/\sqrt{2}$. It will be assumed that deviations from the axis are small compared with L so that (1) and (2) may be replaced by:

$$B_z = \sqrt{2}\ \hat{B} \cos X \quad (3)$$

$$B_r = \sqrt{2}\ \hat{B}\ \frac{\pi r}{L} \sin X \quad (4)$$

If the center of the beam does not coincide with the axis of the magnetic field by an amount δ, we transform the coordinates to the axis of the beam. In (4) above, expression r is replaced by $(r + \delta \cos\theta)$ so that:

$$B_r = \sqrt{2}\ \hat{B}\ \frac{\pi}{L}\ (r + \delta\cos\theta) \sin X \quad (5)$$

There also now appears a component of B in the θ direction:

$$B_\theta = \sqrt{2}\ \hat{B}\ \frac{\pi}{L}\ \delta \sin\theta \sin X \quad (6)$$

In cylindrical coordinates, the expressions for acceleration of particles of mass m, when subjected to forces F_r and F_θ, respectively, are given by:

$$F_r = m\ (\ddot{r} - r\dot{\theta}^2) \quad (7)$$

$$F_\theta = m\ (2\dot{r}\dot{\theta} + \ddot{r}\theta) \quad (8)$$

$$rF_\theta = m\ \frac{d}{dt}\ (r^2\dot{\theta}) \quad (9)$$

In the above expressions, the dots above the symbols represent derivatives with respect to time.

In the TWT beam, it is the forces due to the circumferential magnetic field which cause significant deviation from the trajectories which would be present with the beam on the axis of the magnetic field. Replacing F_θ in (8) with the forces due to the magnetic field, we obtain:

$$r\,(e\dot{r}\,B_z \pm e\dot{z}B_r) = m\,\frac{d}{dt}\,(r^2\dot{\theta}) \qquad (10)$$

$$\eta\,(B_z r\,dr + B_r r\,dz) = d\,(r^2\theta)$$

where $\eta = e/m$, $-e$ is the charge of an electron, and m the mass of an electron.

If (10) is solved for $\delta = 0$, we have the results given by Busch's Theorem. To carry out the solution for $= 0$, it is convenient to reduce variables, taking r_o as the beam radius when entering the magnetic field and $= r/r_o$; z is replaced by XL/2. We shall define as do/dX. Equation (10) may then be written:

$$d(\sigma^2\theta) = 2\eta B\,(\sigma' \cos X - \frac{\sigma^2}{2}\sin X - \frac{\delta\sigma}{2r_o}\sin X \cos\theta)\,dX \qquad (11)$$

The first two terms in the parentheses are integrated into a closed form solution, equivalent to Busch's theorem. Integration is from 0 to X, and the magnetic field, B_c, and the radius at the cathode, r_c, must be taken into account at the 0 limit of integration. The third term remains in integral form, and we have the following solution:

$$\dot{\theta} = \frac{\eta\hat{B}}{\sqrt{2}}\left(\cos X - \frac{B_c r_c^{\,2}}{\sqrt{2}\,\hat{B}r^2} - \frac{\delta}{r_o\,\sigma^2}\int_0^X \sigma\cos\theta\sin X\,dX\right) \qquad (12)$$

Two more normalization factors are introduced. The first, the cathode-shielding parameter, is given by:

$$\kappa = r_c^{\,4}\,B_c^{\,2} / 2\hat{B}\,r_o^{\,4} \qquad (13)$$

The second, the lens-strength parameter, is given by:

$$a = 1/4\,(\frac{L}{\lambda_H})\;;\;\lambda_H = \frac{2\pi\dot{z}}{\eta\hat{B}} \qquad (14)$$

Since $\dot{z}$, the electron velocity in the axial direction, may be assumed constant and much larger than r_o, it is possible to convert $\dot{\theta}$ into $d\theta/dX$. Then, introducing the above normalizing parameters, we have:

$$\frac{d\theta}{dX} = \sqrt{2a}\left(\cos X - \frac{\sqrt{\kappa}}{\sigma^2} - \frac{\delta}{r_o \sigma^2}\int_o^X \sigma \cos\theta \sin X \, dX\right) \qquad (15)$$

When the beam is injected on axis, the following expression for electron motion in a cylindrical beam is given:

$$\sigma'' + a\sigma f^2 - \frac{2\kappa a}{\sigma^3} - \frac{\mathscr{P}}{\sigma} = 0 \qquad (16)$$

In the above, f represents the distribution of magnetic field, given here by $\sqrt{2}$ cos X. $\mathscr{P}$ is the space charge parameter, given by:

$$\mathscr{P} = 1/2\left(\frac{L}{\lambda_p}\right)^2; \quad \lambda_p = \frac{2\pi\dot{z}}{\omega_p} \qquad (17)$$

where ω_p, the plasma frequency, is equal to $\sqrt{\eta\rho/\epsilon_o}$, ρ = charge density, and ϵ_o = the permittivity of space.

For the case of beam injection off axis, the following expression replaces (15):

$$\sigma'' = \frac{\mathscr{P}}{\sigma} - 2a\sigma\cos^2 X + \frac{2\kappa a}{\sigma^3} - (2a)^{1/2}\frac{\delta}{r_o}\sin X \cos(\theta - \theta_o) - 4\frac{\delta a\sqrt{\kappa}}{r_o\sigma^3}\int\sigma \sin X \cos(\theta - \theta_o)dX \qquad (18)$$

For a numerical solution to (18), it is necessary to integrate (15) numerically to find θ at each step, then determine a value for the integral in (18), and then to integrate numerically twice to determine σ.

Distribution and Addresses	DODAAD Code	Number of Copies (Unclassified)
Director, Naval Research Laboratory Washington, D. C. 20375 Attention: Codes 5733 5700 5740 5750 5240 5709	N00173	 3/0 1/0 1/0 1/0 1/0 1/0
Director, Naval Electronic Systems Command 2511 Jefferson Davis Hwy Arlington, Virginia 20360 Attention: Code 304 (Butler)	N00039	3/0
Director, Naval Air Systems Command Jefferson Plaza Washington, D. C. 20361 Attention: AIR 53322D (Whiting)	N00019	3/0
Defense Documentation Center Building 5, Cameron Station Alexandria, Virginia 22314	S47031	2/0
Naval Weapons Center China Lake, California 93555 Attention: Code 3544 (Scott)	N60530	1/0
Watkins-Johnson Company 3333 Hillview Avenue Palo Alto, California 94304 Attention: Mr. G. Wada	14482	1/0
Teledyne MEC Palo Alto, California 94304 Attention: Dr. N. Pond	11312	1/0
ITT Electron Tube Division Easton, Pennsylvania 18042 Attention: Mr. Workman	20948	1/0
Varian Associates Tube Division Palo Alto, California 94304 Attention: Mr. Al Scott	6E845	1/0
Litton Industries Electron Tube Division San Carlos, California 94070 Attention: Mr. S. Weber	80080	1/0

Distribution and Addresses	DODAAD Code	Number of Copies (Unclassified)
Raytheon Power Tube Division Foundry Avenue Waltham, Massachusetts 02054 Attention: Mr. D. Windsor	6H339	1/0
Hughes Aircraft Company Electron Dynamics Division Lomita Boulevard Torrance, California 90509 Attention: Mr. A. Lavik	73293	1/0
Director Naval Electronics Laboratory Center San Diego, California 92152 Attention: Code 3260	N00953	1/0
Director Rome Air Development Center Griffis AFB, New York 13441 Attention: MR. D. Bussey	FY7619	1/0
Microwave Associates, Inc. Burlington, Massachusetts 01803 Attention: Mr. J. Brown, E. W. Components		1/0
Advisory Group on Electron Devices 210 Varick Street New York, New York 10014 Attention: Mr. H. R. Summer		1/0